UNIVERSITY
OF TRENTO - Italy
DEPARTMENT OF INDUSTRIAL ENGINEERING

XXVIII cycle

Doctoral School in Materials Science and Engineering

Development of a design procedure accounting for the anisotropy of the dimensional change in Powder Metallurgy parts

Nicolò Corsentino

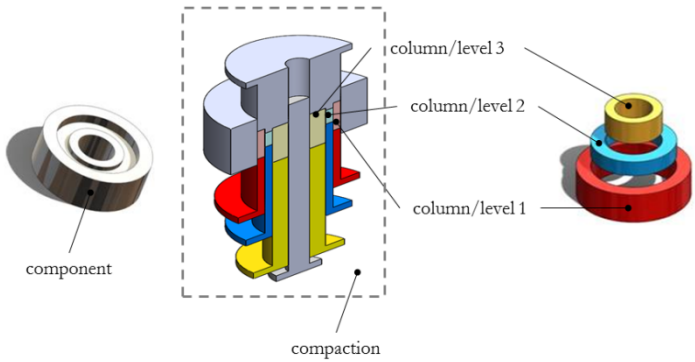

April 2016

DEVELOPMENT OF A DESIGN PROCEDURE ACCOUNTING FOR THE ANISOTROPY OF THE DIMENSIONAL CHANGE IN POWDER METALLURGY PARTS

Nicolò Corsentino

E-mail: n.corsentino @ unitn.it

Approved by:

Prof. Ilaria Cristofolini, Advisor
Department of Industrial Engineering
University of Trento, Italy.

Prof. Alberto Molinari
Department of Industrial Engineering
University of Trento , Italy.

Ph.D. Commission:

Prof. Vigilio Fontanari,
Department of Industrial Engineering
University of Trento, Italy.

Prof. Eugene A. Olevsky,
Department of Mechanical Engineering
San Diego State University,
United States of America.

Prof. Gino Mariotto,
Department of Computer Science
University of Verona, *Italy.*

University of Trento,
Department of Industrial Engineering

April 2016

University of Trento - Department of Industrial Engineering

Doctoral Thesis

Nicolò Corsentino - 2013
Published in Trento (Italy) – by University of Trento

To my love Sbiffa

Abstract

The dimensional control is a crucial aspect for any manufacturing process. In Powder Metallurgy, and in particular in net shape press and sinter process, dimensional control assumes a particular relevance, since sintering of green parts involves dimensional variations that can be from 0 to 2-3% in volume. The dimensional variation in sintering is either shrinkage or swelling. Both depend on the material and on several process parameters relevant to the compaction and the sintering operations.

Experimental evidences proved dimensional variations to be affected by an anisotropic behavior. This important phenomenon affects the effectiveness of the dimensional control if not opportunely taken into consideration in the design process. Professor Ilaria Cristofolini and Professor Alberto Molinari have started a deep investigation on this phenomenon, about five years ago, involving an important experimental campaign. The main idea is to collect a large quantity of data, both on ad-hoc designed samples and on parts produced by qualified PM companies cooperating with the University of Trento. The purpose is to develop a realistic model, able to explain and describe the mechanisms involved in the anisotropy of dimensional changes, and the dependence on the geometry of the parts, building a robust knowledge to improve the design methodologies in the industrial production.

The present work investigates the effect of the geometrical characteristics of the part on the dimensional variations in sintering, giving a particular importance on its anisotropic behavior. The influence of geometry has been investigated using rings and disks with varying heights, external diameters and internal diameters. The influence of the sintering temperature has been also evaluated. The dimensional variation has been measured by a tri-dimensional Coordinate Measuring Machine. The anisotropy has been defined through a specifically determined parameter, which has been used to develop a predictive model estimating the anisotropy of the dimensional variations. This model has been then validated on complex parts produced by a Powder Metallurgy company.

Acknowledgements

This work has been realized under the expertise and the supervision of Professor Ilaria Cristofolini and Professor Alberto Molinari of the University of Trento. All the measurements and the metallographic analyses have been carried out in the laboratories of the Industrial Engineering Department of the University of Trento. The supplied samples have been compacted and sintered by Höganäs AB (Sweden), TFM spa (Italy) and K4sint (Italy). The author is grateful to all the colleagues of the Metallurgy and Machine Design Laboratory of the Industrial Department of the University of Trento in Mesiano (Italy). The author is also thankful to all the students that have been collaborating to this project for their bachelor and master activities.

A special thanks to Professor Ilaria Cristofolini for her precious support during the research activity and the writing of this thesis. Without her help no word of this dissertation would have been written.

TABLE OF CONTENTS

Chapter 1

Introduction.

Metal Powder technology (also known as Powder metallurgy - PM) is getting an ever increasing interest from the industry due to the consolidation of the standard processes and the development of new technologies and materials. The press and sinter process is one of the most common among the PM manufacturing technologies for the production of parts with an excellent combination of dimensional and geometrical precision and technological properties. In this process the part is formed compacting the powder in a rigid die, obtaining an object which is basically pressed powder retained in a shape that is dimensionally very close to the final component, this is the so called green. The green is then ready for the sintering operation. In this operation the part is thermally treated in order to create the metallic bonding between the particles and to achieve the properties required for the specific application. Hereafter some key advantages in using the press and sinter technology are listed:

- Net-shape / near net-shape technology, minimum of post-sintering processes required to reach the final product.
- Limited or even null scrap production.
- Complex geometries are possible with some limitations due to the uni-axial compaction process.
- Technological properties close to the part produced with massive processes.
- High production rate.

The abovementioned characteristics give the process remarkable cost effectiveness.

Dimensional and geometrical precision is a key issue in case of a net-shape technology. Sintering involves dimensional variations that can range from 0 to 2-3% in volume. Usually the dimensional variation in sintering is shrinkage, due to densification. In case of liquid phase formation, it is possible to have swelling. This is a very complex issue, depending on the material and on several process parameters both relative to the compaction and the sintering operations. Moreover, anisotropy of dimensional change depends on the part geometry. The dimensional control, which is a crucial aspect for any manufacturing process, will be in this case of a particular relevance.

Dimensional change of prior cold compacted green parts is anisotropic. Despite the importance of this phenomenon and of its recognized effect on dimensional precision of sintered parts, a reliable design methodology has not yet been developed, and designers frequently use an empiric approach to design parts. The objective of this PhD

thesis is the study of the effect of geometry on dimensional change of pure iron, and the proposal and the validation of a rational design methodology.

1.1 Powder compaction.

Powder compaction is the process by means of which the component is formed, it is the most used technology among the various forming processes. In the press and sinter technology the powder is compacted in a rigid die (Shatt and Witers [1]). A schematic illustration of the compaction process is illustrated in figure [1.1].

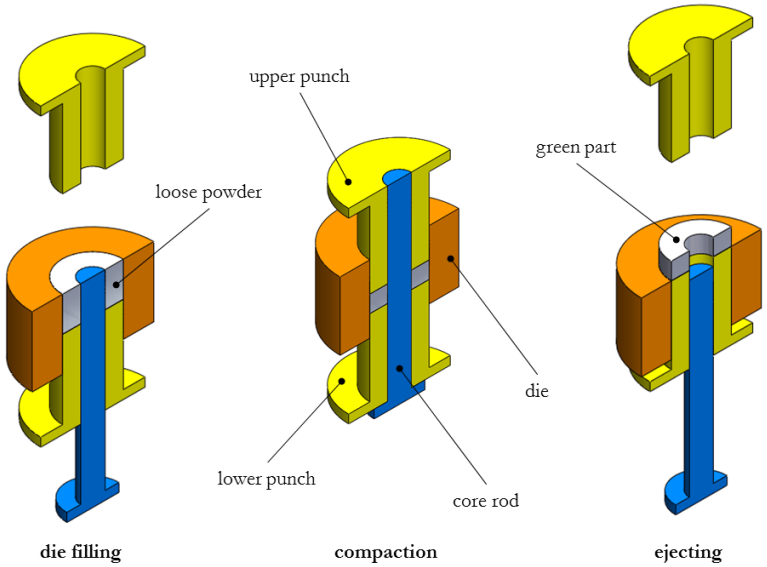

Fig. [1.1] Powder compaction scheme, filling, compaction and ejection.

As reported in figure [1.1], the compaction process can be divided into three main sequential stages, filling, compaction and ejection. Usually the die is filled with a mixture of powder and polymeric lubricant, in order to reduce the friction with the die wall. The die is filled with metallic powder, which is then pressed using a punch. The compaction process can be single-action compaction or double-action compaction. In the first case during the compaction step the lower punch and the die are fixed while the force is applied only by the upper punch; in the second case the load can be applied by moving the upper punch and the lower punch or by moving the upper punch and the die. Compaction provides a densification due to the rearrangement and the plastic

deformation of the powder particles, which implies porosity decrease. This operation also provides the green part with a mechanical strength thanks to the cold-welding of the particle powders at the contact points. The conventional pressure range for this operation is between 150 MPa and 900 MPa (EPMA [2]). In the last step, ejection, the green part is removed from the die, this step is characterized by the recovery of the elastic strain commonly known as "springback". Usually the components produced by press and sinter technology are axi-symmetric and the reachable degree of complexity is strictly linked to the geometry that is possible to form in the compaction step. A rule of thumb in designing components for press and sinter technology is to avoid thin walled components (specifically, wall thickness should never be lower than 1/6 of the height ASSINTER [2]) and the height to diameter ratio should not exceed the value of 3:1. The part presented in figure [1.2] is a "multi-level" component and represents an example of quite complex geometry for powder compaction.

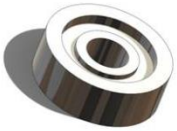

Fig. [1.2] Example of a three level PM part.

The green sample coming from the compaction process needs to have homogeneous density distribution in order to avoid uneven shrinkage and distortion during the sintering stage. To provide the same densification in all the cross-sections each level of the part must be pressed independently, that is using different punches and punch displacements. Generally the higher the number of levels, the higher will be the complexity of the part due to the specific design of the compaction tools. An example is represented in figure [1.3].

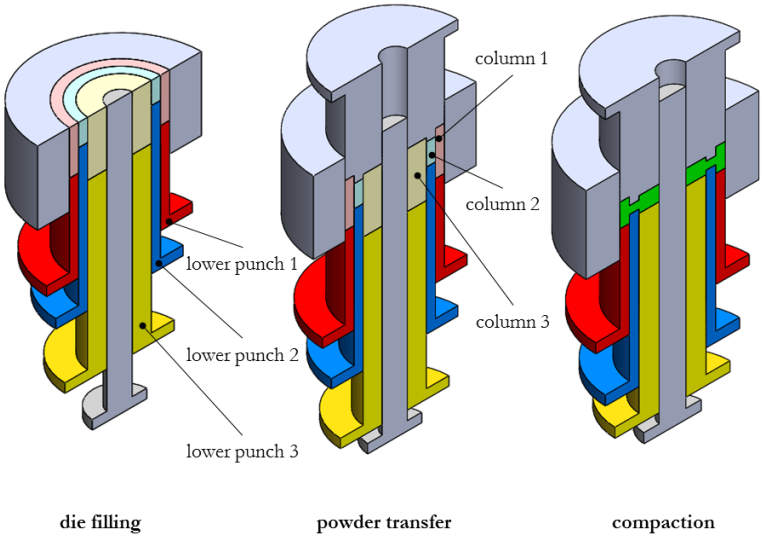

Fig. [1.3] Compacting procedure for a multilevel component.

In figure [1.3] the sample is a three level part, each part is formed by a single powder column, which is pressed by an independent punch that can be moved separately. The number of the punches corresponds to the number of levels. As it is shown in the example the powder is introduced into the die cavity. Before the densification starts, the powder columns are moved after the upper punch is inserted, this step is called "powder transfer" and it is one of the most critical operations in powder compacting (Burch et al. [3]). Once the columns reach the set up position the powder is compacted and the green part is so formed.

During the compaction process the powder is deformed in an elastoplastic regime once the yielding limit is reached during the loading step (Chakrabarty [4]). As mentioned before, the elastic deformation is completely recovered once the load is removed. The stress and the strain states during the compaction step not only depend on the actual pressure, but also on the whole previous load history, thus introducing a further degree of complexity on considering the process parameters influence. In rigid die compaction the densification of the powder is reached under a complex tri-axial stress state (Cocks [5]). A schematic representation of the tri-axial stress in powder compaction is represented in figure [1.4].

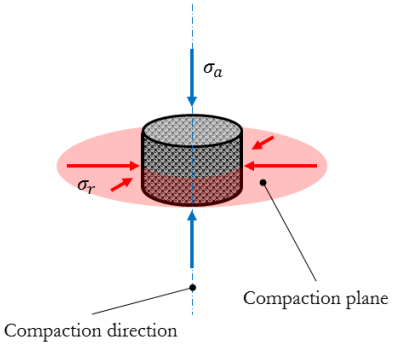

Fig. [1.4] Tri-axial stress in rigid die compaction.

1.2 Sintering.

The sintering process can be defined as a thermal treatment. In this thermal treatment the green part, which is formed by discrete powder particles, goes through a consolidation process. The consolidation process provides the part with an enhanced mechanical strength. The mechanical strength of the green part is ensured by small adhesion forces, thanks to the bonding between the particles; during sintering it increases becoming comparable with the strength of a regular lattice (Thummler and Oberacker [6]). This consolidation occurs either in solid state or in presence of liquid phase (German [7]), this work will be focused on solid state sintering.

From a practical perspective, after compaction the part is placed in a furnace where the sintering process takes place at a well-defined temperature, below the melting point of the main constituent (60% - 90% T_m), within a specific working atmosphere. The protective atmosphere is fundamental for almost all sintering processes, to prevent oxidation and to promote the reduction of surface oxides that could reduce or in some cases inhibit the sintering mechanisms. Usually in furnaces it is common to use partially combusted hydrocarbons, dry hydrogen and nitrogen/hydrogen mixtures (EPMA [2]). The sintering equipment can be implemented with many different technological layouts (Shatt and Witers [1]), the two most common being continuous belt furnaces and batch furnaces. In figure [1.5] a classic sintering cycle is shown.

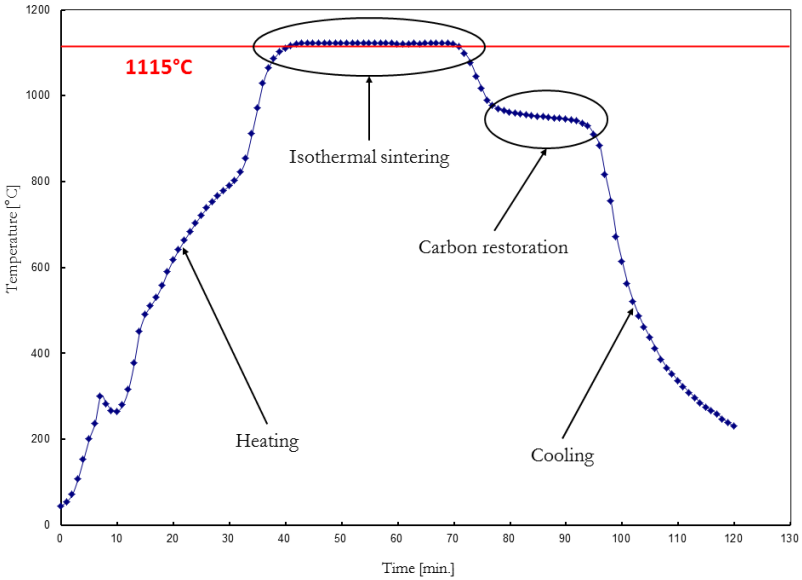

Fig. [1.5] Example of a sintering cycle in a belt furnace, courtesy of T.F.M. automotive spa.

In figure [1.5] some important features of a sintering cycle are shown, heating step, isothermal sintering, carbon restoration (needed in some cases, being sintering a decarburizing process, Shatt and Witers [1]) and cooling step. From an analytical point of view the modeling effort has been focused mainly on the isothermal sintering. Nevertheless every operative condition and parameter of the sintering process play a key role in the densification of the part and the final properties of the material.

On a microscale perspective, sintering is a mass transport phenomenon due to thermally activated diffusion mechanisms, the driving force is the excess of specific surface energy γ due to a high surface to volume ratio of the particles (Suk-Joong L.Kang [8]). In figure [1.6] we can see a schematic evolution of an ideal conglomerate of spherical particles during the sintering process.

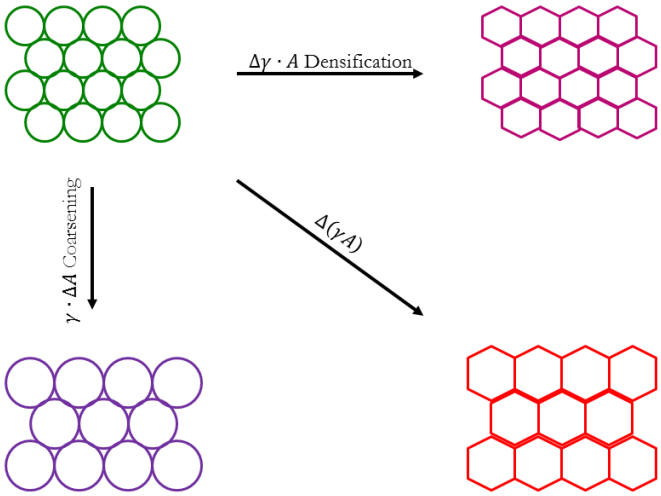

Fig. [1.6] Driving force in sintering and basic phenomena.

$$\Delta(\gamma A) = \Delta\gamma \cdot A + \gamma \cdot \Delta A \qquad \text{Eq. [1.1]}$$

The basic results of mass transport phenomena are densification and grain growth, as schematically depicted in figure [1.6]. In metallic materials sintering grain growth is less enhanced with respect to the densification. The main consequence of densification is the dimensional variation of the part.

1.2.1 Phenomenology of dimensional variation in sintering.

The ability to model and therefore predict the dimensional variation is fundamental for a net-shape technology and enhances the real competitiveness of the process. Several studies investigated the mechanisms involved in sintering and in particular the dimensional variation on sintering. In this work the mechanisms will not be discussed in detail, however a brief list of the main proposed theories will be given in order to understand the complexity of the process and the variables that influence it. In table [1.1] the elementary phenomena in sintering are listed.

	Phenomenon	
No mass transport	• adhesion	
With mass transport	• surface diffusion • volume diffusion via vacancies • volume diffusion via interstitials • grain boundary diffusion • vaporization and re-condensation	single atom movement
	• plastic flow • viscous flow • grain boundary sliding • particle rotation	collective movement

Tab. [1.1] Sintering mechanisms, Thummler and Oberacker [6].

A lot of densification models have been developed, from microscopic mass transport phenomena to macroscopic dimensional variations. Two examples of the earliest shrinkage models are expressed in equation [1.2] and equation [1.3], (Exner and Petzow [9]).

$$\frac{P}{P_0} = (1 + kt)^{-n} \qquad \text{Eq. [1.2]}$$

$$\frac{\Delta L}{L_0} = (kt)^n \qquad \text{Eq. [1.3]}$$

In Skorokhod's model (equation [1.2]) P_0 and P are the green porosity and the porosity at time t, t is the sintering time and the constants k and n are the physical parameters related to the process kinetics. In Kingery and Berg's model (equation [1.3]) ΔL is the dimensional change in the length of a sample having an initial length of L_0, the constant k includes all the physical parameters and the exponent n takes on a different value in function of the single sintering transport mechanism. In this work all the dimensional variations will be expressed as the ratio of the difference between final and initial dimensions to the initial dimensions, this aspect will be discussed in detail in chapter 2. Recently more complex theories have been developed, an example is the Olevsky's continuum theory [10] based on the plastic and nonlinear-viscous deformation of porous bodies. In this model the powder compact is assumed to be an isotropic bi-phase material, the first phase is the "pores skeleton" whereas the second phase is formed by the voids (the first phase could be a multiphase material indeed).

$$\sigma_{ij} = \frac{\sigma(W)}{W}\left(\varphi \dot{\varepsilon}_{ij}{}' + \psi e \delta_{ij}\right) + P_L \delta_{ij} \qquad \text{Eq.[1.4]}$$

In equation [1.4] the general case of the constitutive model is described. The left part of this equation (σ_{ij}) is the external applied stress and takes the null value in case of free sintering, by free sintering is meant all the sintering treatments non pressure-assisted. The term $\frac{\sigma(W)}{W}\left(\varphi\dot{\varepsilon}_{ij}{}' + \psi e\delta_{ij}\right)$ represents the material resistance, where $\dot{\varepsilon}_{ij}$ is the strain rate, e is the shrinkage rate, W is an equivalent strain rate and δ_{ij} is the Kronecker's delta. The term $P_L\delta_{ij}$ is the sintering stress (Thummler and Oberacker [6]). The modeling of sintering shrinkage has been enhanced by software implemented techniques (Suk Hwan Chung et al. [11]) e.g. Monte Carlo simulations, Finite Difference or Finite Elements analysis and so forth. The large variety of models available goes from the two idealized spherical particles to the more complex and realistic macro-mesoscale modeling of sintering developed by Olevsky et al. [12], [13], and Braginsky et al. [14] . In these studies the microstructural and the pore evolution during sintering has been simulated combining the continuum theory of sintering with a Monte Carlo method. In these works the field of simulation is extended even to a tri-dimensional object. Being sintering a complex field with a lot of uncertain parameters the predictive computer models are still poorly accurate, in spite of the good level of complexity reached by computer modeling (German [15]). Also it has to be considered that in literature the majority of predictive models has been developed for ceramic powders.

1.3 Dimensional precision of sintered components.

1.3.1 Dimensional tolerance.

Dimensional control and therefore dimensional precision is a key aspect in sintering (Randall M. German [15]). Designers typically specify component's nominal dimensions such that it fulfils its requirements. Actually, components cannot be made repeatedly to nominal dimensions (Childs [18]). Any given manufacturing technique can only produce a component within a range of accuracy around the specified nominal dimension, this is called capability of the process. The allowed deviation of the actual dimension from the nominal one is the dimensional tolerance. The lower is the tolerance that process capability can guarantee, the higher is the precision of the part. Tolerances are usually normalized with respect to the nominal dimensions in order to compare and evaluate the precision of different dimensions. In this work the precision of the process will be evaluated using a standard, the standard reference will be the UNI EN 20286-1:1995 [16]. In table [1.2] are represented the ISO IT classes of normalized tolerances according to the standard just mentioned.

Nominal dimension		ISO tolerance class													
min	max	IT3	IT4	IT5	IT6	IT7	IT8	IT9	IT10	IT11	IT12	IT13	IT14	IT15	IT16
mm		μm									mm				
0	3	2	3	4	6	10	14	25	40	60	0.1	0.14	0.25	0.4	0.6
3	6	2.5	4	5	8	12	18	30	48	75	0.12	0.18	0.3	0.48	0.75
6	10	2.5	4	6	9	15	22	36	58	90	0.15	0.22	0.36	0.58	0.9
10	18	3	5	8	11	18	21	43	10	110	0.18	0.27	0.43	0.7	1.1
18	30	4	6	9	13	21	33	52	84	130	0.21	0.33	0.52	0.84	1.3
30	50	4	7	11	16	25	39	62	100	160	0.25	0.39	0.62	1	1.6
50	80	5	8	13	19	30	46	74	120	190	0.3	0.46	0.74	1.2	1.9
80	120	6	10	15	22	35	54	87	140	220	0.35	0.54	0.87	1.4	2.2
120	180	8	12	18	25	40	63	100	160	250	0.4	0.63	1	1.6	2.5
180	250	10	14	20	29	46	72	115	185	290	0.46	0.72	1.15	1.85	2.9

Tab. [1.2] ISO IT tolerance classes, according UNI EN 20286-1:1995 [16].

The main idea of this tolerance method is to group the nominal dimensions by size, and to set an equivalent degree of tolerance for each group, so that the same IT tolerance class has different allowed deviations depending on the dimensions. In this way it is possible to compare the precision of different dimensions, for example a diameter of 35 mm with a tolerance of ±0.05 mm has the same precision of a height of 70 mm with an error of ±0.07 mm, both of them belonging to the tolerance class IT 9.

1.3.2 Influence of process parameters.

The main advantage of producing sintered parts is that they can be manufactured directly to the specified dimensions, markedly reducing the amount of machining required or eliminating it completely. The evaluation of the process capability of press and sinter technology is therefore very important. One of the first assessment of the generalized dimensional precision of this process has been reported by Shatt and Witers [1] and it is represented in figure [1.7].

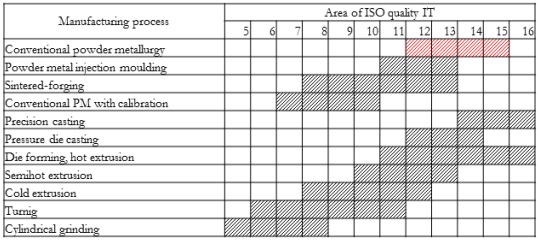

Fig. [1.7] Summary of manufacturing tolerances obtained using various processes for the manufacture of components according to W. Michaeli, (Shatt and Witers [1]).

In figure [1.7] the manufacturing tolerances of conventional powder metallurgy are compared with the tolerances achievable for other manufacturing processes. For conventional powder metallurgy the highest precision achievable is IT 12. Nevertheless, the development of compaction tools and control technologies have improved the precision of the process significantly. In a technical document containing the guidelines for the design of sintered components issued by ASSINTER [2] the precision level is reported to be IT9 up to IT8 for low complexity geometries, when referring to dimensions perpendicular to the compacting axis. As opposed to these normalized tolerance classes, German [17] recently reported the absolute tolerance for the press and sinter process of ferrous parts, as being of ±135 μm in the compaction direction and ±25 μm perpendicular to the compaction direction. The precision associated to the process is still an open issue due to the many parameters that influence it. Despite the generalizations just mentioned, the dimensional precision of the sintered components is the result of several contributions due to the complexity of the process.

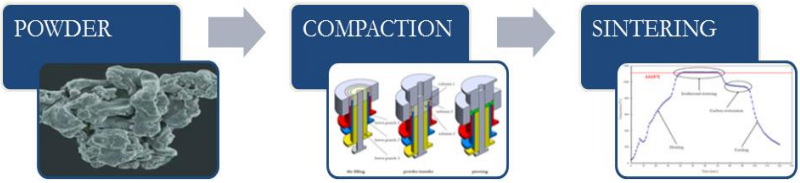

Fig. [1.8] Schematic representation of the press and sinter process.

With respect to the PM production sequence shown in figure [1.8], Bocchini [18] proposed a systematic approach for the evaluation of the influence of the process parameters on the dimensional precision of the sintered component, analyzing individually the effect of the powder characteristics, the compaction step and the sintering step. The final tolerances will be the sum of the individual contributions. The powder plays a crucial role in the process precision by influencing the homogeneity of the green compact and therefore the sintered part.

Powder is the first part of the PM production chain. Its effect on precision is mainly relevant to the influence of the powder characteristics on the compaction operations and the sintering process. Hereafter are listed the main characteristics of the powder:

- chemical composition
- alloying grade (pre-mixed → diffusion bonded → pre-alloyed)
- particle size and size distribution
- particle shape

The choice of powder characteristics is normally based on compromise, since many of the factors are in direct opposition to each other (EPMA [2]). If the irregularity of the powder grain increases, the apparent density decreases, and so the reduction in volume that occurs on compaction increases, in turn giving greater green strength to the compact. The increase in contacting surfaces promotes in the end a more efficient sintering. In addition, the greater reduction in volume giving the required green density may need higher pressure and consequently larger presses and stronger dies. The efficiency and the ease of packing the powder in the die depend to a large extent on a wide particle size distribution, so that the voids created between large particles can be progressively filled with those of smaller size. Fine particles tend to leave smaller pores, which are easily closed during sintering. An excess of small particles, however, reduces flowability due to a higher inter-particle friction. All these aspects influence the homogeneity of the green compact, directly affecting the dimensional precision of the produced part, which may show uneven dimensional variation. According to Bocchini [18], in the sintering step the main powder parameter affecting the dimensional precision is segregation, this is basically due to the homogeneity of the chemical composition. Pre-alloyed powders usually require higher compaction pressures than pre-mixed powder due to the intrinsic higher mechanical strength of the former ones, in spite of the pre-alloyed powders providing the part with a better homogeneity. Rapp et al. [19] studied the influence of the powder alloy grade on the dimensional and geometrical precision of iron-copper steel. In this work it is found that with respect to the pre-mixed powder the diffusion bonded powder deals with a considerable higher dimensional accuracy, which is in part the consequence of a more homogeneous density distribution.

Analyzing the compaction process Bocchini [18] evaluated a list of parameters that influence the dimensional precision of the part.

- Precision of the tooling equipment (die, core rods, punches)
- Wearing of the die and the core rods
- Compliance of the punches
- Springback variation (axial to radial) of the compact
- Tool design and geometrical complexity
- Compaction strategy and type of press

In addition to these factors the attitude of the powder to be compacted, discussed in advance, must be considered, and the presence of lubricant as well. The main effect of the compaction process on the dimensional precision is related to the height of the part. The precision of the height is systematically significantly lower than the diameter precision. This is the result of three main aspects. The first is the filling step, any difference in the quantity of powder introduced into the die causes an unavoidable difference in the height. The second aspect is relevant to the displacement of the punch in the compaction step, due to its compliance. The last aspect is the elastic recovery of the pressed part once it is ejected, the springback, which is higher in the axial direction due to the uniaxial compaction. Moreover the precision is influenced by the friction phenomena, as studied by Al-Qureshi et al. [20], and by the cold work hardening of the metallic particles, which again has a remarkable effect on the homogeneity of the green compact introducing an axial gradient of the density. Figure [1.8] shows the decrease in density in the axial direction, related to the decrease in height from H_0 to H in a cylindrical specimen obtained by single action compaction, as simulated by Druyanov and Nepershin [21] for different compaction conditions.

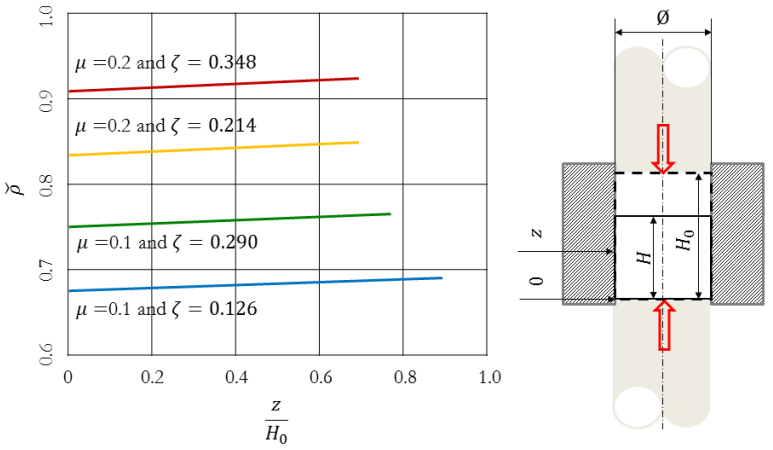

Fig. [1.8] Relative density ($\breve{\rho}$) versus powder compaction ($\zeta = 1 - \frac{H}{H_0}$) of a cylindrical specimen with instantaneous and original heights H and H_0, and the aspect ratio $\frac{H}{Ø} = 0.3$; (Druyanov and Nepershin [21]).

Sintering is the last step of the process and it is influenced by all the aforementioned aspects, in addition to the operative parameters relevant to the sintering process itself. The way this step affects the dimensional precision is very complex. The main phenomenon associated with sintering is dimensional variation due to the enhanced densification. The dimensional variation is the main aspect affecting the dimensional precision and its modelling is very complex as just explained. Bocchini [18] studied the influence of the green density and the alloying elements on the precision of ferrous PM

parts. The density of the green part has a different effect on the dimensional variations for different types of powders, for sponge iron the increase in density leads to a reduction of dimensional variations, this effect is opposite for water atomized powders, where an increase of density leads to an increase of the dimensional variations. The effect of the addition of copper and nickel has been analyzed, showing that the addition of copper enhances the precision of the sintered parts, while the effect of the addition of nickel was negligible if compared with that of copper addition, in any case the addition of an alloying element causes a loss of precision. Summarizing the main aspects concerning the dimensional precision, two main conclusions are evident. Firstly, the dimensional precision of axial dimensions is always result lower compared to that of radial dimensions. Secondly, there is a size effect on the dimensional precision of sintered components, the bigger is the part the higher is the tolerance class associated to the dimensional precision.

1.4 Anisotropy of dimensional variations.

The anisotropy of the dimensional variations is an important aspect concerning the densification during sintering. This has a deep impact in the prediction of dimensional variation and therefore on the overall precision of the process. This phenomenon mainly affects rigid die compacted PM parts. In a cylindrical specimen uni-axially cold compacted, the anisotropy of dimensional variations basically means that the dimensional variation of the height (parallel to the compaction direction) is different from the dimensional variation of the diameter (perpendicular to the compaction direction), as schematically represented in figure [1.9].

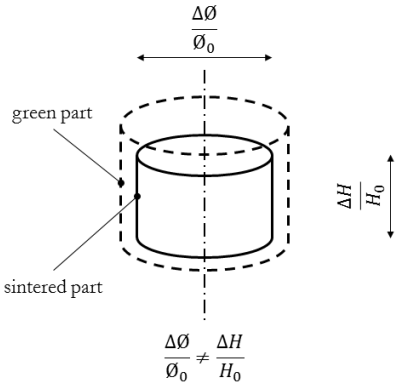

Fig. [1.9] Schematic representation of an anisotropic dimensional variation.

A clear evidence of this phenomenon can be highlighted by dilatometry tests. In figure [1.10] an example of a dilatometry test is shown.

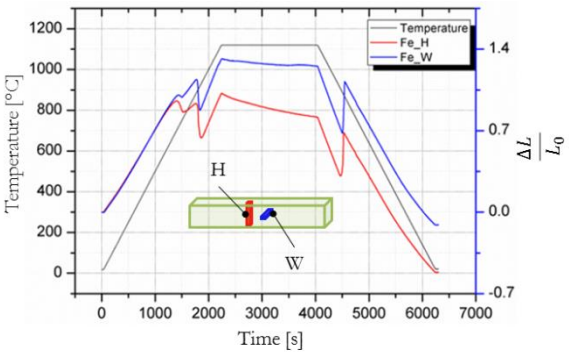

Fig. [1.10] Dilatometry test on iron powder compact, the specimen "H" has been carried out along the compaction direction (longitudinal), the specimen "W" has been carried out in the compaction plane (transversal) of a plain iron impact test specimen, courtesy of Prof. Alberto Molinari.

In this dilatometry test two prismatic samples have been cut form the axial direction "H" and from the transversal direction "W". The same sintering cycle has been performed on both samples and the dimensional variation has been instantaneously recorded. What is evident from this test is the significant difference between the dimensional variation of the two samples at the end of the sintering cycle. Moreover the difference can be observed even in the first stages of the sintering cycle meaning that the anisotropy of the dimensional variations is a phenomenon starting very early in the whole sintering stage.

1.4.1 Mechanisms enhancing the anisotropy.

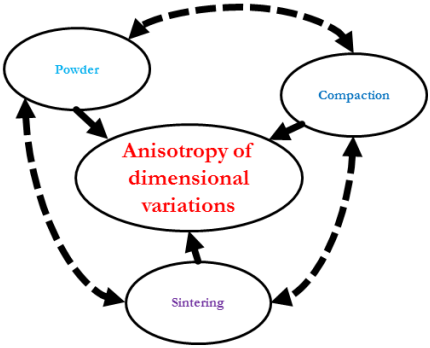

Fig. [1.11] Schematic representation of the influence of process parameters on the anisotropy of the dimensional variations.

The explanation of the mechanisms involved in the anisotropy of dimensional change on sintering is very complex. This phenomenon depends on each of the three main parameters of the process, as schematically described in figure [1.11]. One of the first remarkable explanations of the anisotropy of dimensional change on sintering has been done by Olevsky and Skorohod [22]. In that work, the origin of anisotropy has been found in the morphology of the pores due to the oriented structure of the particles. The model has been idealized to an anisotropic-porous body with texture of ellipsoidal pores. The result of the computations show a spheroidization of the pore due to the higher strain rate on the radial direction compared to the axial direction as represented in figure [1.12].

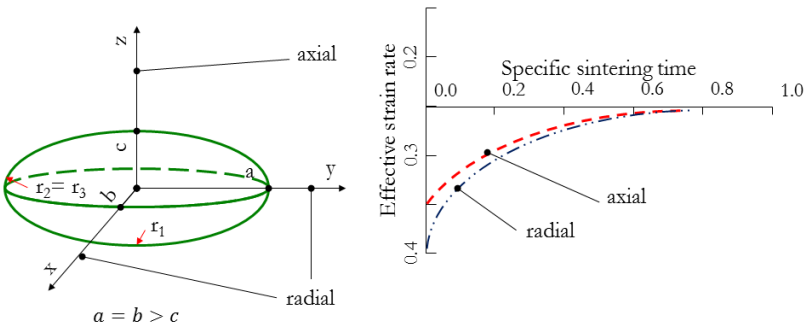

Fig. [1.12] Elliptic pore and effective strain rate.

This behavior is imputable to the Laplace stress which is inversely proportional to the curvature radius, being $r_1 = \frac{a^2}{c}$ higher than $r_2 = r_3 = \frac{a^2}{c}$ it leads to higher stress in the radial direction than in the axial direction that tends to increase the ratio $\frac{c}{a}$ to reach the value of one typical of a sphere. According to Wakai et al. [23] there are three main causes explaining the non-uniformity of the dimensional changes on sintering. The first is the heterogeneity in the structure of powder compact, density gradients for example, that indeed is the cause of shape distortion. The second cause is the presence of an external field of forces as gravity, which may determine an anisotropic shrinkage as studied also by Olevsky and German [24]. The last cause is the anisotropic oriented microstructure due to the arrangement of elongated particles during the compaction process. The theories just mentioned are more suitable for ceramic powders that are not deformed during the compaction step. Zavaliangos et al. [25], simulating a two dimensional array of particles, suggested that deformation of powder particles during powder compaction is the main cause of the anisotropy of the dimensional variations. Axial compaction determines plastic deformation of the powder particles, leading to a different extension of the neck's size, in particular the necks perpendicular to the axial direction have an higher extension than the necks parallel to the axial direction. This difference in the neck size increases on proceeding compaction, resulting in substantially different grain boundary fluxes and therefore in a different shrinkage strain. Molinari et al. [26] developed a theory based on experimental measurement of the effective diffusion coefficient in sintering of ferrous green parts, investigated by dilatometry. According to this theory, since the compaction pressure is higher than the radial one during uniaxial cold compaction, diffusion coefficients result larger along the compaction direction than along the transversal one, and this is highlighted as the main cause to the anisotropy of dimensional change. Under the hypothesis that the enhanced diffusivity is due to the large dislocation density in the particle contact regions, the model has been developed considering that such a high dislocation density is expected to change during isothermal holding, due to recovery and/or recrystallization. This leads to introduction of a time depending diffusion coefficient. A kinetic model has therefore been elaborated, assuming volume diffusion as responsible for mass transport towards the neck region, introducing a time depending effective diffusion coefficient $D_{eff}(t)$. Shrinkage has been measured to be larger along the compaction direction than in the compaction plane, and the volume diffusion coefficient determined by the shrinkage curves has been computed to be definitely higher than that corresponding to an equilibrium concentration of structural defects. The time dependence of the effective diffusion coefficient at different temperatures and along the two directions has been introduced in an equation that can be introduced in the classical model for shrinkage, described by equation [1.3], to include the effect of the anisotropy.

1.4.2 Influence of the anisotropy on the dimensional precision.

The most critical effect of the anisotropy of the dimensional variations is the influence on the dimensional precision of the part. Dimensional variations could be either negative (shrinkage) or positive (swelling), the last possibility is linked to the presence of liquid phase during the sintering step, for example due to the addition of copper.

Cristofolini et al. [27] investigated the dimensional change on sintering and its effect on the dimensional precision of Fe-Cu-C ring-shaped parts produced by powder metallurgy. The liquid phase due to the melting of the copper particles in sintering has an important effect on the observed anisotropy of the dimensional changes. Anisotropy is due both to the larger shrinkage along the compaction direction, which occurs in the early solid phase sintering, and to the smaller swelling along the compaction direction, which is observed in correspondence to the formation and spreading of the liquid phase. The main conclusion is that anisotropy is somehow contrasted by the presence of liquid phase, and it was observed that 2%Cu-0.8%C steel show less anisotropic dimensional change than 3%Cu-0.5%C steel. This phenomenon has been investigated by Corsentino et al. [28], finding that the larger shrinkage along the transversal direction is due to a preferential spreading of the liquid phase between the "weaker" inter-particle contacts parallel to the compaction direction. The presence of copper also contributes to reduce anisotropy of dimensional change due to solid state diffusion at lower temperatures. The effect of the liquid phase on decreasing anisotropy of the dimensional variations was confirmed.

The prediction of the dimensional variations is an important aspect of the design of a PM part. Cristofolini et al. [29] studied the dimensional characteristics of ring-shaped parts produced with Fe–Cu–P alloy. An important achievement has been the introduction of the theoretical isotropic dimensional change defined on the basis of the measured volumetric change.

$$1 + \frac{\Delta V}{V_0} = \left(1 + \frac{\Delta l}{l_0}\right)^3 \qquad \text{Eq. [1.5]}$$

An interesting approach has been applied in order to evaluate the error that can result by implementing a design process considering the dimensional variation, $\frac{\Delta l}{l_0}$, to be isotropic. It has been observed that the anisotropic behavior has a negligible effect on the precision of the height and the internal diameter, whereas the effect on the precision of the external diameter is significant. An anisotropy parameter has been defined as the ratio of the real dimensional variation to the theoretical isotropic variation.

$$R_a = \frac{\Delta R}{R_0} \qquad \text{Eq. [1.6]}$$

R_a is the radial dimensional variation computed as the variation of the thickness of the ring-shaped part.

$$Z_a = \frac{\Delta Z}{Z_0}$$ Eq. [1.7]

Z_a is the dimensional variation of the height.

$$R_i = Z_i = \sqrt[3]{1 + \frac{\Delta V}{V_0}}$$ Eq. [1.8]

Given the theoretical dimensional change, $R_i = Z_i$, the anisotropy parameters have been calculated as $K_R = \frac{R_a}{R_i}$ and $K_Z = \frac{Z_a}{Z_i}$.

These results have been generalized by considering larger volume variations and anisotropy parameters, so the relationships between anisotropy parameters and the attainable ISO tolerance classes have been built as represented in figure [1.13].

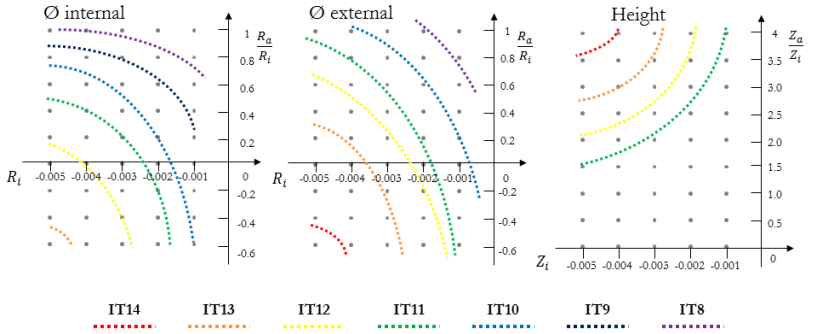

Fig. [1.13] ISO tolerance map for the internal diameter, external diameter and height, as a function of the isotropic radial/axial dimensional change and of the anisotropy parameter.

Concerning height, the design of the green part based on an isotropic dimensional change leads to acceptable precision, even in the case of a pronounced anisotropy, provided that the volume contraction is very small. When the volume contraction is more than 1.5%, the dimensional precision is lost for an anisotropy parameter of approximately 2. Considering the diameters, the isotropic approach for design always fails when the anisotropy parameter becomes negative (it works only for R_i lower than -0.001, corresponding to a volume contraction of 0.3%). In the case of a positive anisotropy parameter, the approach works for any volume contraction that decreases with increasing anisotropy, corresponding to the zones identified by IT9 and IT10 in Figure [1.13]. These conclusions are relevant to the dimensions of the ring reported above, but a calculation of the maps can be performed for any ring-shaped part with a different height or diameter.

This approach has been applied also to a structural part made by low Cr and Mo steel by Cristofolini et al. [30]. This structural part has been sintered at two different temperatures, 1180 °C and 1360 °C. The dimensional and geometrical characteristics were measured both in the green state and in the sintered state by a Coordinate Measuring Machine (CMM), which provides an accurate representation of the surfaces of the part. The part is two-level compacted and it is displayed in figure [1.14].

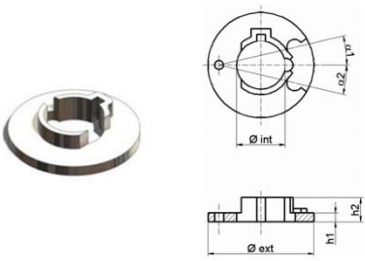

Fig. [1.14] Studied structural part.

The dimensional variations of this part have been measured and they resulted anisotropic at both the sintering temperatures. To evaluate the anisotropy, the anisotropy parameter K has been defined as the ratio between the dimensional variation of the height, $\frac{\Delta h}{h_0}$, over the radial dimensional variation; the radial dimensional variation has been evaluated as the dimensional variation of the ring's wall, $\frac{\Delta t}{t_0}$.

$$K = \frac{\Delta h / h_0}{\Delta t / t_0} \qquad \text{Eq. [1.9]}$$

Cristofolini et al. observed that the increase of the dimensional variation is accompanied to a decrease of the anisotropy parameter K. The results of the isotropic design approach are shown in figure [1.15].

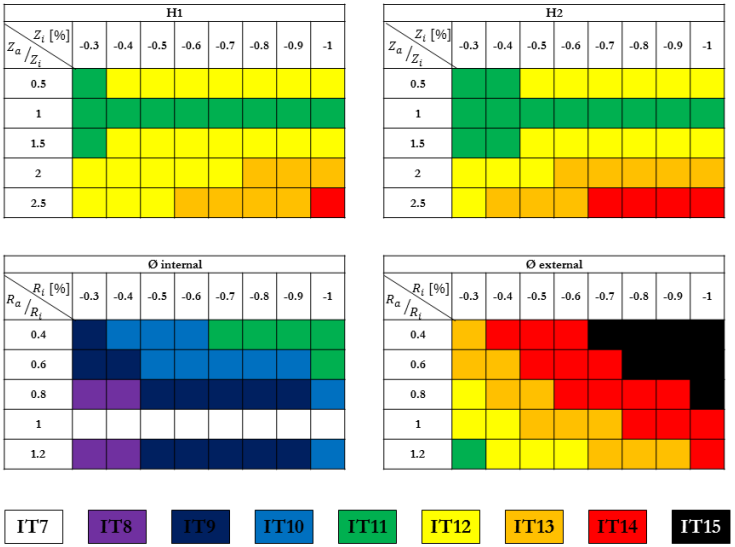

Fig. [1.15] ISO IT tolerance map of heights and diameters as a function of isotropic shrinkage and of the anisotropy coefficient.

With reference to the tolerances commonly related to press-and-sinter process, already discussed, the results in figure [1.15] show that an isotropic design leads to acceptable results for height and for the internal diameter in most cases, while the precision of the external diameter is acceptable in only a few cases.

The influence of the anisotropy on the geometrical precision of the part has also been evaluated after sintering and the same tolerances as those of the green compact were kept. This aspect is very important if the sintering process is pushed to higher temperatures in order to achieve better mechanical properties.

1.5 Scope of this work.

The anisotropy of dimensional variation is a very complex issue. This phenomenon is strongly related to the densification during sintering, which is in turn influenced by several parameters belonging to all the three main sequences on press and sinter process (powder, compaction, sintering, figure [1.11]). According to the literature examined in this work, there are two main approaches to describe this phenomenon. The first is micro-modeling, and investigates the mechanisms that are involved in the

sintering stage. This leads to the development of several models which can be used to predict the dimensional variations mainly in the micro-scale and they are still not completely satisfactory for the prediction of dimensional variations in complex parts. The second approach is related to the measure of the effect of this phenomenon on the dimensions of the object. This is more focused on the industrial application and has the aim to provide the designer with robust design models and procedures in order to improve the quality of the process, which are based on strong correlations experimentally obtained. The purpose of this Ph.D. work is to develop a predictive model for the anisotropy of dimensional variation, studying the influence of the geometry on the anisotropy of the dimensional variations using a sampling of axi-symmetric geometries. The anisotropy coefficient as the parameter for the evaluation of the anisotropy has been introduced in several works in literature, examples are given by Cristofolini [29 and 30] and Zavaliangos [25]. In this work a new anisotropy coefficient will be introduced on the basis of some concepts that concern the measure of the dimensional variations. The experimental data obtained from the measurements will be used to build a correlation between the anisotropy, the process parameters and the geometry. A model to predict the amount of anisotropy will be based on the experimental correlations and will be implemented in a procedure developed to predict the dimensional variations of complex parts. This model will be tested and its reliability will be evaluated using a Monte Carlo method based on the procedure. The aim of this model is to enhance the dimensional precision of sintered components.

This work is subdivided as follows:

- Analysis of the dimensional variation of an axi-symmetric part.
- Definition of an anisotropy parameter to quantify the anisotropy.
- Measurement of the dimensional variation of several geometries.
- Correlation between the anisotropy and the geometry.
- Development of a predictive model.
- Development of a design procedure.
- Validation of the predictive design procedure on complex sintered parts.

1.6 References.

1. Schatt, Werner and Wieters, Klaus-Peter Powder metallurgy : processing and materials. (1997) European Powder Metallurgy Association, Shrewsbury, U.K.
2. ASSINTER - Guida alla progettazione dei componenti sinterizzati - (technical gudelines from the Italian society of PM parts producers)
3. S.F. Burch, A.C.F. Cocks, J.M. Prado and J.H. Tweed, Die Fill and Powder Transfer, Modelling of Powder Die Compaction, (2008) Editors: P. R. Brewin, O. Coube PhD, P. Doremus PhD, J. H. Tweed PhD,Springer, pp 131 - 150

4. J. Chakrabarty, Theory of Plasticity, (2006) 3rd ed. Elsevier Butterworth-Heinemann
5. A.C.F. Cocks - Mechanics of Powder Compaction - Modelling of Powder Die Compaction 3rd ed. Elsevier Butterworth-Heinemann, (2008) Editors: P. R. Brewin, O. Coube PhD, P. Doremus PhD, J. H. Tweed PhD, Springer, pp 31 - 42
6. F. Thummler; R. Oberacker, An Introduction to Powder Metallurgy, (1993), London : The Institute of Materials
7. R.M. German - Introduction to Liquid Phase Sintering, (1985), Springer Science + Business Media LLC
8. Suk-Joong L.Kang, Sintering. Densification,Grain Growth and Microstructure, (2005), 1st ed. Elsevier Butterworth-Heinemann
9. H.E. Exner; G. Petzow, A critical evaluation of shrinkage equations, Proceedings of the fifth international conference on sintering and related phenomena, (1980), Material Science Research: 13, Plenum Press G. C. Kuczynsky Editor
10. Eugene A. Olevsky, Theory of sintering: from discrete to continuum, Materials Science and Engineering R23 (1998) pp 41- 100
11. Suk Hwan Chung; Young-Sam Kwon; Seong Jin Par; Randall M. German, Modeling and Simulation of Press and Sinter Powder Metallurgy, ASM Handbook 22B (2010) pp 323 - 324
12. Eugene A. Olevsky; Veena Tikare; Michael V. Braginsky, Combined macro-meso scale modeling of sintering. Part II: mesoscale simulations, NATO SCIENCE SERIES SUB SERIES III COMPUTER AND SYSTEMS SCIENCES; 176; (2001) pp 94 - 104; Advanced research workshop on recent developments in computer modeling of powder metallury processes; Multiscale computational methods in chemistry and physics by Ohmsha, IOS Press
13. Eugene A. Olevsky; Veena Tikare, Combined macro-meso scale modeling of sintering. Part I: continuum approach, NATO SCIENCE SERIES SUB SERIES III COMPUTER AND SYSTEMS SCIENCES; 176; (2001) pp 85 - 93; Advanced research workshop on recent developments in computer modeling of powder metallury processes; Multiscale computational methods in chemistry and physics by Ohmsha, IOS Press
14. Michael Braginsky; Veena Tikare; Eugene Olevsky, Numerical simulation of solid state sintering, International Journal of Solids and Structures 42, 2, (2004) pp 621 - 636
15. Randall M. German, Sintering: From Empirical Observations to Scientific Principles (2014) 1st ed. Elsevier Butterworth-Heinemann
16. UNI EN 20286-1:1995, ISO 286/1
17. Randall M. German, European Powder Metallurgy Association, Green body homogeneity effects on sintered toerances - Powder Metallurgy 47 Euro PM2004 Shrewsbury (2004), pp 495 - 500
18. G.F. Bocchini, Influence of process parameters on precision of PM parts, Powder Metallurgy 28 (1985) pp 155 - 165

19. H. Rapp; P. Beiss; T. Hoster; K.H. Lindner - Dimensional stability of iron-copper steel - Metal Powder Report 46, 3, (1991) pp 25 - 29
20. H.A. Al-Qureshi; A. Galiotto; A.N. Klein - On the mechanics of cold die compaction for powder metallurgy - J. Mater. Process. Technol. 166, 1, (2005) pp 135 - 143
21. B.A. Druyanov; R.I. Nepershin, Problems of Technological Plasticity (1994) Studies in Applied Mechanics, Elsevrier
22. E.A. Olevsky; V. Skorokhod, Deformation aspects of anisotropic-porous bodies sintering, La Societe Francaise de Metallurgie et de Materiaux in JOURNAL DE PHYSIQUE (1993) 4; 3, 7//v1; C7-739-C7-742; Euromat 93
23. Fumihiro Wakai; Kentarou Chihara; Michiyuki Yoshida, Anisotropic shrinkage induced by particle rearrangement in sintering, Acta Materialia 55, 13 (2007) pp 4553 - 4566
24. E.A. Olevsky; R.M. German, Effect of gravity on dimensional change during sintering - I. shrinkage anisotropy, Acta Materialia 48, 5, (2000) pp 1153 - 1166
25. Zavaliangos; J.M. Missiaen; D. Bouvard, Anisotropy in Shrinkage During Sintering, Science of Sintering 38, 1, (2006) pp 13 -26
26. Molinari; C. Menapace; E. Torresani; I. Cristofolini; M. Larsson, A study of sintering shrinkage kinetics of cold compacted ferrous green parts Metal Powder Industries Federation in ADVANCES IN POWDER METALLURGY AND PARTICULATE MATERIALS; 1; 05-25-05-32; Powder metallurgy & particulate materials (2013)
27. Cristofolini; M. Pilla; A. Molinari; C. Menapace; M. Larsson, DOE investigation of anisotropic dimensional change during sintering of Iron-Copper-Carbon INTERNATIONAL JOURNAL OF POWDER METALLURGY; 48, 4; (2013) pp 33 - 44
28. N. Corsentino; I. Cristofolini; S. Libardi; A. Molinari - Effect of high sintering temperature on the dimensional and geometrical precision of PM Cr-Mo steel parts - Proceeding EURO PM2014 Congress & Exhibition (2014)
29. Cristofolini; C. Menapace; M. Cazzolli; A. Rao; W. Pahl; A. Molinari - The effect of anisotropic dimensional change on the precision of steel parts produced by powder metallurgy - Journal of Materials Processing Technology 212, 7 (2012) pp 1513 - 1519
30. I. Cristofolini; F. Selber; C.Menapace; M. Pilla; A. Molinari; S. Libardi - Anisotropy of Dimensional Variation and its Effect on Precision of Sintered Parts - Proceedings EURO PM2012 Congress & Exhibition 1 (2012)

Chapter 2

Materials and methods

2.1 Sampling.

This work has been developed following two main paths to understand the influence of geometry on the anisotropy of the dimensional change and to provide a tool to be implemented in a design procedure. The first part of this work has been focused on the relation between geometry and anisotropy by investigating the dimensional variation of specific basic geometries in order to build a model, where the relation between anisotropy and geometry can be generalized and used for any given component. To investigate the influence of geometry on the anisotropy of the dimensional variation a set of axi-symmetric geometries has been chosen, in particular the rings and disks shown in figure [2.1].

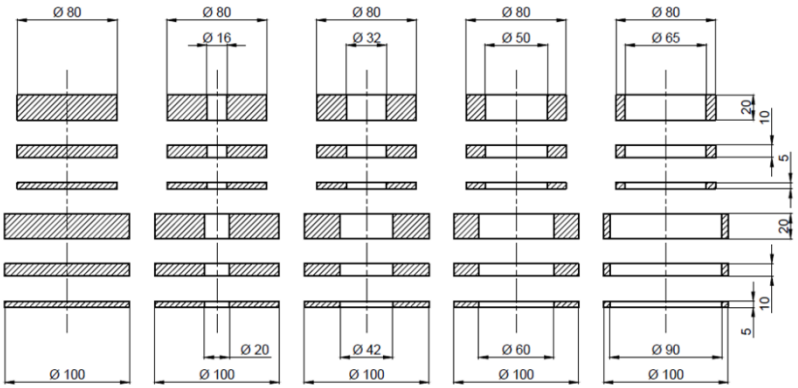

Fig. [2.1] Sampling of compacted iron powder, nominal dimensions are reported.

In figure [2.1] six different disks and twenty four different rings are shown. The sampling, provided by Höganäs AB Sweden, has been chosen to represent a wide domain of feasible sizes commonly used in the press and sinter industry.

The second part of the work has been focused on the validation of the model proposed in the first part by applying the relevant design procedure on four mechanical components produced by press and sinter technology.

The four cases of study, provided by TFM s.p.a., are presented in figure [2.2] and they will be discussed in detail in chapter five along with the procedure to validate the model.

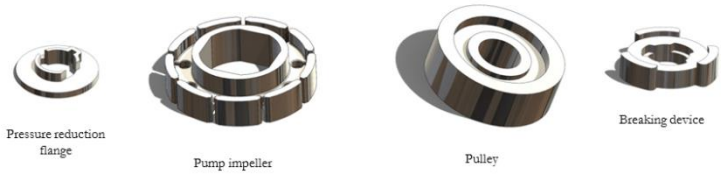

Fig. [2.2] Structural parts for the model validation. Courtesy of TFM s.p.a.

The material used for the first part is water atomized pure iron powder produced by Höganäs AB[1] , commercially identified by ASC 100.29. Pure iron powder has been chosen for two main reasons. First reason is chemical composition, which allows avoiding any liquid phase formation during sintering or uncontrolled volume change expected for phase transition different from ferrite-austenite reaction (German [2]). Second reason is related to the industrial use, being the majority of the press and sinter powders based on iron alloys according to Shatt and Witers [3]. All the geometries have been compacted up to green density of 6.7 g/cm³. The sintering process has been carried out using two standard industrial furnaces. For the 1120°C conventional sintering temperature (Shatt and Witers [3]) a belt furnace has been used, with a low carbon potential atmosphere to minimize the carbon intake. For the other two sintering temperatures (1220 °C and 1280 °C) a batch furnace has been used. Sintering operations in the batch furnace have been carried out in vacuum with $95\%N_2/5\%H_2$ backfill. The operative conditions such as the heating rate, the sintering time (isothermal sintering) and the cooling rate have been kept constant for all the three processes. Five samples each geometry have been sintered at each temperature in order to have a reasonable consistency of the measured value. The sintering conditions are summarized in table [2.1].

Sintering temperature [°C]	Heating rate [°C/min]	Sintering time [min]	Sintering atmosphere	Cooling rate [°C/min]
1120	5	30	Carbon low potential	5
1220	5	30	Vacuum + N_2 backfill	5
1280	5	30	Vacuum + N_2 backfill	5

Tab. [2.1] Sintering conditions.

The experimental campaign has been conducted on thirty different geometries, sintered at three different temperatures, leading to a total of ninety different experimental conditions. The main part of the experimental work has been focused on the measurement of the samples. Each sample has been carefully labeled to be recognizable among the others, therefore every sample has been tracked through all the process from compaction to sintering. Each specimen has been measured before and after sintering. The dimensional variations of height and diameters have been calculated as the variation between the corresponding dimension in the green sample and in the same specimen as sintered. The definition of dimensional variation and the formal equations will be detailed in chapter three.

2.2 Measurement.

The measurement has been carried out using a tri-dimensional Coordinate Measuring Machine (CMM).

2.2.1 Equipment.

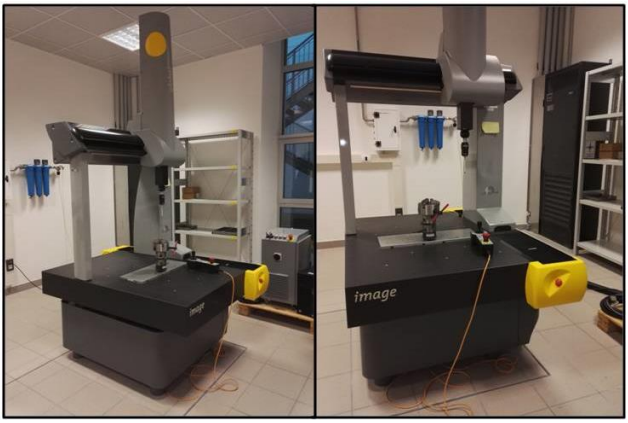

Figure [2.3] C.M.M.

The equipment presented in figure [2.3] is a DEA Global image 07-07-07 Coordinate Measuring Machine (in this work it will be referred as its acronym C.M.M, which allows acquiring the samples' surfaces, and obtaining the dimensional features of the scanned geometry. The surfaces of the specimens are acquired in continuous scan mode (accuracy 3.4/120 μm/s according to ISO 10360-4 [4], giving the scanning probe error referred to a well defined scan path, performed over 120 s). This C.M.M. has a measurement volume of a cube, the side of which is 700 mm, where the probe can move approaching the specimen to be measured. The path can be optimized thanks to its three degrees of freedom in translation, and two in rotation. An example of sample measurement is shown in figure [2.4].

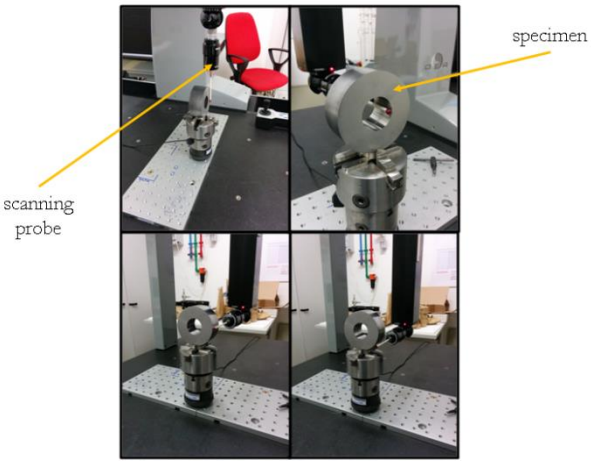

Figure [2.4] Sample measurement in the CMM.

2.2.2 Measurement Procedure.

Both the iron samples and the mechanical components have been measured using a specific measurement procedure, giving the information for the path of the scanning probe on the sample's surface. Due to the differences in size and feature, the measurement procedure has been tailored to fit the specific geometry of each sample, keeping as consistent as possible the quantity of information and therefore the accuracy of the measurement. The measurement procedure is schematically shown in figure [2.5].

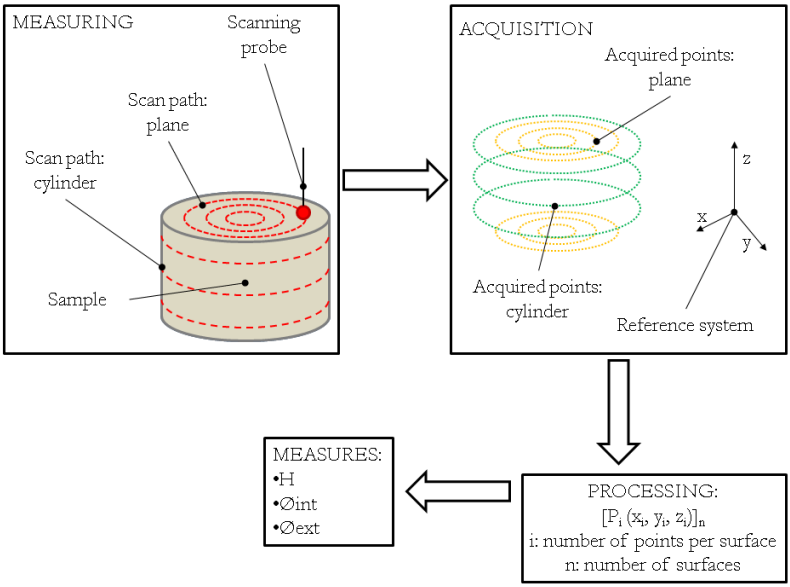

Fig. [2.5] Measurement procedure.

As mentioned before, the scanning probe moves contacting the sample's surface, and acquires a certain quantity of points. The number of the points that are recorded by the probe is related to a sampling frequency that has been set up to five points per millimeter. The scanning probe is controlled by the machine's electronics which has been programmed in advance. The specific path of the scanning probe has been chosen circular according with the axi-symmetric feature of the parts.

Particular attention has been dedicated to the clamping of the sample within the measurement volume of the machine. The clamping of the specimens has two main issues. First problem is related to the mechanical strength of the green samples, since the strength is due basically to slight adhesion forces and to micro cold welding, the sample has to be carefully handled. The touching pressure of the probe has been set to 0.1 Newton, so the specimen does not move when in contact with the probe and its position is maintained invariant during all the measurement. Second issue deals with the clamping system that has to keep the sample safe and still in the same position. The presence of the clamping system can represent a consistent obstacle to the probe movements. Moreover, there is a shadowing effect of the clamping system so some portions of the sample's surface cannot be reached by the probe and therefore not acquired. In figure [2.6] an example of the solution adopted. The clamping system acts with a force in the compacting direction, which is the direction along which the green

sample offers the highest strength since it has been compacted up to 700 MPa. In this way both the integrity and the stability of the green sample are preserved during measurement.

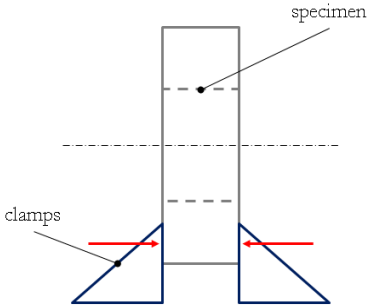

Fig. [2.6] Schematic representation of the clamping system.

This solution has been optimized to minimize the shadow effect of the clamping system. Same solution has been adopted both for the iron specimens having a simple geometry and for the structural parts.

The control algorithm has been implemented using the PC-Dmis software by Hexagon Metrology. Basically the control algorithm has been programmed to execute the following operations:

- Define the machine parameters (movement speed, wrist rotation, scanning parameters)
- Define the movement sequence (approach distance to the sample)
- Define the alignment (defining the Cartesian reference system)
- Define the scanning sequence (path)
- Define the post processing operations on the acquired points

Particular attention has been paid to the alignment procedure, that is the definition of the Datum system, to which refer every acquired point. Each part has been measured with a specific self-alignment, in particular z-axis has been aligned with the external cylinder's axis, which is more reliable (its precision is related to the rigid die's precision), the x-y plane has been aligned with the upper plane of the part. Being the parts axi-symmetric, the alignment procedure does not need a third alignment. With this alignment strategy the measurement does not depend on the positioning of the part. The scansion sequence has been defined differently for planes and cylinders. The scanning path on the plane surfaces has been defined by circles with a radius ranging between the external and the internal one of the specimen. Two or more circular paths

have been scanned, depending on the thickness of the specimen. The cylindrical surface has been scan by circular paths, open for the external cylinder to avoid the clamps. The cylinder has been scanned on three or more levels (depending on the height) in order to appreciate any distortion effect, either due to the springback or to the gravity (Olevsky et al. [5]).

2.2.3 Post processing.

The acquired points of sample are reported in figure [2.7].

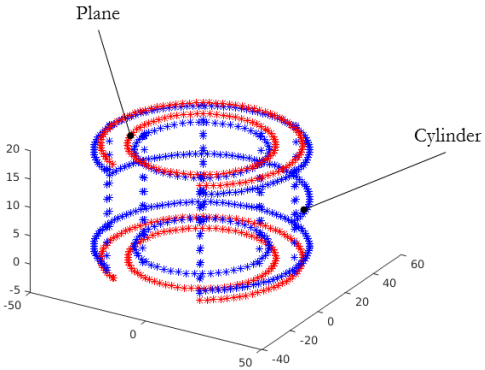

Figure [2.7] Acquired points derived from the measurement of a Øext 80 mm, Øint 50 H 20 mm specimen.

In figure [2.7] the shadowing effect due to the presence of the clamps is clearly visible, showing that the part has not been scanned along a small sector of the external surface. Despite this effect the quantity of processed points is sufficient to have a coherent representation of the external surface. The acquired points have been processed in order to build the best fitting surface using the least square method. The built surfaces are basically planes and cylinders, as reported in figure [2.8].

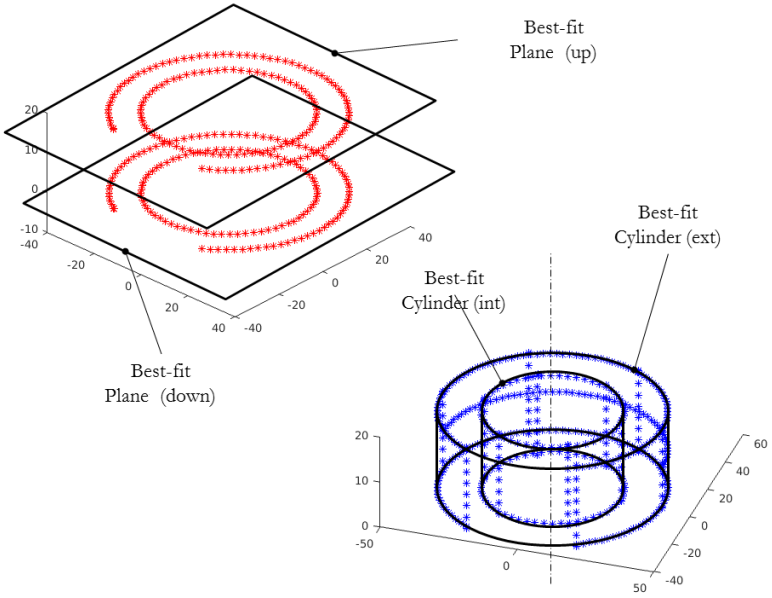

Figure [2.8] Best fit surfaces on the acquired points.

The dimensions derived from the processed points are the diameters (internal and external) and the height of the ring. The diameter is the best fit cylinder's diameter and the height is the distance between two best fit planes. An example is given in figure [2.9].

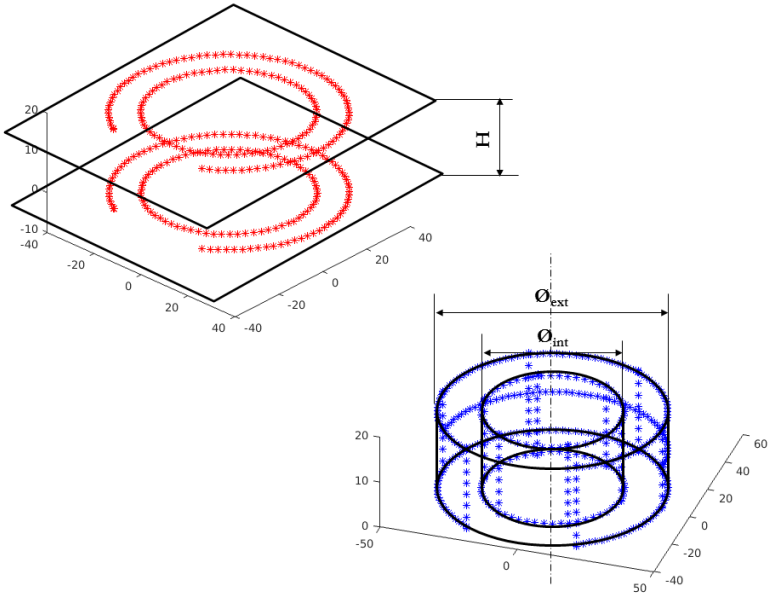

Figure [2.9] Sample dimensions.

2.3 References.

1. Hoganas, ASC100.29 iron powder technical datasheet
2. R. M. German - Introduction to Liquid Phase Sintering, (1985), Springer Science + Business Media LLC
3. Schatt, Werner and Wieters, Klaus-Peter Powder metallurgy : processing and materials. (1997) European Powder Metallurgy Association, Shrewsbury, U.K.
4. ISO 10360 – 4: (2000) Geometrical Product Specifications (GPS) -- Acceptance and reverification tests for coordinate measuring machines (CMM) -- Part 4: CMMs used in scanning measuring mode
5. E.A. Olevsky; R.M. German, Effect of gravity on dimensional change during sintering : I. shrinkage anisotropy, Acta Materialia 48, 5, (2000) pp 1153 - 1166

Chapter 3

3.1 Dimensional variations in axi-symmetric geometry.

Recalling the definition already given in chapter one, the dimensional variation due to the densification mechanism occurred during the sintering process is significantly different if measured along two independent directions. The first step is the definition of the dimensional variation. In powder metallurgy the dimensional variation $\frac{\Delta l}{l_0}$ occurred during the sintering process is described using the kinetic models (Exner and Petzow [1]) based on the shrinkage in the isothermal sintering step.

$$\frac{\Delta l}{l_0} = kt^n \qquad \text{Eq. [1.3]}$$

Nevertheless, this study will be focused on the dimensional changes as a result of the whole process, as given by the relationship of the measured dimensions of the sintered and the green part, so that the kinetic model will not be further investigated

For a generic cubic system, represented in figure [3.1] the general definition of dimensional variation in the three independent directions x, y and z, is described by the following equations.

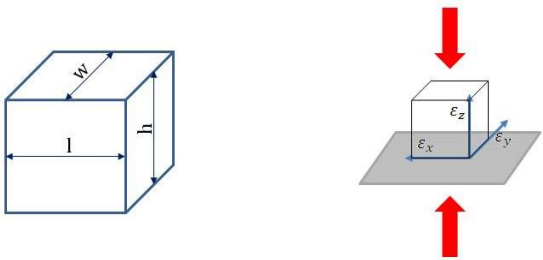

Figure [3.1] Elementary cubic system.

$$\varepsilon_x = \frac{[l]_s - [l]_g}{[l]_g}$$ Eq. [3.1]

$$\varepsilon_y = \frac{[w]_s - [w]_g}{[w]_g}$$ Eq. [3.2]

$$\varepsilon_z = \frac{[h]_s - [h]_g}{[h]_g}$$ Eq. [3.3]

$$\varepsilon_V = \frac{[V]_s - [vV]_g}{[V]_g}$$ Eq. [3.4]

Where the notation s stands for sintered and g stands for green. The volumetric variation, ε_V, is the parameter directly related to the densification ($\Delta\rho$), under the assumption that the mass of the metal remains constant.

$$\Delta\rho = \frac{[\rho]_s - [\rho]_g}{[\rho]_g} = \frac{1}{\varepsilon_V + 1} - 1$$ Eq. [3.5]

Usually solid state sintering is characterized by an increase of density and therefore the volumetric change results negative (Suk-Joong L.Kang [2]). As mentioned in chapter one, the density in the green compact is not homogeneously distributed and this affects the dimensional variations according to German [3]. Despite this implication, in this work the dimensional variation will be computed on the dimensions directly measured on the part and the computation will be referred to their mean value. In figure [3.2] a ring-shaped axi-symmetric geometry is represented, which is the most suitable geometry for rigid die powder compaction.

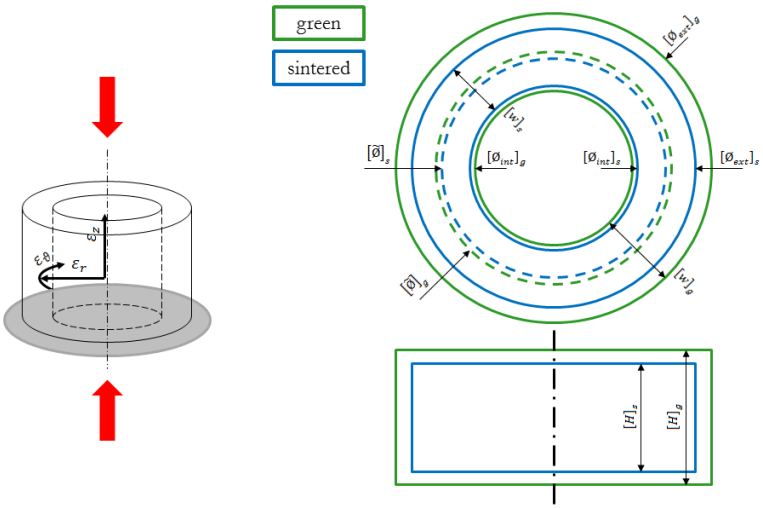

Figure [3.2] Generic ring, axi-symmetric geometry.

$$\varepsilon_\vartheta = \frac{[\bar{\phi}]_s - [\bar{\phi}]_g}{[\bar{\phi}]_g} \qquad \text{Eq. [3.6]}$$

$$\varepsilon_r = \frac{[t]_s - [t]_g}{[t]_g} \qquad \text{Eq. [3.7]}$$

$$\varepsilon_z = \frac{[h]_s - [h]_g}{[h]_g} \qquad \text{Eq. [3.8]}$$

$$\varepsilon_V = \frac{[V]_s - [V]_g}{[V]_g} \qquad \text{Eq. [3.9]}$$

Where $\bar{\phi}$ is the mean diameter

$$\bar{\phi} = \frac{\phi_{ext}+\phi_{int}}{2}$$ Eq. [3.10]

and t is the wall thickness

$$t = \frac{\phi_{ext}-\phi_{int}}{2}$$ Eq. [3.11]

The relations just defined are the starting point to develop the model that describes the anisotropy of the dimensional changes based on the dimensions of the part.

3.2 Anisotropy of dimensional variations.

For the axi-symmetric geometry the three independent directions correspond to the cylindrical coordinates ϑ, r, and z. According to the compaction mechanics (Cocks [4]) in a generic axi-symmetric geometry the compaction direction is z and the compaction plane is defined by the $\overline{r\vartheta}$ plane. In literature, as already mentioned in chapter one, the anisotropy of the dimensional variation during sintering has been evaluated basically as the ratio between the dimensional variations measured in two independent direction, usually the compaction direction versus one direction laying on the compaction plane. As examples, the anisotropy parameters defined by Cannon et al. [5] (equation [3.12]) and Cristofolini et al. [6] [7] (equations [3.13], [3.14] and [1.8]), are reported.

$$K_A = 100\left(1 - \frac{\varepsilon_x}{\varepsilon_y}\right)$$ Eq. [3.12]

$$K_R = \frac{R_a}{R_i}$$ Eq. [3.13]

$$K_Z = \frac{Z_a}{Z_i}$$ Eq. [3.14]

$$K = \frac{\Delta h/h_0}{\Delta t/t_0}$$ Eq. [1.8]

The information given in form of ratio is rather limiting and not satisfactory, since when only the ratio is known the problem can't be solved in a closed form, in other words it is impossible to know the value of each single dimensional variation.

In this work the main idea is to build a tool for macro modeling, which is able to estimate the dimensional variations in all the independent directions of any given axi-symmetric geometry. In order to provide the minimum amount of information for the modeling, a new analytical description of anisotropy has been implemented. This analytical description is based on some basic assumptions, giving the boundary conditions in order to solve the dimensional problem in closed form. The first assumption is the absence of shape distortion, so the volume of the ring can always be computed by the measured dimensions (ϕ_{ext}, ϕ_{int}, H).

$$V = \pi \bar{\phi} t H$$ Eq. [3.15]

The volumetric variation can be therefore written as a function of the dimensional variations measured in the three directions.

$$\varepsilon_V = \frac{[V]_s - [V]_g}{[V]_g} = (\varepsilon_\vartheta + 1)(\varepsilon_r + 1)(\varepsilon_z + 1) - 1$$ Eq. [3.16]

The second assumption is related to the definition of an isotropic dimensional variation, which verifies for example on sintering cold isostatic compacted samples (Exner and Petzow [1]). The isotropic dimensional variation corresponds to the dimensional variation measured in any direction, as by equation [3.18].

$$\varepsilon_i = \varepsilon_\vartheta = \varepsilon_r = \varepsilon_z$$ Eq. [3.17]

ε_i can be written as function of the volume, as by the definition presented in chapter one in equation [1.5].

$$(\varepsilon_i + 1)^3 = \varepsilon_V + 1 \text{ con } \varepsilon_i = \varepsilon_\vartheta = \varepsilon_r = \varepsilon_z \qquad \text{Eq. [3.18]}$$

$$\varepsilon_i = \sqrt[3]{(\varepsilon_V + 1)} - 1 \qquad \text{Eq. [3.19]}$$

From equations [3.19] and [3.16], the following equalities can be written:

$$(\varepsilon_i + 1)^3 = (\varepsilon_\vartheta + 1)(\varepsilon_r + 1)(\varepsilon_z + 1) \qquad \text{Eq. [3.20]}$$

$$\sqrt{\frac{(\varepsilon_i+1)^3}{(\varepsilon_z+1)}} = \sqrt{(\varepsilon_\vartheta + 1)(\varepsilon_r + 1)} \qquad \text{Eq. [3.21]}$$

In case of isotropy ($\varepsilon_i = \varepsilon_\vartheta = \varepsilon_r = \varepsilon_z$) the equality [3.20] becomes a tautology.

$$(\varepsilon_i + 1) = (\varepsilon_i + 1) \qquad \text{Eq. [3.22]}$$

Equation [21] represents the relationships between the dimensional change in the compaction direction (on the left) and the dimensional change in the compaction plane (on the right). Plotting these entities on the graph in figure [3.3], the value in abscissa represent the right terms of the equation [3.21] and [3.22], and the terms in ordinate are the left terms of the equation [3.21] and [3.22]. The points relevant the different dimensional changes will lie on the bisector line, and the far they will be from the point relevant to the isotropic dimensional changes, the larger the anisotropy of dimensional changes.

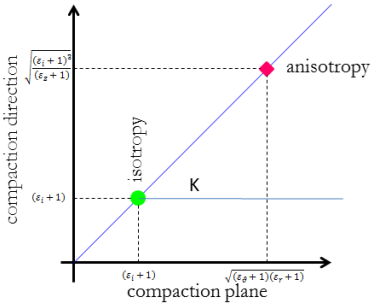

Figure [3.3] Graphical description of anisotropy.

The graphical description of anisotropy in figure [3.3] describes a general anisotropic situation (red square), as by the equation [3.21], compared to the isotropic dimensional variations (green circle), as by the equation [3.22]. An anisotropy parameter K' is consequently defined as the difference between the coordinates representing the anisotropic dimensional variation and the isotropic one, as by equation [24]

$$K' = \sqrt{(\varepsilon_\vartheta + 1)(\varepsilon_r + 1)} - (\varepsilon_i + 1) \qquad \text{Eq. [3.23]}$$

The parameter K' is zero in condition of isotropy.

The parameter K' is then divided by the parameter ε_i.

$$K = \frac{K'}{\varepsilon_i} = \frac{\sqrt{(\varepsilon_\vartheta+1)(\varepsilon_r+1)}-(\varepsilon_i+1)}{\varepsilon_i} \qquad \text{Eq. [3.24]}$$

The coefficient K represents the magnitude of anisotropy and the higher is the value of K, the higher is the anisotropy. Under the hypothesys that the dimensional variation in the compaction plane is independent with respect to the direction Cristofolini et al. [6], therefore $\varepsilon_\vartheta = \varepsilon_r$. Given this relation the anisotropy coefficient can be written simply as by equation [3.25].

$$K = \frac{\varepsilon_r - \varepsilon_i}{\varepsilon_i} \qquad \text{Eq. [3.25]}$$

The parameter ε_i, by definition, is directly related to the change in volume, which is mainly affected by to the material and the production process. Both the influence of geometry, through ε_r, and the influence of the material and production process, through ε_i, are thus represented in the anisotropy parameter K. Nevertheless, up to now the dimensional variations have been defined on the basis of parameters as the mean diameter and the thickness, which are never used by the designers. Dimensional variations are thus more usefully defined considering the inner and the outer diameters of the ring-shaped samples (ϕ_{ext}, ϕ_{int}) , as by equations [3.26] and[3.27].

$$\varepsilon_{\phi_{int}} = \frac{[\phi_{int}]_s - [\phi_{int}]_g}{[\phi_{int}]_g} \qquad \text{Eq. [3.26]}$$

$$\varepsilon_{\phi_{ext}} = \frac{[\phi_{ext}]_s - [\phi_{ext}]_g}{[\phi_{ext}]_g} \qquad \text{Eq. [3.27]}$$

Introducing the geometrical parameter $R = \frac{[\phi_{int}]_g}{[\phi_{ext}]_g}$, the dimensional variations ε_ϑ and ε_r and the volumetric variation can be written as functions of $\varepsilon_{\phi_{int}}$ and $\varepsilon_{\phi_{ext}}$.

$$\varepsilon_\vartheta = \frac{(\varepsilon_{\phi_{ext}}+1)+R\left(\varepsilon_{\phi_{int}}+1\right)}{(1+R)} - 1 \qquad \text{Eq. [3.28]}$$

$$\varepsilon_r = \frac{(\varepsilon_{\phi_{ext}}+1)-R\left(\varepsilon_{\phi_{int}}+1\right)}{(1-R)} - 1 \qquad \text{Eq. [3.29]}$$

$$\varepsilon_V = \frac{(\varepsilon_{\phi_{ext}}+1)^2 - R^2\left(\varepsilon_{\phi_{int}}+1\right)^2}{(1-R^2)}(\varepsilon_z + 1) - 1 \qquad \text{Eq. [3.30]}$$

Consequently, the anisotropy coefficient in represented by equation [3.31].

$$K = \frac{\sqrt{\frac{\left(\varepsilon_{\phi_{ext}}+1\right)^2 - R^2\left(\varepsilon_{\phi_{int}}+1\right)^2}{(1-R^2)}} - (\varepsilon_i+1)}{\varepsilon_i} \qquad \text{Eq. [3.31]}$$

Assuming $\varepsilon_\vartheta = \varepsilon_r$ the equality $\varepsilon_{\phi_{int}} = \varepsilon_{\phi_{ext}}$ is necessarily true, so the anisotropy coefficient can be again simplified.

$$K = \frac{\varepsilon_{\phi_{ext}} - \varepsilon_i}{\varepsilon_i} \qquad \text{Eq. [3.32]}$$

The coefficient K can be represented in the same graphical way as it is shown in figure [3.4].

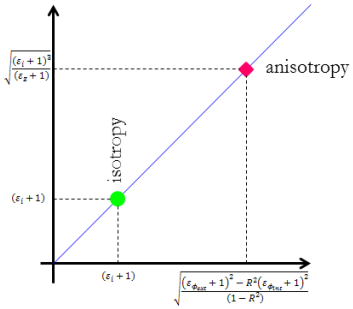

Figure [3.4] Graphical and analytic description of anisotropy.

In this chapter the anisotropy of the dimensional variations has been described using dimensional variations that can be directly measured on ring-shaped parts, see equations [3.8], [3.26], and [3.27]. The parameter ε_i defined as the isotropic dimensional variation is directly related to the densification since it has been defined through the volume variation by equation [3.19].

The anisotropy coefficient K defined by equation [3.31] takes into account both the influence of the geometry (through $\varepsilon_{\phi_{int}}$, $\varepsilon_{\phi_{ext}}$,and R) and the influence of the material and process parameters (through ε_i), so that it can be used as a tool in a design procedure, which aims at considering the anisotropic dimensional variation on sintering, as it will be discussed in the next chapter.

3.3 References

1. H.E. Exner; G. Petzow, A critical evaluation of shrinkage equations, Proceedings of the fifth international conference on sintering and related phenomena, (1980), Material Science Research: 13, Plenum Press G. C. Kuczynsky Editor
2. Suk-Joong L.Kang, Sintering. Densification,Grain Growth and Microstructure, (2005), 1st ed. Elsevier Butterworth-Heinemann
3. Randall M. German, European Powder Metallurgy Association, Green body homogeneity effects on sintered toerances - Powder Metallurgy 47 Euro PM2004 Shrewsbury (2004), pp 495 - 500
4. A.C.F. Cocks - Mechanics of Powder Compaction - Modelling of Powder Die Compaction 3rd ed. Elsevier Butterworth-Heinemann, (2008) Editors: P. R. Brewin, O. Coube PhD, P. Doremus PhD, J. H. Tweed PhD, Springer, pp 31 - 42
5. W. Roger Cannon; P. Markondeya Raj, Evolution of Sintering Anisotropy Using a 2D Finite Difference Method Journal of the American Ceramic Society; 92, 7 (2009) pp 1391 - 1395
6. I. Cristofolini; M. Pilla; A. Molinari; C. Menapace; M. Larsson, DOE investigation of anisotropic dimensional change during sintering of Iron-Copper-Carbon INTERNATIONAL JOURNAL OF POWDER METALLURGY; 48, 4; (2013) pp 33 – 44
7. I. Cristofolini; F. Selber; C.Menapace; M. Pilla; A. Molinari; S. Libardi - Anisotropy of Dimensional Variation and its Effect on Precision of Sintered Parts - Proceedings EURO PM2012 Congress & Exhibition 1 (2012)

Chapter 4

Results.

4.1 Dimensional variations.

The analysis of the measured data allows to describe the correlation between the dimensional variations, the geometry, and the process parameters. In this first part the dimensional variations have been processed in order to describe the mean dimensional variation associated with the geometry and the temperature of sintering, as a specific process parameter. The iron disks and rings have been measured using the procedure described in chapter two. For each geometry the mean dimensional changes ($\varepsilon_{\emptyset int}$, $\varepsilon_{\emptyset ext}$, ε_z) have been computed on five specimens using the definitions given in equations [3.7], [3.26] and [3.27] in chapter three. As explained in chapter two, the measured dimensions came from the best fit analysis of a large quantity of points collected on the sample's surfaces. As highlighted in chapter three, according to the hypothesis of no distortions occurring, in this work the analyzed geometries will be considered ideal and therefore their volume can be computed using the mean measured dimensions. On this basis, the mean volumetric variation ε_V has been computed for each geometry. Using the definition given in equation [3.19] the isotropic dimensional variation ε_i has been computed.
From figure [4.1] to figure [4.9] all the mean dimensional variations and scatter bands are reported along with the computed isotropic dimensional variation.

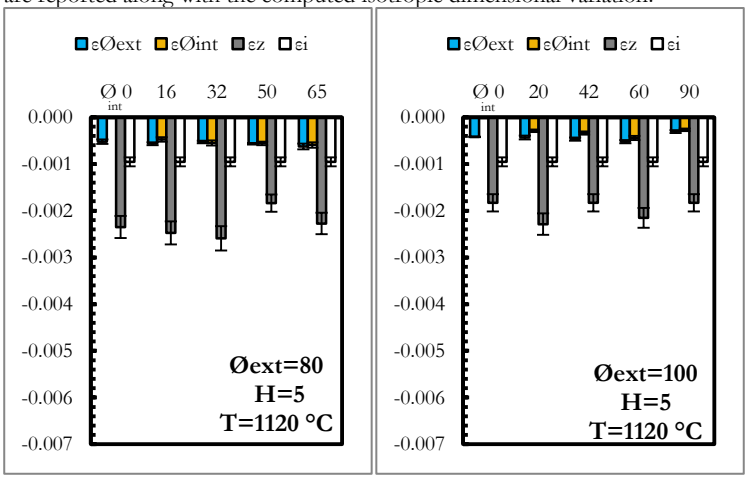

Fig. [4.1] Dimensional variations of the samples having the height of 5 mm, sintered at 1120 °C.

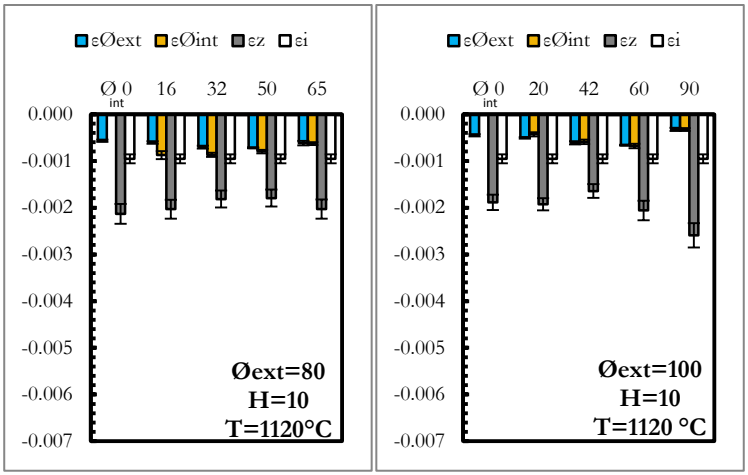

Fig. [4.2] Dimensional variations of the samples having the height of 10 mm, sintered at 1120 °C.

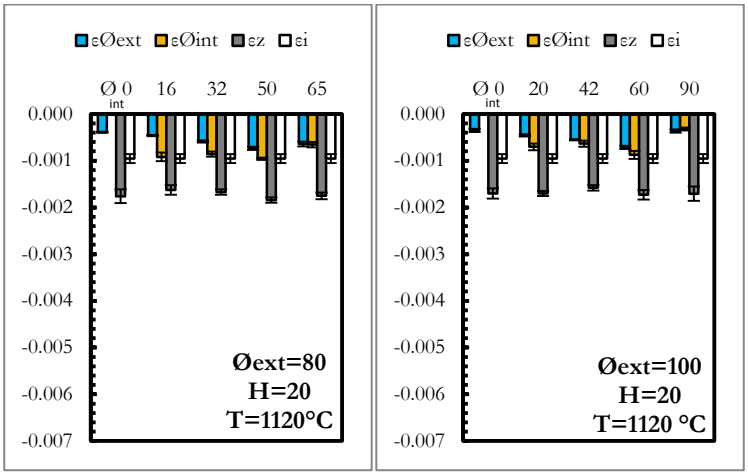

Fig. [4.3] Dimensional variations of the samples having the height of 20 mm, sintered at 1120 °C.

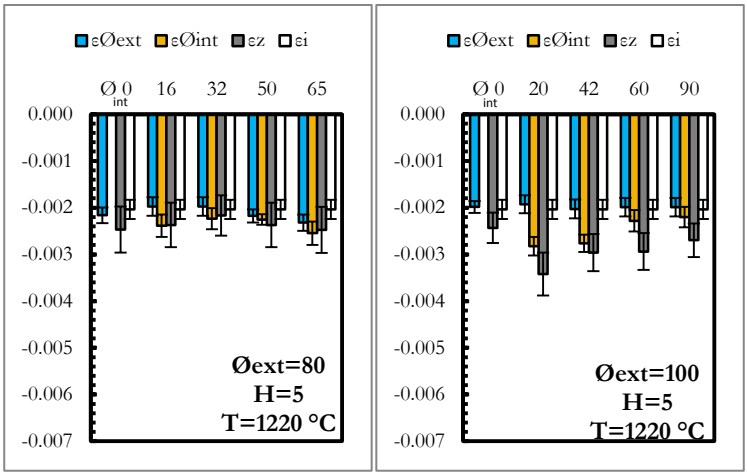

Fig. [4.4] Dimensional variations of the samples having the height of 5 mm, sintered at 1220 °C.

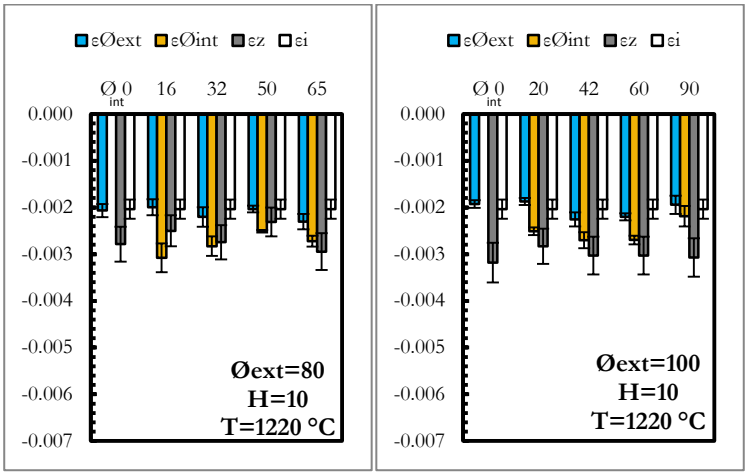

Fig. [4.5] Dimensional variations of the samples having the external diameter of 100 mm and height of 10 mm, sintered at 1220 °C.

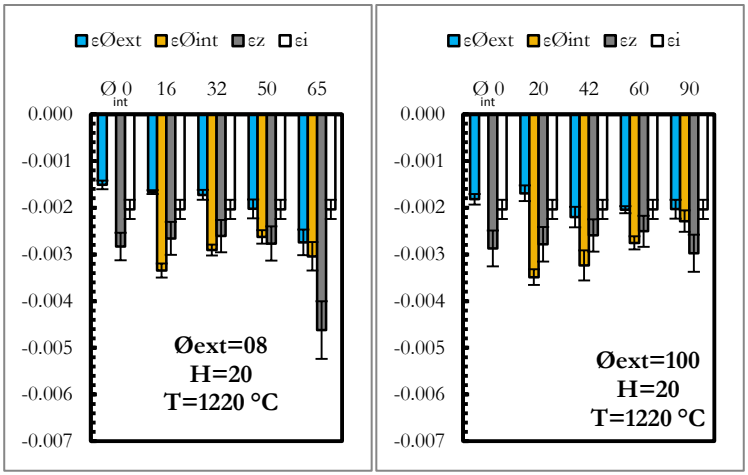

Fig. [4.6] Dimensional variations of the samples having the height of 20 mm, sintered at 1220 °C.

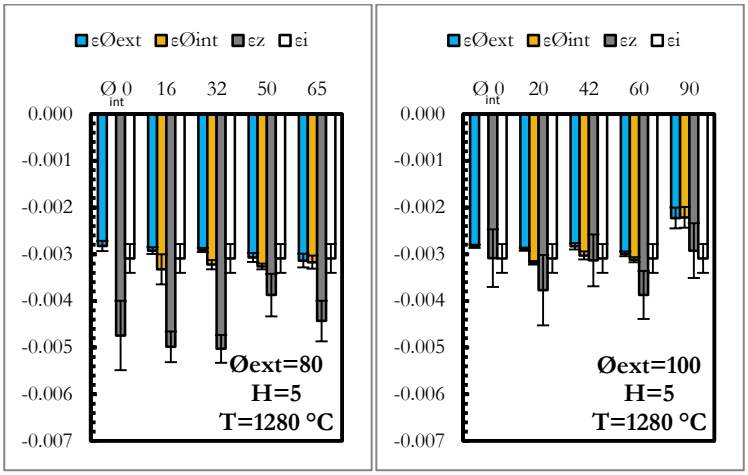

Fig. [4.7] Dimensional variations of the samples having the height of 5 mm, sintered at 1220 °C.

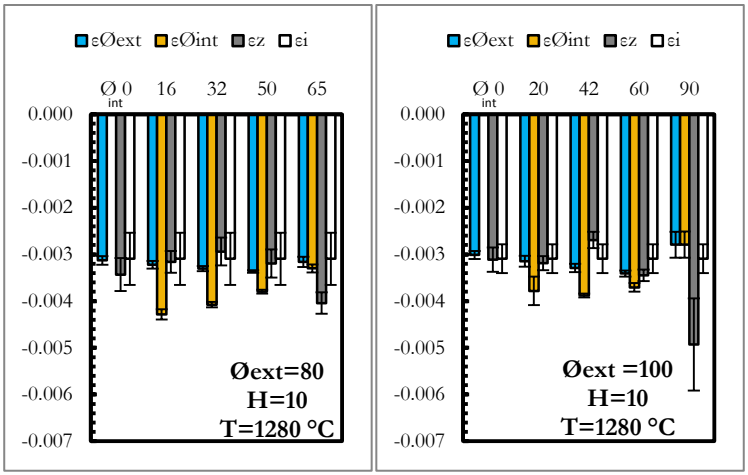

Fig. [4.8] Dimensional variations of the samples having the height of 10 mm, sintered at 1280 °C.

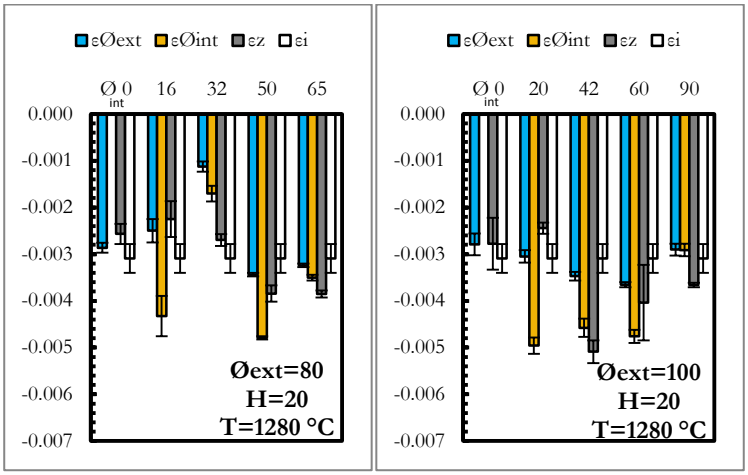

Fig. [4.9] Dimensional variations of the samples having the height of 20 mm, sintered at 1280 °C.

Analyzing the dimensional variations occurring at the three different sintering temperatures important considerations have been highlighted. First of all, on increasing the sintering temperature the isotropic dimensional variation increases as well. This trend can be easily observed if the isotropic dimensional variations are compared simultaneously.

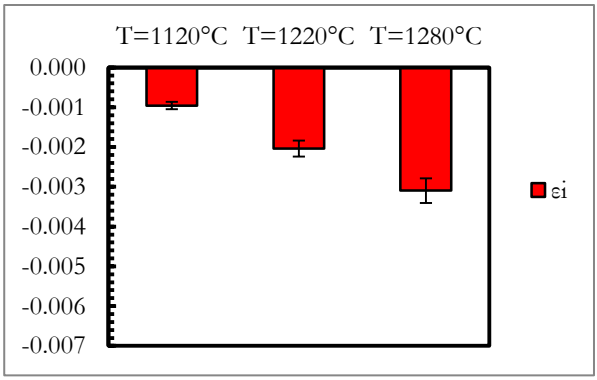

Fig. [4.10] Isotropic dimensional variation at the three different sintering temperatures.

In figure [4.10] the isotropic dimensional change has been compared for the three different sintering temperatures. As considered earlier, this parameter is linked to the densification. As expected, the increase in sintering temperature induces a higher densification (this assuming the process without significant mass losses). Nevertheless, on increasing the sintering temperature the anisotropy of dimensional change tends to decrease, as confirmed by the smaller difference between the dimensional changes in the compaction plane and in the axial direction in the samples sintered at the highest temperature.

Secondly, the dimensional variations are more stable on the diameters than on the heights (despite some exceptions), since the scatter band is in most cases higher for heights than for diameters. The influence of geometry and sintering temperature was also observed. According to Al-Qureshi [1] the higher the compacted sample is, the less homogenous the green density will be due to the pressure gradient, furthermore, the filling operations have an intrinsic variability. This effect, which is enhanced by the temperature, induces an enlargement of the scatter deviation. On the other hand parts with a high height to diameter ratio, are critical for the geometrical stability and some distortion effect, due to the ejection of the part from the die or/and intensified by the temperature gradients, could arise. Although the geometrical aspect of the part is of a crucial importance in the process know-how, it will not be discussed in this work. The parts will always be assumed to have ideal (not warped) geometrical features. However, the hypothesis of no significant distortions has been verified by checking the geometrical characteristics of the features used to derive the measured dimensions (flatness and cylindricity for planes and cylinders, respectively).

The third aspect deals with the dimensional variations measured in the compaction plane, $\varepsilon_{\emptyset int}$ and $\varepsilon_{\emptyset ext}$. It has been found that in several cases they are significantly, and unexpectedly, different. In fact the anisotropy has always been considered, due to the differences in the dimensional variation in the directions perpendicular and parallel to

the compaction direction, as the result of prior axial compaction, according to Molinari et al. [2] and Zavaliangos et al. [3]. This fundamental point will be discussed in detail in the next part of this chapter.

Given the strict relationship between densification and dimensional changes, interesting information can be drawn considering the dimensional variations of the sizes directly related to the mass of the material. Aiming at estimating this phenomenon the parameters ε_z and ε_r have been compared for the different geometries. The mean dimensional change related to the thickness, ε_r, has also been computed. The results are displayed for each sintering cycle in figures [4.11] to [4.19].

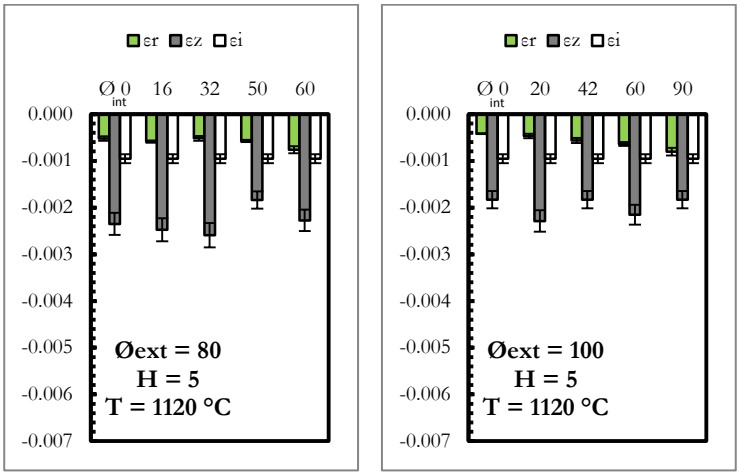

Fig. [4.11] ε_r, ε_z *and* ε_i *for samples having a height of 5 mm, sintered at 1120 °C.*

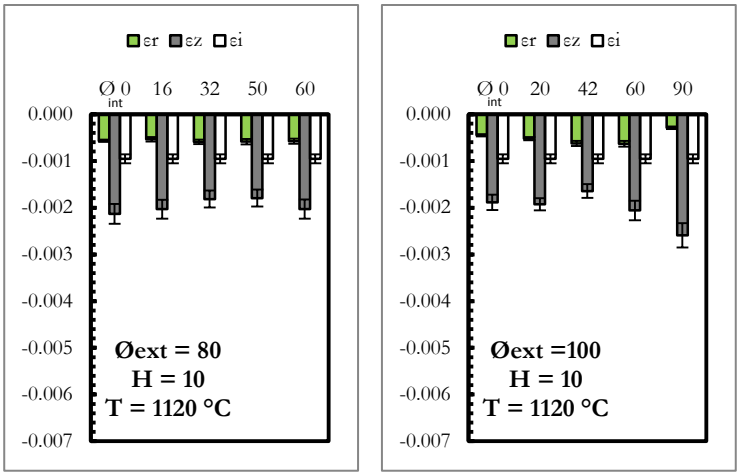

Fig. [4.12] ε_r, ε_z *and* ε_i *for samples having a height of 10 mm, sintered at 1120 °C.*

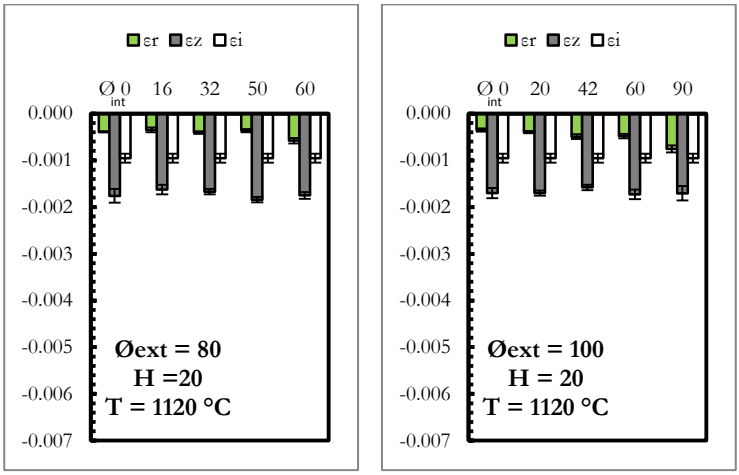

Fig. [4.13] ε_r, ε_z *and* ε_i *for samples having a height of 20 mm, sintered at 1120 °C.*

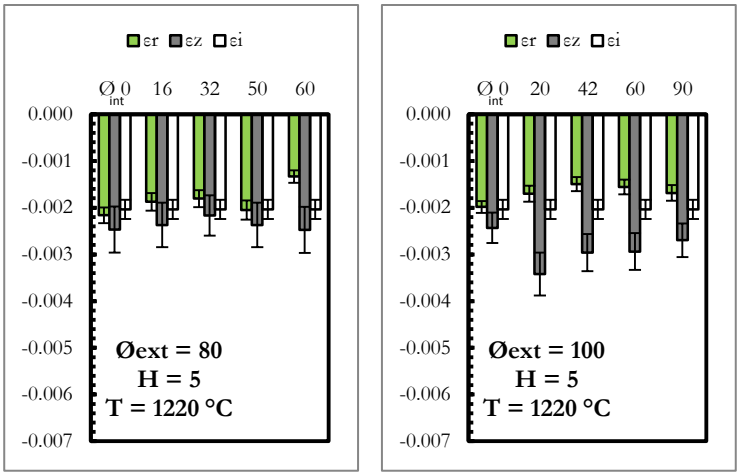

Fig. [4.14] ε_r, ε_z *and* ε_i *for samples having a height of 5 mm, sintered at 1220 °C.*

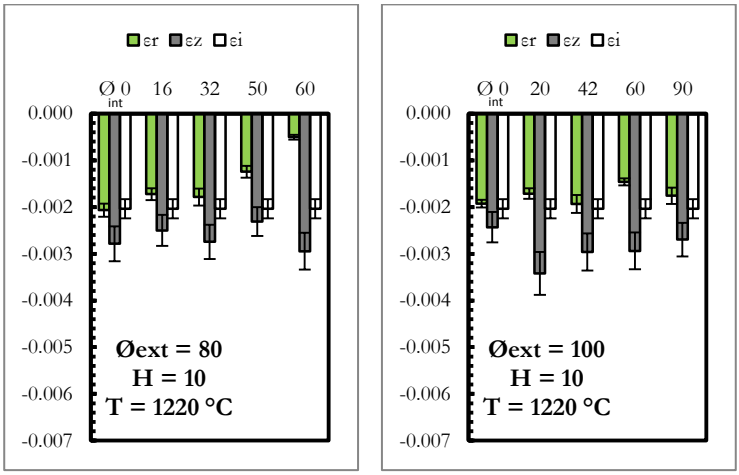

Fig. [4.15] ε_r, ε_z *and* ε_i *for samples having a height of 10 mm, sintered at 1220 °C.*

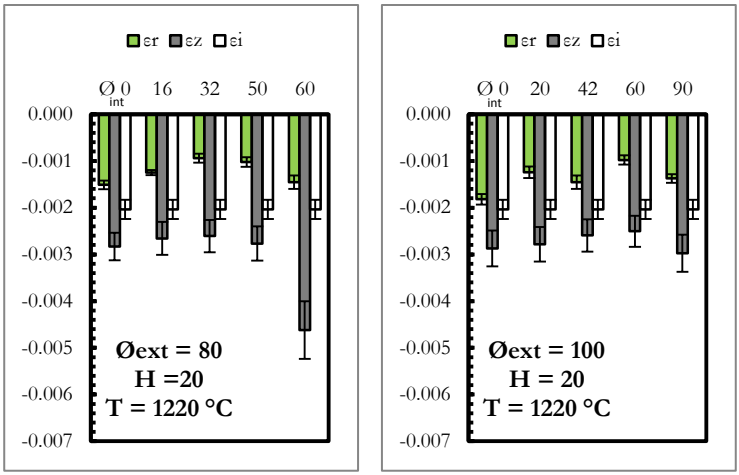

Fig. [4.16] ε_r, ε_z *and* ε_i *for samples having a height of 20 mm, sintered at 1220 °C.*

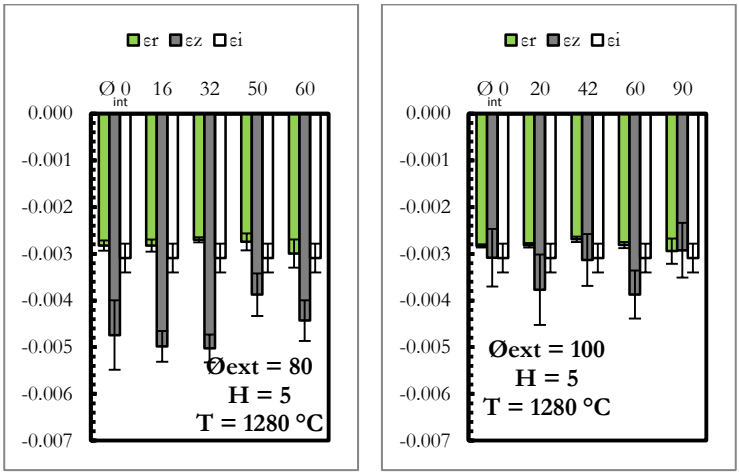

Fig. [4.17] ε_r, ε_z *and* ε_i *for samples having a height of 5 mm, sintered at 1280 °C.*

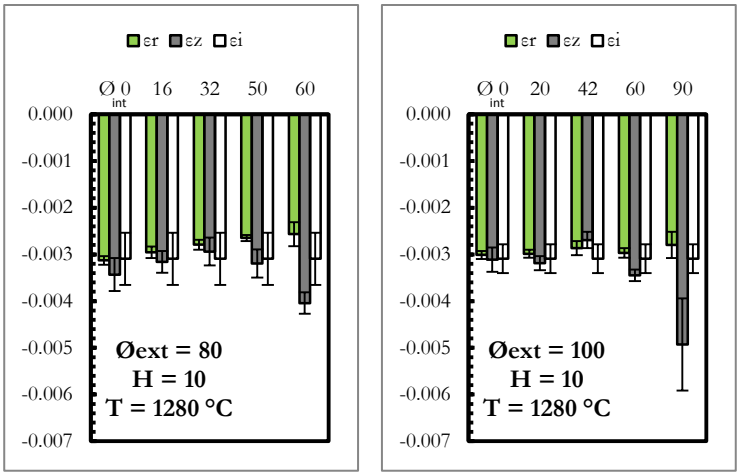

Fig. [4.18] ε_r, ε_z *and* ε_i *for samples having a height of 10 mm, sintered at 1280 °C.*

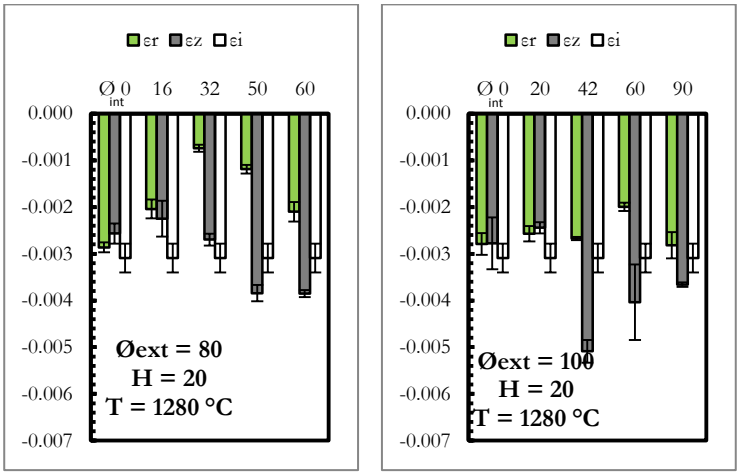

Fig. [4.19] ε_r, ε_z *and* ε_i *for samples having a height of 20 mm, sintered at 1280 °C.*

The dimensional variation of the wall thickness has been identified as the dimensional variation in the radial direction. Thanks to ε_r and ε_z the influence of sintering temperature is clearly highlighted in most cases. These two parameters significantly differ at the lowest sintering temperature, and their difference tends to decrease on increasing the sintering temperature, thus confirming that the anisotropy of the

dimensional change decreases on increasing the sintering temperature. This result was already highlighted by comparing the dimensional changes in terms of internal, external diameter and height, but less clearly, mainly due to the differences between the dimensional change in the internal and external diameter, which will be detailed in the following.

4.2 Dimensional variation of the diameters.

The dimensional variations in figures from [4.1] to [4.9] clearly show that the hypothesis $\varepsilon_{\emptyset int} = \varepsilon_{\emptyset ext}$ is not confirmed. These dimensional variations have been deeper investigated in order to understand if this behavior has a systematic base. Figure [4.20] shows $\varepsilon_{\emptyset int}$ versus $\varepsilon_{\emptyset ext}$ at the three different sintering temperatures.

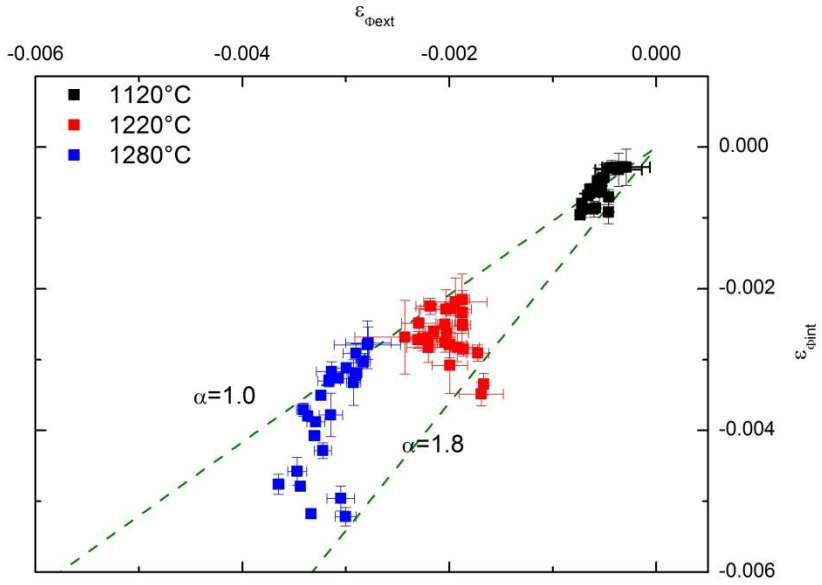

Fig. [4.20] $\varepsilon_{\emptyset int}$ *versus* $\varepsilon_{\emptyset ext}$.

Examining the data in figure [4.20] it is clear that on increasing the temperature the difference between $\varepsilon_{\emptyset int}$ and $\varepsilon_{\emptyset ext}$ increases as well: all the measured data lie within the domain defined by the straight lines of equation $\varepsilon_{\emptyset int} = \alpha \varepsilon_{\emptyset ext}$ where the coefficient $\alpha = [1; 1.8]$. The occurrence of a density gradient in the compaction plane, and not only in the compaction direction, might thus be reasonably hypothesized.

Picking out the data belonging to each single shape the influence of the geometry on the parameter α has been highlighted.

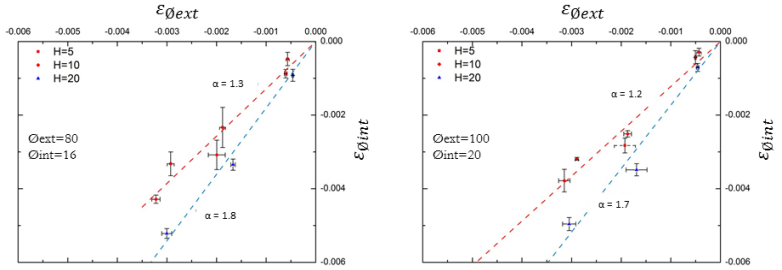

Fig. [4.21] $\varepsilon_{\emptyset int}$ *versus* $\varepsilon_{\emptyset ext}$, *specimens having* $\frac{\emptyset_{int}}{\emptyset_{ext}} = \frac{16}{80}$ *and* $\frac{\emptyset_{int}}{\emptyset_{ext}} = \frac{20}{100}$.

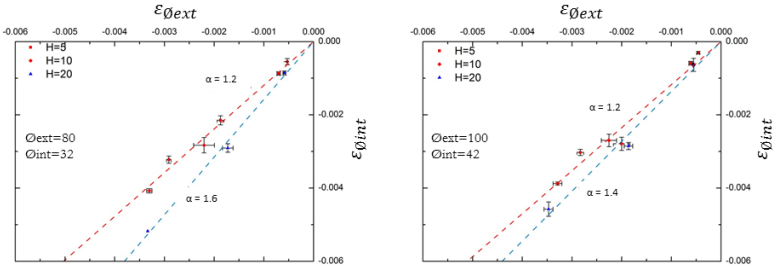

Fig. [4.22] $\varepsilon_{\emptyset int}$ *versus* $\varepsilon_{\emptyset ext}$, *specimens having* $\frac{\emptyset_{int}}{\emptyset_{ext}} = \frac{32}{80}$ *and* $\frac{\emptyset_{int}}{\emptyset_{ext}} = \frac{42}{100}$.

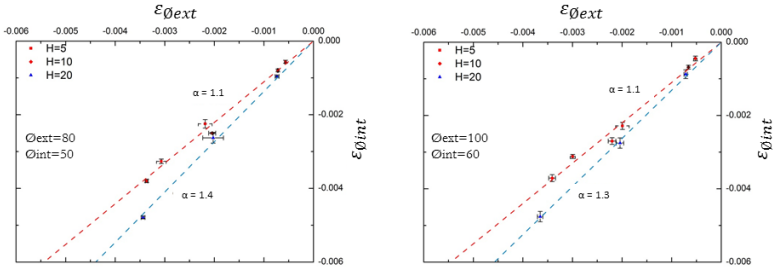

Fig. [4.23] $\varepsilon_{\emptyset int}$ *versus* $\varepsilon_{\emptyset ext}$, *specimens having* $\frac{\emptyset_{int}}{\emptyset_{ext}} = \frac{50}{80}$ *and* $\frac{\emptyset_{int}}{\emptyset_{ext}} = \frac{60}{100}$.

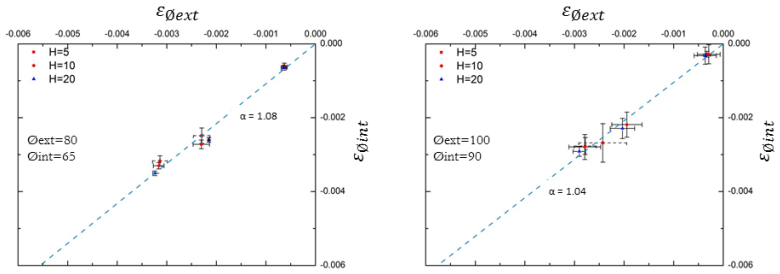

Fig. [4.24] $\varepsilon_{\emptyset int}$ *versus* $\varepsilon_{\emptyset ext}$, *specimens having* $\frac{\emptyset_{int}}{\emptyset_{ext}} = \frac{65}{80}$ *and* $\frac{\emptyset_{int}}{\emptyset_{ext}} = \frac{90}{100}$.

From figure [4.21] to figure [4.24] the data of the dimensional variation of the diameters are ordered by increasing the ratio $\frac{\emptyset_{int}}{\emptyset_{ext}}$, and it is clearly shown that the relationship between $\varepsilon_{\emptyset int}$ and $\varepsilon_{\emptyset ext}$ markedly depends on the geometry. Increasing the diameter ratio, the difference between $\varepsilon_{\emptyset int}$ and $\varepsilon_{\emptyset ext}$ decreases. Besides, this trend needs to be addressed with respect to the influence of the height. The $\varepsilon_{\emptyset int}$ versus $\varepsilon_{\emptyset ext}$ data have been processed for two blocks of outputs, grouped by the height. The specimens having a nominal height of 20 in one group and the other specimens (heights lower or equal to 10) in the second group. Data have been then fitted by a linear relation using the parameter α.

$$\varepsilon_{\emptyset int} = \alpha \varepsilon_{\emptyset ext} \qquad \text{Eq. [4.1]}$$

The coefficients resulted from the linear regressions have been evaluated with reference to the related diameter ratio, $\frac{\emptyset_{int}}{\emptyset_{ext}}$.

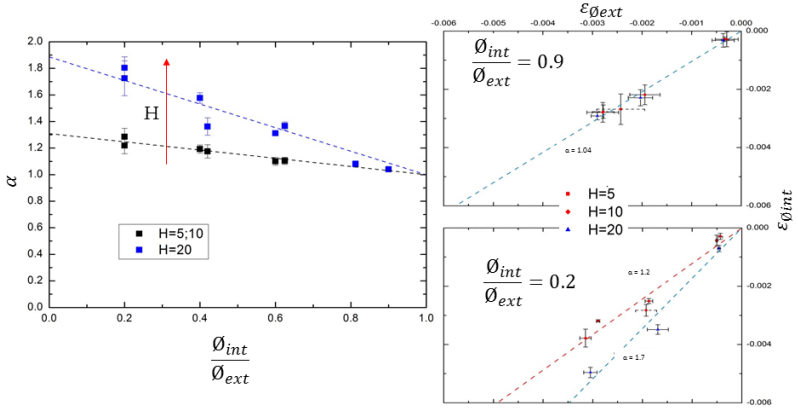

Fig. [4.25] Influence of the geometry (H and $\frac{Ø_{int}}{Ø_{ext}}$) on the parameter α.

The combined influence of the height and the diameter ratio on the coefficient α has been highlighted in figure [4.25]. The influence of the geometrical parameters on the coefficient α can be described by a simple linear equation. The limits highlighted for m are derived from the analyzed data.

$$\alpha = m\frac{Ø_{int}}{Ø_{ext}} + (1-m) \qquad \begin{cases} m = -0.3 \\ m = -0.9 \end{cases} \qquad \text{Eq. [4.2]}$$

Hence, the definition of the anisotropy coefficient can be updated using the coefficient α in equation [3.31].

$$K = \frac{\sqrt{\frac{\left(\varepsilon_{\phi_{ext}}+1\right)^2 - R^2\left(\alpha\varepsilon_{\phi_{ext}}+1\right)^2}{(1-R^2)}} - (\varepsilon_i+1)}{\varepsilon_i} \qquad \text{Eq. [4.3]}$$

In the current definition given in equation [4.3] the influence of the dimensional variation $\varepsilon_{\phi_{int}}$ is thus obtained through $\varepsilon_{Øext}$. The influence of the geometry is thus represented in the anisotropy parameter K through the variables $R^2 = \left(\frac{Ø_{int}}{Ø_{ext}}\right)^2$ and α.

4.3 The coefficient of anisotropy.

According to the definition of K by equation [4.3], the anisotropy of the dimensional variations in a ring-shaped specimen is a function of two classes of parameters. The first class comprehends the geometrical coefficients, while the second includes the dimensional variations $\varepsilon_{\phi_{ext}}$ and ε_i, by way of explanation $K = f(R,\ \alpha,\ \varepsilon_i,\ \varepsilon_{\phi_{ext}})$. Under the hypothesis that the parameter K and the isotropic dimensional variation can be somehow quantified, the dimensional variation in the compaction plane can be computed by isolating the variable $\varepsilon_{\phi_{ext}}$ in equation [4.3].

4.3.1 Anisotropic versus isotropic dimensional variation.

The value of K has been computed for every geometry by means of equation [3.31] with the intent to investigate the correlation with the dimensional variation ε_i. The results have been processed and reorganized in order to separate the effect of the geometrical dimensions ($\emptyset_{int}$, $\emptyset_{ext}$ and H) from the factor ε_i. The computed value of K have then been embedded in a chart versus the parameter ε_i. The results are summarized in figure [4.26].

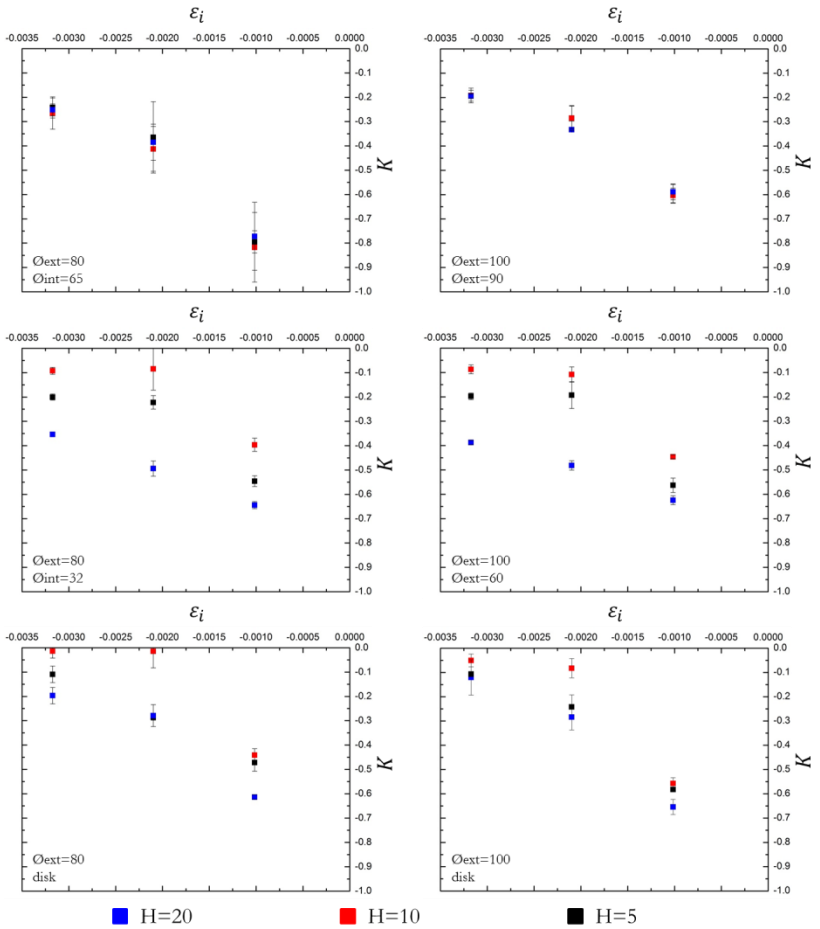

Fig. [4.26] Anisotropic versus isotropic dimensional variation.

In figure [4.26] the anisotropy parameter K shows a regular trend in function of the isotropic dimensional variation ε_i. The graphs dealing with the geometries, not reported in figure [4.26], evidenced intermediate trends. The anisotropy of the dimensional variations is mitigated on the isotropic dimensional variation's growth, that means on the proceeding of the densification. This is supported by the hypotheses introduced by Molinari et al. [2], where the magnitude of the mechanisms enhancing the anisotropy behavior has been proven to be higher at the early stage of the sintering phase and then

to decrease progressively. Such behavior has already been confirmed in the works of Cristofolini et al. [4] and [5] for ring-shaped specimens sintered at different temperatures.

4.3.2 K as a function of the isotropic dimensional variation.

All data of the computed anisotropy parameter *K* have been compared with the isotropic dimensional variation corresponding to each geometry. In this work the geometry has been identified by one or more parameters being a certain combination of the nominal dimensions of the specimens ($\emptyset_{int}$,$\emptyset_{ext}$, H), for instance $\frac{\emptyset_{int}}{\emptyset_{ext}}$. As expected, geometry does influence the anisotropy of the dimensional variations, but no univocal clear monotonic trend can be highlighted. In particular the data do not show a systematic trend dealing with the influence of the height, saving an exception for the geometries with higher $\frac{\emptyset_{int}}{\emptyset_{ext}}$ ($\frac{\emptyset_{int}}{\emptyset_{ext}} = \frac{65}{80}$ and $\frac{\emptyset_{int}}{\emptyset_{ext}} = \frac{90}{100}$), where no effect of the height is observed.

Based on the main evidence which sees the anisotropy decreasing on increasing the densification, a simple inversely proportional relation has been suggested, in order to constitute a general law that links the parameter K with the parameter ε_i.

$$K = \frac{C}{\varepsilon_i} + D \qquad \text{Eq. [4.4]}$$

The coefficients $C = [3.5 \cdot 10^{-4} \;\; ; \;\; 8.5 \cdot 10^{-4}]$ and $D = [-0.1 \;\; ; \;\; 0.1]$ have been found for each geometry using a non-linear regression tool. C and D have been related to the diameter ratio and, although the parameter D has an unreliable trend with respect to the parameter $\frac{\emptyset_{int}}{\emptyset_{ext}}$, the relation between C and $\frac{\emptyset_{int}}{\emptyset_{ext}}$ can be explicated by a second order polynomial.

$$C = C_0 + C_1\left(\frac{\emptyset_{int}}{\emptyset_{ext}}\right) + C_2\left(\frac{\emptyset_{int}}{\emptyset_{ext}}\right)^2 \qquad \text{Eq. [4.5]}$$

In equation [4.5] $C_0 = 7 \cdot 10^{-4}$, $C_1 = -7 \cdot 10^{-4}$ $C_1 = 7 \cdot 10^{-4}$.

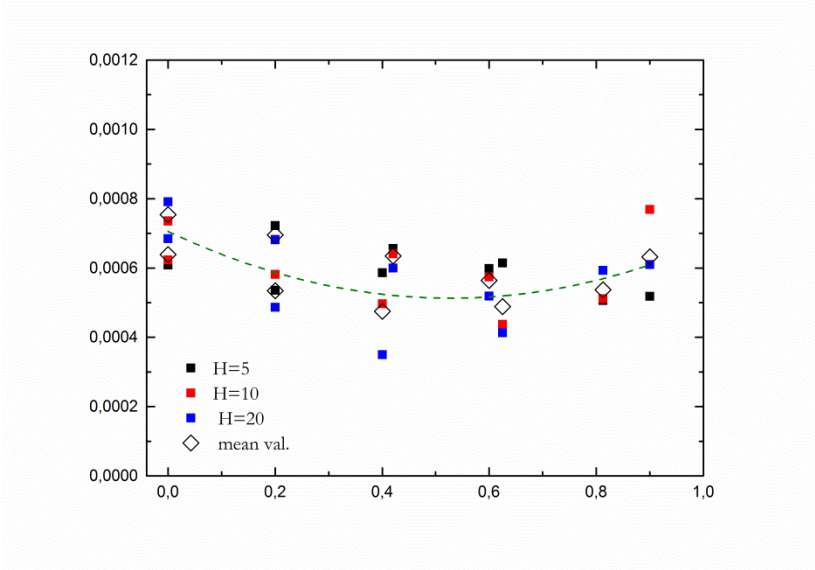

Fig. [4.27] C versus $\frac{\emptyset_{\text{int}}}{\emptyset_{\text{ext}}}$.

The densification, in this work identified with the parameter ε_i, is influenced by all the process parameters and the material. Equation [4.4] can be interpreted as the connection of the anisotropy of the dimensional variations with the process, the material and the geometry.

Equation [4.4] can therefore be set equal to the equation [4.3].

$$\frac{C}{\varepsilon_i} + D = \frac{\sqrt{\frac{\left(\varepsilon_{\phi_{ext}}+1\right)^2 - R^2\left(\alpha\varepsilon_{\phi_{ext}}+1\right)^2}{(1-R^2)}} - (\varepsilon_i+1)}{\varepsilon_i} \qquad \text{Eq. [4.6]}$$

$$\alpha = m\frac{\emptyset_{int}}{\emptyset_{ext}} + (1-m) \qquad \begin{cases} m = -0.3 & H \leq 10 \\ m = -0.9 & H = 20 \end{cases} \qquad \text{Eq. [4.2]}$$

$$\varepsilon_{\emptyset int} = \alpha\varepsilon_{\emptyset ext} \qquad \text{Eq. [4.1]}$$

$$C = C_0 + C_1\left(\frac{\emptyset_{int}}{\emptyset_{ext}}\right) + C_2\left(\frac{\emptyset_{int}}{\emptyset_{ext}}\right)^2 \qquad \text{Eq. [4.5]}$$

$$(\varepsilon_i + 1)^3 = (\varepsilon_\vartheta + 1)(\varepsilon_r + 1)(\varepsilon_z + 1) \qquad \text{Eq. [3.20]}$$

Combining equation [4.6] with the auxiliary equations [4.2], [4.1] and [4.5], plus the equation [3.20], which embodies the dimensional variation along the axis, the problem of the dimensional variations in a ring-shaped part can be likely solved in closed form.

4.5 Conclusions.

The iron disks and rings described in chapter two have been measured before and after the sintering process. Three different sintering temperatures have been considered, under the same operative conditions of heating rate, sintering time and cooling rate. The measured dimensional variations have been compared with the computed isotropic dimensional variation. Analyzing the results important aspects have been highlighted:

- The measured dimensional variations confirm that at all three temperatures shrinkage occurs.
- Shrinkage, represented by the change in volume and described in terms of isotropic dimensional change, increases on increasing the sintering temperature.
- The scatter band relevant to the dimensional variation of the height is generally wider than the scatter band relevant to the dimensional variation of the diameters.
- The anisotropy of the dimensional variation is clearly highlighted if the dimensional variation of thickness (rather than of internal and external diameters) is compared to the dimensional variation of the height. Thickness and height are in fact the parameters directly related to the volume of the mass shrinking during the sintering stage.
- A linear relation between the dimensional variation of the external diameter and the internal diameter has been defined, this relation depends on the geometrical parameters.
- The anisotropy of the dimensional variations (parameter K) has been computed using the analytical definition.
- This parameter K has been compared with the isotropic dimensional variation, ε_i.
- The relation between K and ε_i has been described by an empirical equation [4.4].

The anisotropy of the dimensional variations has been analytically defined and then correlated with the isotropic dimensional variation through a solid experimental relation. This analytical and empirical equality is the milestone for building a model able to predict the dimensional variation of an axi-symmetric part.

4.6 References

1 H.A. Al-Qureshi; M.R.F. Soares; D. Hotza; M.C. Alves; A.N. Klein, Analyses of the fundamental parameters of cold die compaction of powder metallurgy, Journal of Material Processing Technology 199, 1 - 3 (2008) pp 417 - 424

2 A. Molinari; C. Menapace; E. Torresani; I. Cristofolini; M. Larsson - Working hypothesis for origin of anisotropic sintering shrinkage caused by prior uniaxial cold compaction - Powder metallurgy 56, 3 (2013) pp 189 - 185

3 A. Zavaliangos; J.M. Missiaen; D. Bouvard, Anisotropy in Shrinkage During Sintering, Science of Sintering 38, 1, (2006) pp 13 -26

4 I. Cristofolini; C. Menapace; M. Cazzolli; A. Rao; W. Pahl; A. Molinari, The effect of anisotropic dimensional change on the precision of steel parts produced by powder metallurgy, Journal of Materials Processing Technology 212, 7 (2012) pp 1513 - 1519

5 I. Cristofolini; N. Corsentino; A. Molinari; M. Larsson - A design procedure accounting for the anisotropic dimensional change on sintering of ferrous PM parts - Advances in metallurgy and Particulate materials 1 (2014)

Chapter 5

Design of axi-symmetric PM part.

The anisotropic dimensional change on sintering should be properly evaluated in the design step, aiming at guaranteeing the required precision in the final parts. The model developed in the previous chapter, represented as a main result by equation [4.7], is the starting point to develop a design procedure accounting for anisotropic dimensional change, under the assumptions that the considered geometry is a disc or ring and that the parameter ε_i, representative of the densification of the material under given process conditions, is known in advance.

$$\frac{C}{\varepsilon_i} + D = \frac{\sqrt{\frac{\left(\varepsilon_{\phi_{ext}}+1\right)^2 - R^2\left(\alpha\varepsilon_{\phi_{ext}}+1\right)^2}{(1-R^2)}} - (\varepsilon_i+1)}{\varepsilon_i} \qquad \text{eq. [4.7]}$$

The quantity ε_i can be either estimated on theoretical basis, or derived from experience. The theory of the densification in sintering developed several models to estimate the linear shrinkage, as the Kingery and Berg's model in equation [1.1] (Exner and Petzow [1]) or the continuum theory (Olevsky [2]). In the industry practice designers can rely on the sintering master curves (Hunghai Su et al. [3]) that can predict the densification under a particular process condition with an acceptable precision.

Following, in this chapter a procedure to predict the anisotropy of the dimensional change on sintering will be presented. This procedure has been successively adopted and implemented for a pool of four multi-level PM structural parts of different materials, and different sintering conditions. Only the results coming from one part will be presented and discussed, the others are reported briefly in the appendix.

5.1 Prediction of dimensional variations of a ring-shaped PM part.

The design procedure outline is shown in figure [5.1].

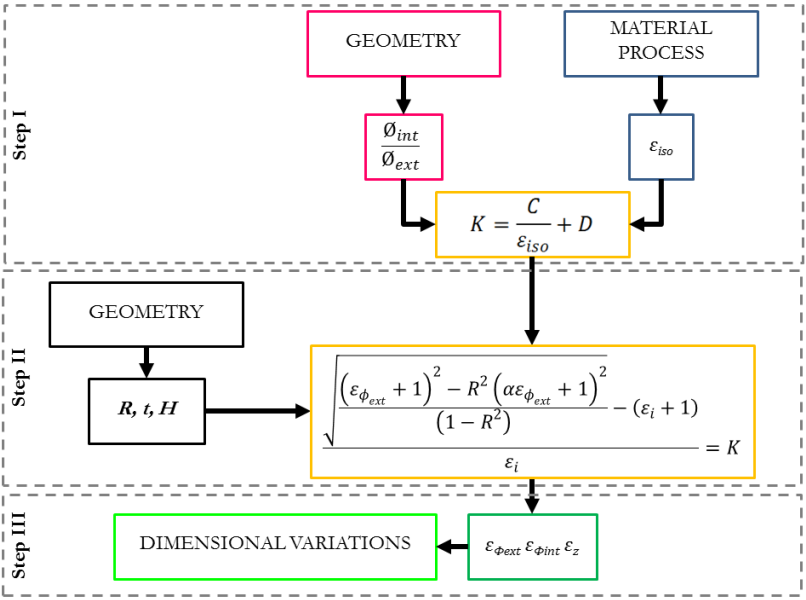

Fig [5.1]. Design procedure for a ring-shaped part.

This procedure has been implemented in three main steps, following a logic pathway from the input (the nominal dimensions and the process parameters), towards the output (the real dimensions of the sintered part).

5.1.1 Step I. Estimation of the amount of anisotropy induced by the process.

In chapter four an empirical relation has been developed to predict the anisotropy parameter K of any ring-shaped part on the basis of the isotropic dimensional change.

$$K = \frac{C}{\varepsilon_i} + D. \qquad \text{Eq. [4.5]}$$

The value of C can be computed as a function of the ratio of the internal diameter to the external diameter $\frac{\emptyset_{int}}{\emptyset_{ext}}$, as by equation [4.6]. As a first assumption, parameter D has been set equal to -0.05, being the mean value of the computations.

Figure [5.2] schematically represents that the anisotropy parameter *K* is representative both of the influence of the geometry and of the influence of the material and process parameters, the main advantage is that the only inputs required are the densification (given by the change in volume) and the nominal dimensions. Assuming that the mass remains constant, the amount of loose lubricant during sintering or any other contamination such as oxygen intake or carbon depleting is neglected [German [4]]. Moreover the densification is assumed to be independent of the geometry and the mass of the component. In principles this model can be used to predict the anisotropy of the dimensional variation due to sintering of any material formed with a rigid die compaction with a single exception for liquid phase sintering conditions which has been proven by Corsentino et al. [5] to have an active effect on reducing the anisotropy.

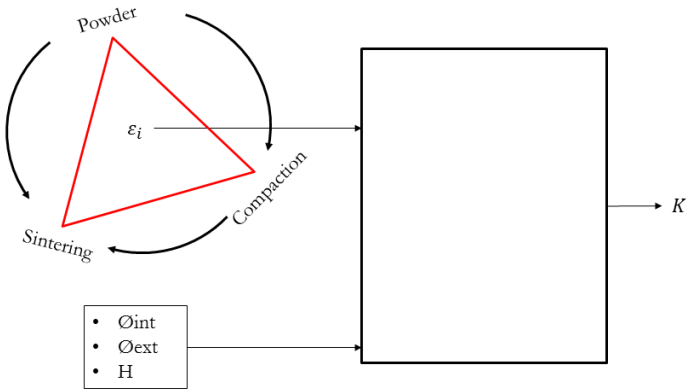

Fig [5.2]. Input parameters determining K.

5.1.2 Step II. Analytical description of anisotropy.

The analytical description of anisotropy is the link between the amount of anisotropy and the dimensional variations. It has been represented by equation [3.31].

$$K = \frac{\sqrt{\frac{(\varepsilon_{\emptyset ext}+1)^2 - R^2(\varepsilon_{\emptyset int}+1)^2}{1-R^2}} - (1+\varepsilon_i)}{\varepsilon_i}$$ Eq. [3.31]

This relation can be conveniently modified as a function of $\varepsilon_{\emptyset ext}$ and ε_i by the addition of some opportune parameters.

$$K = \frac{\sqrt{\gamma \varepsilon_{\emptyset ext}{}^2 + \delta \varepsilon_{\emptyset ext} + 1} - (1+\varepsilon_i)}{\varepsilon_i}$$ Eq. [5.1]

Where $\gamma = \frac{1-\alpha^2 R^2}{1-R^2}$, $\delta = 2\frac{1-\alpha R^2}{1-R^2}$, and α is the function in equation [4.3]. This last equation has been further modified by introducing the wall thickness ($t = \frac{\emptyset_{int} - \emptyset_{ext}}{2}$) instead of the diameter ratio ($\frac{\emptyset_{int}}{\emptyset_{ext}}$) as a geometrical parameter, obtaining a new relationship describing parameter α, more useful in the development of the prediction model. This relation is represented in figure [5.3].

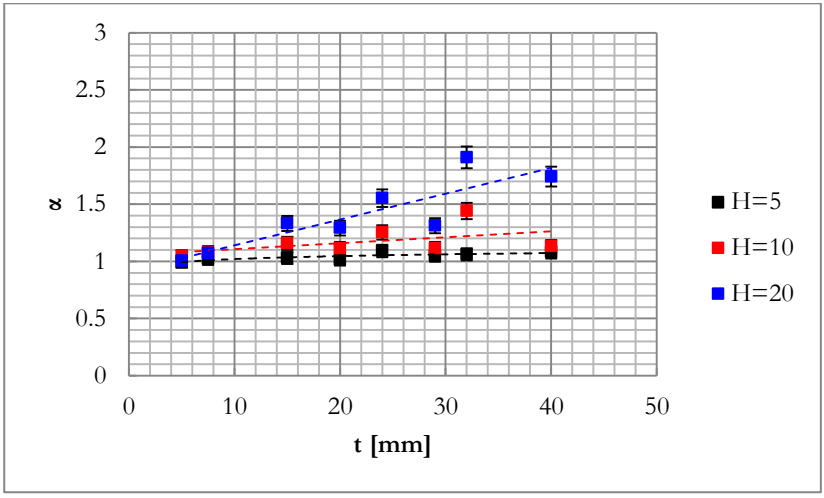

Fig. [5.3] α versus t, for three heights.

The new relationship, from $\alpha = \nexists \left(\frac{\emptyset_{int}}{\emptyset_{ext}}\right)$ to $\alpha = \nexists(t)$ results in equation [5.2].

$$\alpha = \alpha_0 + \alpha_1 t \qquad \begin{cases} \alpha_0 \approx 1 \quad , \quad \alpha_1 = 0.02 \quad ; \quad H = 20 \\ \alpha_0 \approx 1 \quad , \quad \alpha_1 = 0.005 \quad ; \quad H = 10 \\ \alpha_0 \approx 1 \quad , \quad \alpha_1 = 0.002 \quad ; \quad H = 5 \end{cases} \qquad \text{Eq. [5.2]}$$

The data exposed in figure [5.3] can be analyzed with the same criterion adopted in chapter four, assuming that the data belonging to rings with height equal to 10 mm are not significantly different to the ones having height equal to 5 mm, and choose a mean trend.

At this point equation [5.1] can be imposed equal to equation [4.5]. The result is the equation [5.3] where the variable $\varepsilon_{\emptyset ext}$ can be explicated and finally computed.

$$\frac{C}{\varepsilon_i} + D = \frac{\sqrt{\gamma {\varepsilon_{\emptyset ext}}^2 + \delta \varepsilon_{\emptyset ext} + 1} - (1 + \varepsilon_i)}{\varepsilon_i} \qquad \text{Eq. [5.3]}$$

5.1.3 Step III. Dimensions of the sintered ring.

By the definition of K the dimensional variation of the outer diameter has been computed. The dimensional variation occurring on the internal diameter can be in turn computed using the experimental relation described by the equation [4.2].

$$\varepsilon_{\emptyset int} = \alpha \varepsilon_{\emptyset ext} \qquad \text{Eq. [4.2]}$$

Furthermore the dimensional variation of the height can be computed by imposing the boundary condition relative to the volume change.

$$(1+\varepsilon_i)^3 = \frac{(1+\varepsilon_{\emptyset ext})^2 - R^2(1+\varepsilon_{\emptyset int})^2}{1+R^2}(1+\varepsilon_z) \quad \text{Eq. [5.4]}$$

Equation [5.4] is the result of the equality between equation [3.30] and equation [3.20]. In this relation the variable ε_z can be easily isolated and computed.

The dimensional variations accounting for anisotropy, $\varepsilon_{\emptyset int}$, $\varepsilon_{\emptyset ext}$ and ε_z are estimated and therefore the dimensions of the sintered part can be predicted. The prediction of the sintered dimensions can be simply derived by the definitions of the dimensional variations given in chapter three.

$$\varepsilon_z = \frac{[H]_s - [H]_g}{[H]_g} \quad \text{Eq. [3.8]}$$

$$\varepsilon_{\phi_{int}} = \frac{[\phi_{int}]_s - [\phi_{int}]_g}{[\phi_{int}]_g} \quad \text{Eq. [3.27]}$$

$$\varepsilon_{\phi_{ext}} = \frac{[\phi_{ext}]_s - [\phi_{ext}]_g}{[\phi_{ext}]_g} \quad \text{Eq. [3.28]}$$

Hence the dimensions of the sintered ring-shaped part can be computed.

$$[H]_s = [H]_g(1+\varepsilon_z) \quad \text{Eq. [5.5]}$$

$$[\emptyset_{int}]_s = [\emptyset_{int}]_g(1+\varepsilon_{\emptyset int}) \quad \text{Eq. [5.6]}$$

$$[\emptyset_{ext}]_s = [\emptyset_{ext}]_g(1+\varepsilon_{\emptyset ext}) \quad \text{Eq. [5.7]}$$

The procedure is summarized in figure [5.4].

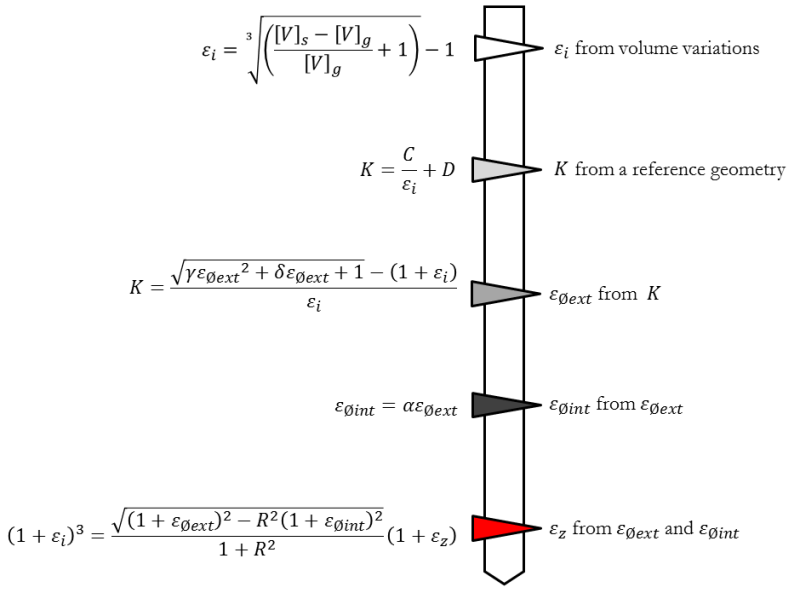

Fig. [5.4] Summarized design procedure.

This simple design procedure can be used in two different ways. The first approach, which has been shown above, is the prediction of the dimensions of a sintered part starting, for a given green sample, with known dimensions and a given sintering process. The second approach is the design of the green sample by imposing the dimensions of the sintered part and the sintering process. The second approach can be more interesting for an industrial application considering that the press and sintering process is a near net-shape technology, the dimensions of the sintered component and therefore the compacting process with a higher efficiency.

In this session it has been presented a basic procedure predicting the dimensions of a sintered cylinder of any given dimension and densification. The most suitable geometry for the press and sinter technology is the axi-symmetric one, but in general, a PM part is more complex than a ring. The procedure needs to be implemented and adapted for more complex geometries since the aim of this work is to give a tool to improve the design of PM components. To validate this model four different components have been studied. Each sample is a mechanical component made in an industry and sintered under different conditions. Each part has been measured before and after sintering using the method already explained in the chapter two, by implementing a specific procedure tailored for each one of the four components.

5.2 Prediction of the dimensional variations of a multi-level PM part

5.2.1 Main hypotheses and general procedure.

The design procedure for a complex part is based on two hypotheses:

1. The sintering process does not influence the geometrical accuracy of the component. This statement is equivalent to the assumption of having no shape distortions, discussed in chapter three, relative to the analytical description of anisotropy. Therefore the geometrical features of the component are still within the tolerances required, despite the densification due to the sintering process, meaning that after the sintering process the distortion is negligible. Moreover, if an excess of distortion appears, it does inhibit the functionality of the component, so the production process by sintering technique is not feasible or needs to be re-designed. There are several studies supporting that the geometrical precision of the component is only slightly decreased on increasing the densification, this has been proven by Cristofolini et al [6] and Corsentino et al. [7].

2. Any geometry can be described as an assembly of simpler geometries. Any axi-symmetric component formed by the rigid die compaction technology can be broken down to two or more concentric rings with different heights. In figure [5.5] a schematic example of an exploded geometry is represented.

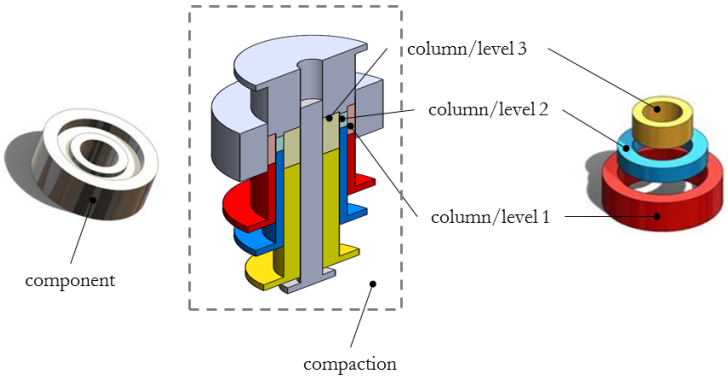

Figure [5.5] Example of part breakdown by the multi-level compaction approach.

This splitting is the same used to design the column movements during the compaction process of an axi-symmetric part having a varying cross-section. As mentioned in chapter one, to provide the same densification in all the cross-sections each level of the part must be pressed independently. The result is a complex axi-symmetric part, which is represented by the sum of several concentric rings, named as levels in this work. This approach has been evaluated to be the most coherent since the major cause of the anisotropy of dimensional variations of PM part is the compaction process as reported by Zavaliangos [8] and Molinari [9]. Consequently, each column will be considered separately. Each level in sintering expresses an amount of anisotropy, which is directly related to the corresponding powder column in the compaction step.

3. The dimensional variation of each ring can be predicted using the procedure already described in this session. In the end there is the need to restore the congruency at equivalent dimensions when the dimensional variations and the related sintered dimensions are known for each level. The dimensional changes are still related to each single level, meaning that there are two different variations for the same dimension, as represented in figure [5.6]. The congruence is restored by computing the weighted average of the dimensional changes referred to the same dimension using the volume of the level, according to equation [5.8].

$$\emptyset_{i+1} = \frac{[\emptyset_{int}]_{Vi}+[\emptyset_{ext}]_{Vi+1}}{Vi+Vi+1} \qquad i = [1 \quad ; \quad n-1] \qquad \text{Eq. [5.8]}$$

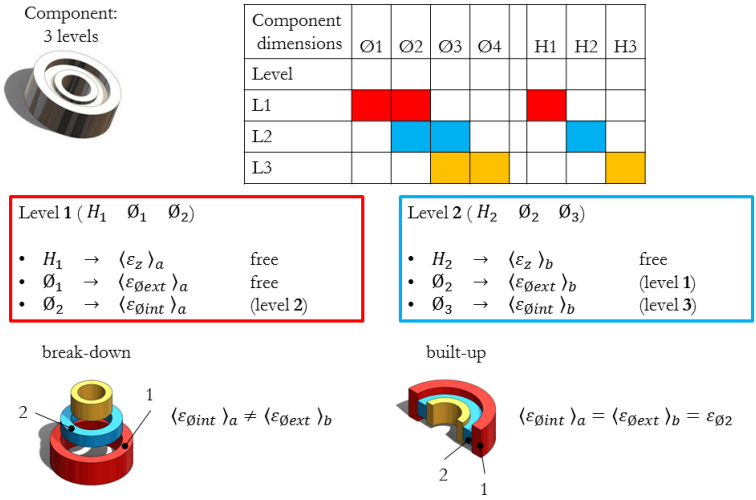

Fig. [5.6] Congruence conflict in the level approach.

In figure [5.6] there is an example of a prediction conflict that needs to be solved in order to restore the geometrical congruence. The design procedure implied breaking-down the component and predicting the dimensional variation on each ring. A this point the dimensional variation of the diameter Ø2 is predicted by both the dimensional variation on the external diameter of the blue level and the dimensional variation on the internal diameter of the red level. Equation [5.8] allows to solve this problem under the simple but effective assumption that the higher is the mass of the material that is shrinking, the higher is the influence on the overall dimensional variation affecting the part.

The designer is therefore able to compute the sintered dimensions of the part since the dimensional changes are known for each dimension of the part. The design procedure is summarized in figure [5.7].

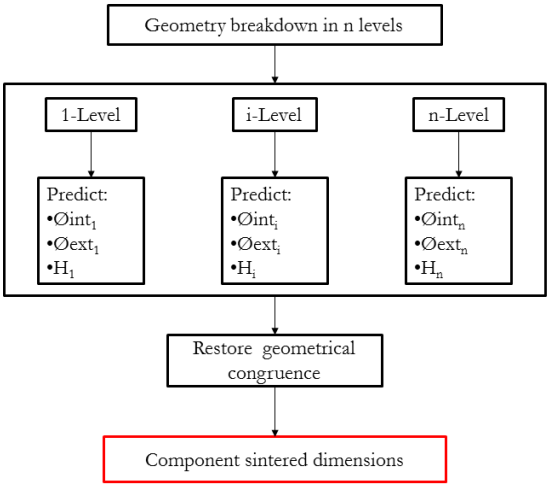

Figure [5.7] Design procedure for an n-levels component.

Commonly the most of the mechanical components are also characterized by several details and features (grooves, chamfers, holes etc., Mott [10]), which are small if compared with the main dimensions of the component itself. Usually these features are obtained by secondary operations in order to fulfill the dimensional requirements. The dimensional variation of small details and features will no longer be considered, as it will be demonstrated in the following that they do not dramatically affect the dimensional variations of the main dimensions. This model has been developed on the experimental behavior of main heights and diameters, so that the design procedure will be focused only on the critical dimensions identified by diameters and heights (Bocchini [11]). The components analyzed in the four cases of study are made of commercial grade steel powders, compacted and sintered in different conditions in order to investigate the influence of the main process parameters. In this chapter only one of the four parts will be discussed in detail, all the other results will be presented in the appendices.

5.2.2 Part and process description.

The component analyzed in the first case of study is an impeller produced with chromium steel powder (0.55%C 3%Cr 0.5%Mo), green density up to 6.7 g/cm^3. The samples have been sintered in a batch furnace under the same operational conditions at five different temperatures. The component is described in figure [5.8]. The sintering conditions are summarized in table [5.1].

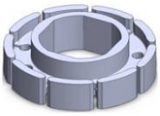

Fig. [5.8] Chromium steel impeller.

Sintering Temperature [°C]	Heating rate [°C/min]	**Sintering** time [min]	Sintering atmosphere	Cooling rate [°C/min]
1150	5	30	Vacuum + N_2 backfill	5
1200	5	30	Vacuum + N_2 backfill	5
1250	5	30	Vacuum + N_2 backfill	5
1300	5	30	Vacuum + N_2 backfill	5
1350	5	30	Vacuum + N_2 backfill	5

tab. [5.1] Sintering conditions.

5.2.3 Part breakdown strategy

The part layout has been processed to obtain the break-down structure following the approach already described. In this case the component is a three level part. In figure [5.9] the component is represented in its broken-down structure.

Fig. [5.9] Component break-down.

In figure [5.10] the scheme of the component is displayed, showing the critical dimensions evaluated in the design procedure.

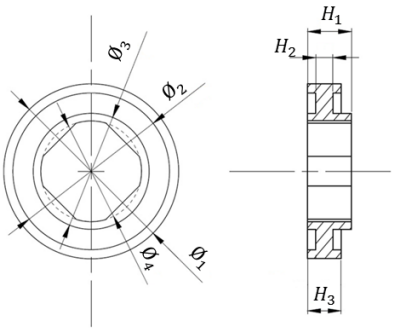

Ø1	Ø2	Ø3	Ø4		H1	H2	H3
68.3	59.9	44.7	38.9		13.5	6.4	17.3

Fig. [5.10] Rotor scheme and main nominal dimensions.

5.2.4 Actual dimensions, before and after sintering.

Each sample has been measured before and after sintering using the measuring procedure well described in chapter three. The measures are reported in table [5.2] and summarized in figure [5.10].

	Ø1	Ø2	Ø3	Ø4		H1	H2	H3
	68.304	59.902	44.651	38.949		13.495	6.392	17.267

Tab. [5.2a] Dimensions of the green samples.

	Ø1	Ø2	Ø3	Ø4		H1	H2	H3
1150°C	-0.002	-0.002	-0.002	-0.002		-0.004	-0.003	-0.004
1200°C	-0.003	-0.003	-0.003	-0.003		-0.005	-0.005	-0.006
1250°C	-0.004	-0.004	-0.004	-0.004		-0.007	-0.006	-0.007
1300°C	-0.006	-0.006	-0.006	-0.006		-0.008	-0.008	-0.009
1350°C	-0.007	-0.008	-0.007	-0.007		-0.010	-0.009	-0.011

Tab. [5.2b] Dimensional variations on sintering.

	Ø1	Ø2	Ø3	Ø4	H1	H2	H3
1150°C	68.191	59.801	44.580	38.886	13.442	6.369	17.193
1200°C	68.108	59.729	44.525	38.835	13.415	6.357	17.163
1250°C	68.031	59.665	44.472	38.795	13.388	6.343	17.139
1300°C	67.934	59.581	44.402	38.734	13.371	6.336	17.116
1350°C	67.791	59.457	44.301	38.645	13.371	6.347	17.106

Tab. [5.2c] Dimensions of the sintered samples.

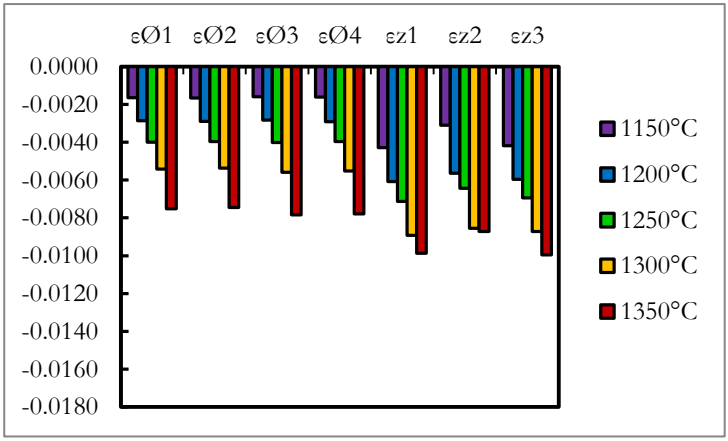

Fig. [5.10] Measured dimensional variations.

Figure [5.10] highlights that, for each considered dimension, the dimensional variation is higher on increasing the sintering temperature, and it is not isotropic: as expected the dimensional variation of the heights is higher than that of the diameters.

5.2.5 Design procedure. Estimation of the dimensional variation.

Using the dimensions in table [5.2] it is possible to compute the volume of the single levels (red, blue and yellow in figure [5.9]) and to estimate the volume densification (ε_V). Given the volume densification, the isotropic dimensional change, ε_i, can be computed. Therefore the anisotropy coefficient K can be estimated using equation [4.3]. The results are reported in table [5.3].

	εi	K	K	K
1150°C	-0.002	-0.300	-0.279	-0.299
1200°C	-0.004	-0.206	-0.193	-0.206
1250°C	-0.005	-0.170	-0.159	-0.169
1300°C	-0.007	-0.141	-0.133	-0.141
1350°C	-0.008	-0.123	-0.116	-0.122

Tab. [5.3] Measured isotropic dimensional variations and computed anisotropy parameters.

The dimensional variations due to the sintering process can thus be computed by equations [4.3, 4.4, 4.5, 4.6]. In table [5.4] the predicted dimensional variations are reported.

	V1			V2			V3		
	εØext	εØint	εZ	εØext	εØint	εZ	εØext	εØint	εZ
1150°C	-0.0017	-0.0017	-0.0038	-0.0018	-0.0019	-0.0035	-0.0016	-0.0016	-0.0039
1200°C	-0.0031	-0.0031	-0.0054	-0.0033	-0.0033	-0.0049	-0.0029	-0.0030	-0.0055
1250°C	-0.0042	-0.0043	-0.0067	-0.0045	-0.0045	-0.0060	-0.0040	-0.0040	-0.0069
1300°C	-0.0058	-0.0058	-0.0084	-0.0061	-0.0061	-0.0075	-0.0055	-0.0055	-0.0087
1350°C	-0.0074	-0.0074	-0.0102	-0.0078	-0.0078	-0.0091	-0.0070	-0.0070	-0.0106

Tab. [5.4] Predicted dimensional variations for each level.

The congruence of the geometry has been restored for diameter Ø2 (level1 and level2) and for diameter Ø3 (level2 and level3). Using the predicted dimensional changes it is possible to estimate the dimensions of the sintered component. The dimensions estimated with the model are reported in table [5.5b], along with the measured ones (table [5.5a]).

	Ø1	*Ø2*	*Ø3*	*Ø4*	*H1*	*H2*	*H3*
1150°C	*68.191*	*59.801*	*44.580*	*38.886*	*13.442*	*6.369*	*17.193*
1200°C	*68.108*	*59.729*	*44.525*	*38.835*	*13.415*	*6.357*	*17.163*
1250°C	*68.031*	*59.665*	*44.472*	*38.795*	*13.388*	*6.343*	*17.139*
1300°C	*67.934*	*59.581*	*44.402*	*38.734*	*13.371*	*6.336*	*17.116*
1350°C	*67.791*	*59.457*	*44.301*	*38.645*	*13.371*	*6.347*	*17.106*

Tab. [5.5a] Actual dimensions. Measured dimensions of the sintered parts.

	Ø1	*Ø2*	*Ø3*	*Ø4*	*H1*	*H2*	*H3*
1150°C	*68.186*	*59.795*	*44.573*	*38.885*	*13.448*	*6.367*	*17.198*
1200°C	*68.091*	*59.711*	*44.511*	*38.833*	*13.424*	*6.362*	*17.170*
1250°C	*68.014*	*59.641*	*44.459*	*38.791*	*13.394*	*6.346*	*17.140*
1300°C	*67.909*	*59.547*	*44.391*	*38.734*	*13.378*	*6.342*	*17.117*
1350°C	*67.800*	*59.449*	*44.319*	*38.674*	*13.366*	*6.345*	*17.095*

Tab. [5.5b] Predicted dimensions. Computed dimensions of the sintered parts.

5.2.6 Error of estimation.

After the prediction of the dimensions in sintering the error of estimation has been evaluated. The evaluation of this error has been performed in two steps. The first is the computation of the difference of the actual value $\langle X \rangle_a$ from the predicted one $\langle X \rangle_p$.

$$e = \langle X \rangle_p - \langle X \rangle_a \qquad \text{Eq. [5.9]}$$

The results of this computation are listed in table [5.6].

	Ø1	Ø2	Ø3	Ø4	H1	H2	H3
1150°C	-0.004	-0.007	-0.007	-0.001	0.006	-0.002	0.005
1200°C	-0.017	-0.018	-0.014	-0.002	0.009	0.005	0.007
1250°C	-0.017	-0.024	-0.013	-0.003	0.006	0.003	0.001
1300°C	-0.025	-0.034	-0.011	0.000	0.007	0.006	0.000
1350°C	0.009	-0.008	0.017	0.029	-0.005	-0.003	-0.011

Tab. [5.6] Errors of estimation.

The second step is the evaluation of the precision of the predicted value. This has been provided by assigning the relevant ISO IT tolerance class according to the standard UNI EN 20286-1 [12]. As already explained in chapter one this method permits a comparison between the allowed deviation of an actual value from the nominal value of a dimension and the nominal dimension itself. The tolerance for any dimension can therefore be expressed as a dimensionless integer number corresponding to a tolerance class. In this case the tolerance class assumes a different meaning, since the nominal dimensions of the finished part are not considered. The tolerance class associated with the deviation of the predicted value from the actual value is used to estimate and rank the goodness of the prediction, and not to evaluate the precision of a process. The results are listed in table [5.7].

	Ø1	Ø2	Ø3	Ø4	H1	H2	H3
1150°C	3	4	4	3	5	3	4
1200°C	6	6	6	3	6	5	5
1250°C	6	7	5	3	5	4	3
1300°C	7	7	5	3	5	5	3
1350°C	4	4	6	7	4	4	6

Tab. [5.7] ISO-IT tolerances, values lower than 3 have been considered with the tolerance class IT 3.

All errors are reported in a chart in figure [5.11], and in figure [5.12], they are compared with the relative tolerance level.

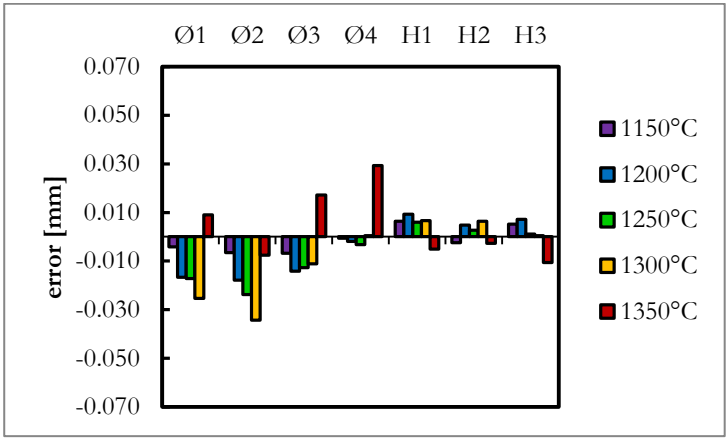

Fig [5.11] Difference between the actual value and the predicted one.

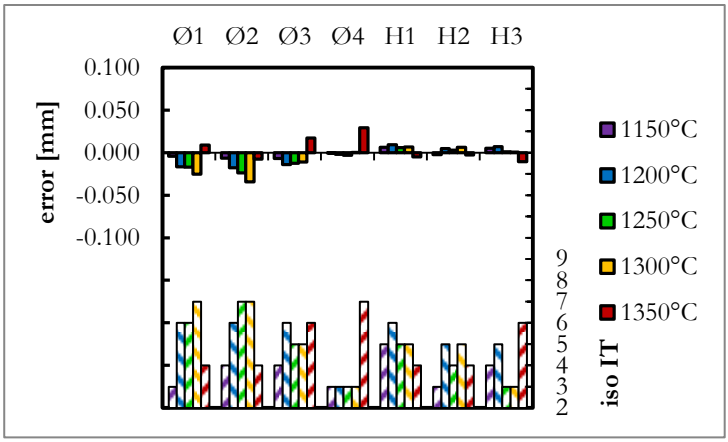

Fig. [5.12] Error and relative tolerance class.

The maximum absolute error of estimation is 34 μm, while the average deviation is around 10 μm. The widest tolerance class achieved is IT 7. Comparing these results with the precision usually assigned to the press and sinter technology, according to the ASSINTER [13] indications, the overall goodness of estimation is acceptable. The estimation of the diameter dimensions is generally less accurate than the estimation for the heights, in fact the prediction of the heights is generally overestimated (predicted heights are usually higher than the actual ones) and the prediction of the diameters is generally underestimated (predicted diameters are usually bigger than the actual ones). This last condition on the diameters has to be evaluated carefully during the design process, some unexpected coupling interference may occur. About the influence of the sintering temperature, the prediction accuracy tends to decrease on increasing the temperature. The error evaluated at the highest temperature seems to have an opposite trend with respect to the others.

5.3 Monte Carlo simulation.

The model developed to predict the anisotropy of the dimensional variations can be compared to a system, where the state variables are the isotropic dimensional variations ε_i and the green dimensions. In the scheme reported in figure [5.2] the variable ε_i is the way the process parameters influence the anisotropy. This model can be slightly modified in order to include the final dimensional variations. Figure [5.13] shows the variables affecting the estimation error.

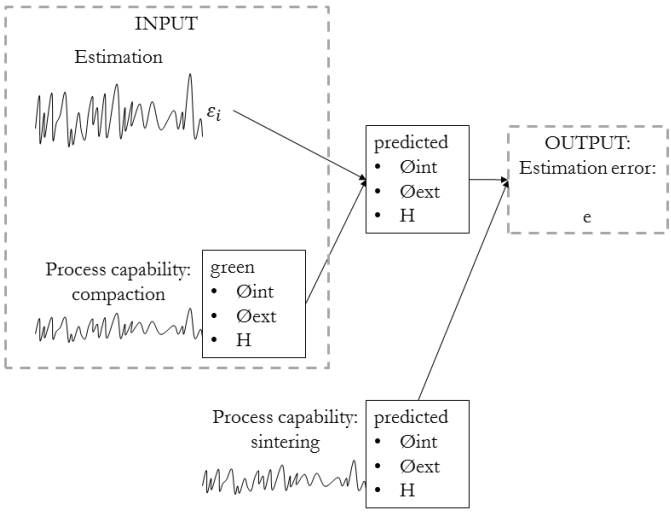

Fig. [5.13] Influence of the input variability on the error of estimation.

From the designer point of view, ε_i and the dimensions of the green part can be estimated on the basis of process parameters. The aim of this work is to provide a tool for the prediction of the dimensional variations. The model developed has proven to be successful when the input values are actual values. The behavior of this model compared with the variability of this input needs to be evaluated. The variability of the isotropic dimensional variation is due to the accuracy of the method used to estimate it, the variability of the green dimensions is due to the compacting process capability. Moreover the error of estimation, which is used to rank the goodness of the prediction, is computed by the deviation of the predicted value from the actual value. This actual value is not a nominal dimension but a measured dimension, thus implies a certain variability, which is directly related to the overall process capability. Summarizing, the model prediction accuracy is affected by three parameters:

1. the distribution of the green sample dimensions due to the process capability of the compaction step;
2. the densification estimation, which can be predicted or measured within a certain error; in this work the error of estimation has been evaluated as $\pm$ 10% of the value ε_i;
3. the distribution of the sintered sample dimensions due to the process capability of the sintering step.

5.3.1 Parameter simulation.

The process capability has been simulated by varying the dimensions. The variation is centered in the mean measured value between a lower boundary and an upper boundary identified with the minimum measured value and the maximum measured value through a specific distribution of probability that will be later explained in detail. The validation of this model, by means of random values simulating the process capability, estimates the degree of reliability of the model itself. A Monte Carlo simulation has been performed to test the model reliability. In figure [5.14] is shown a flow chart explaining how the simulation has been implemented using the software Matlab®.

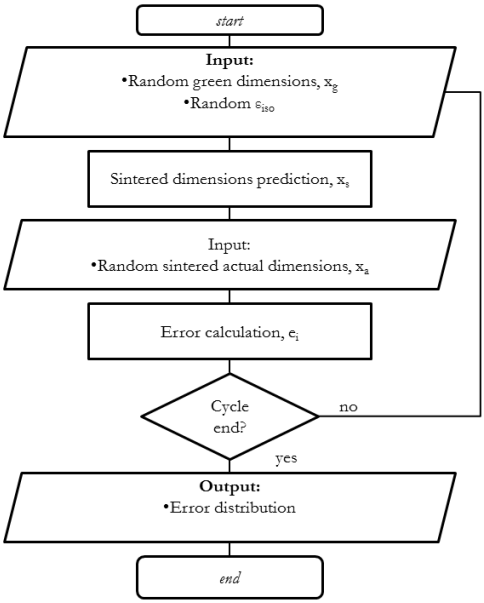

Fig. [5.14] Monte Carlo simulation flow chart.

The test shown in figure [5.14] is built of two main parts, the first is a cycle where the test is performed several times by opportunely varying some parameters, the second part gives the frequency distribution of all the results collected during the cycle. The cycle is made by a sequence of four main operations:

1. input the green dimensions and the expected densification $[X]_g$, ε_i

2. predict the sintered dimensions using the developed procedure $\langle [X]_s \rangle_p$
3. input the actual sintered dimensions $\langle [X]_s \rangle_a$
4. calculate the error $[e] = \langle [X]_s \rangle_p - \langle [X]_s \rangle_a$

The green dimensions, the actual sintered dimensions and the expected densification are the varying parameters which assume a different value every cycle. The variation of those parameters has been simulated using a uniform distribution (Ross [14]).

$$\begin{cases} p = 0 & x < x_{min} \\ p = \frac{1}{x_{max} - x_{min}} & x_{min} \leq x \leq x_{max} \\ p = 0 & x_{max} < x \end{cases}$$

Given a uniform distribution (figure [5.4]) any value x within the interval between the minimum value, x_{min} and the maximum value, x_{max} has the same probability p. Usually an industrial process has a distribution closer to a Gaussian one (Ullman [15]), so the probability p of a value x is higher the closer to the mean value the value x is. Using a uniform distribution leads to a precautionary analysis. The value of each parameter ($[X]_g$, $[X]_s$, ε_i) has been chosen from its related distribution as a random value generated within the interval. The number of iteration has been optimized to 10^5.

Concerning the reliability of this model three different tests have been performed.

1. Stability test. The model stability has been evaluated by varying the parameters that are influenced by the designer's decisions, assuming the process to be ideal, with no variability. The parameters related to the process ($[X]_g = [\bar{X}]_g$, $[X]_s = [\bar{X}]_s$) have been kept constant and equal to their mean value every cycle iteration, only varying the parameter related to the densification.
2. Robustness test. The robustness has been evaluated assuming that the model precision is affected only by external variability as the process capability. The parameters related to the process have been assumed varying with every iteration while the parameter ε_i has been kept constant and equal to the mean value.
3. Reliability. This third test is a combination of the two former tests, in this case all the parameters have been varied at every iteration, giving the reliability of the whole design model.

The operating conditions of the three tests are summarized in table [5.8].

	Test1: stability	Test2: robustness	Test3: reliability
$[\boldsymbol{X}]_{\boldsymbol{g}}$	$[\mathrm{X}]_{\mathrm{g}} = [\overline{\mathrm{X}}]_{\mathrm{g}}$	varying	varying
$[\boldsymbol{X}]_{\boldsymbol{s}}$	$[\mathrm{X}]_{\mathrm{s}} = [\overline{\mathrm{X}}]_{\mathrm{s}}$	varying	varying
$\boldsymbol{\varepsilon_i}$	varying	$\varepsilon_{\mathrm{i}} = \overline{\varepsilon_{\mathrm{i}}}$	varying

Tab. [5.8] Test1, test2, test3 (stability, robustness, reliability) parameters.

The tests have been performed for each component and for each condition using the design procedure already described for the four cases of study.

5.3.2 Stability.

As mentioned before, the stability of this model has been studied varying the parameter $\boldsymbol{\varepsilon_i}$ and keeping constant the green and the sintered dimensions. The test conditions are summarized in table [5.9].

	Test1: stability
$[\boldsymbol{X}]_{\boldsymbol{g}}$	$[\mathrm{X}]_{\mathrm{g}} = [\overline{\mathrm{X}}]_{\mathrm{g}}$
$[\boldsymbol{X}]_{\boldsymbol{s}}$	$[\mathrm{X}]_{\mathrm{s}} = [\overline{\mathrm{X}}]_{\mathrm{s}}$
$\boldsymbol{\varepsilon_i}$	varying

Table [5.9] Stability test parameters.

At the end of the simulation the mean error has been computed as well as the maximum error and the minimum error. The results are summarized in the following, figures from [5.15] to [5.19].

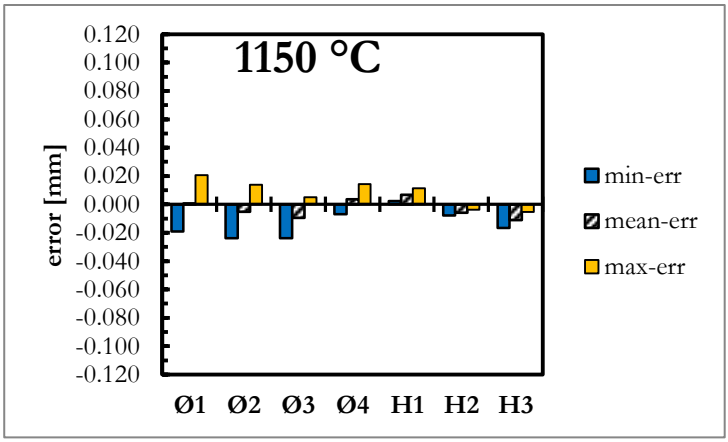

Fig. [5.15] Stability test results, 1150 °C.

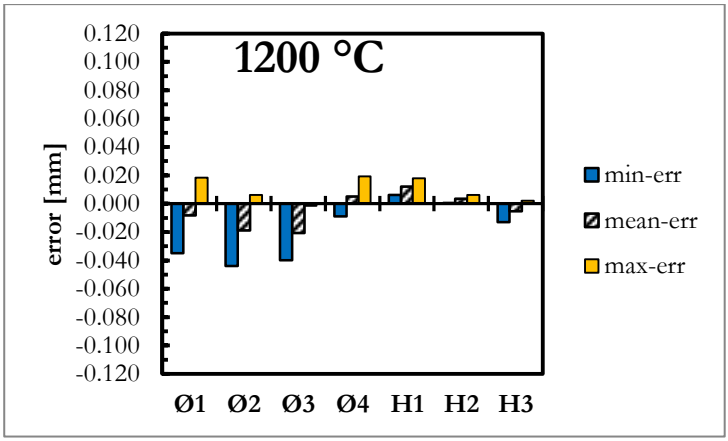

Fig. [5.16] Stability test results, 1200 °C.

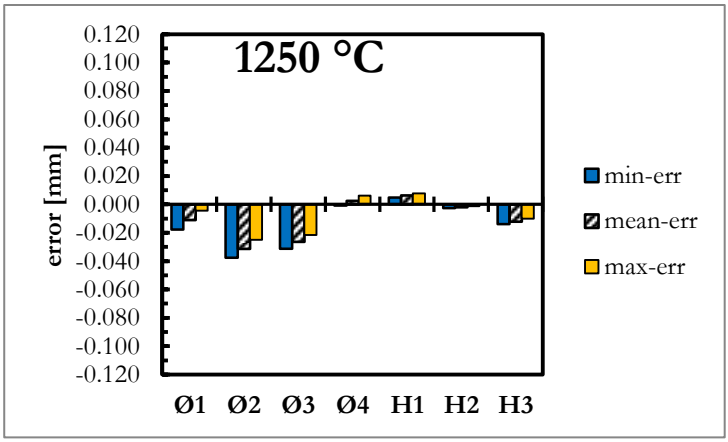

Fig. [5.17] Stability test results, 1250 °C.

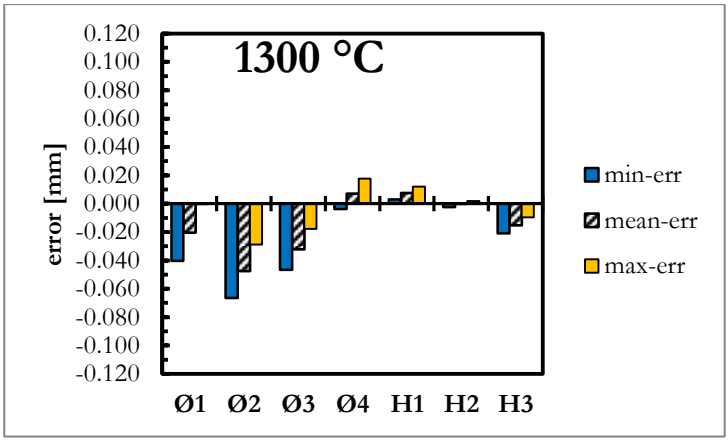

Fig. [5.18] Stability test results, 1300 °C.

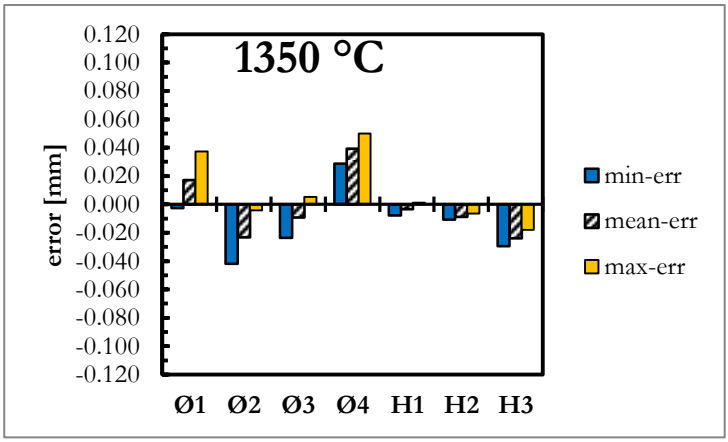

Fig. [5.19] Stability test results, 1350 °C.

Figures from [5.15] to [5.19] show that the stability is affected more by the prediction of the diameter dimensions than by that of the heights dimensions, despite the difference being small. No significant trends with respect to the temperature have been observed. The model has proven to be rather stable since the maximum and the minimum errors are close to the mean error.

5.3.3 Robustness.

The robustness of the model has been studied varying the process parameters such as the green dimensions and the actual sintered dimensions, keeping constant the densification parameter $\varepsilon_i = \overline{\varepsilon_i}$. The test conditions are summarized in table [5.10].

	Test2: robustness
$[X]_g$	varying
$[X]_s$	varying
ε_i	$\varepsilon_i = \overline{\varepsilon_i}$

Tab. [5.10] Robustness test parameters.

At the end of the simulation the mean error has been computed as well as the maximum error and the minimum error. The results are summarized in figures from [5.20] to [5.24].

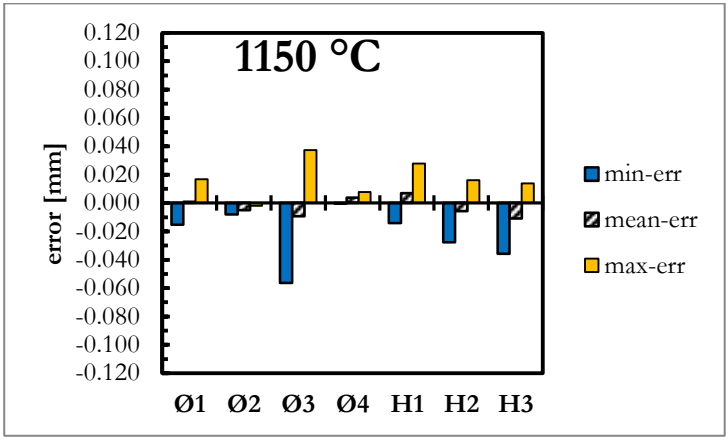

Fig. [5.20] Robustness test results, 1150 °C.

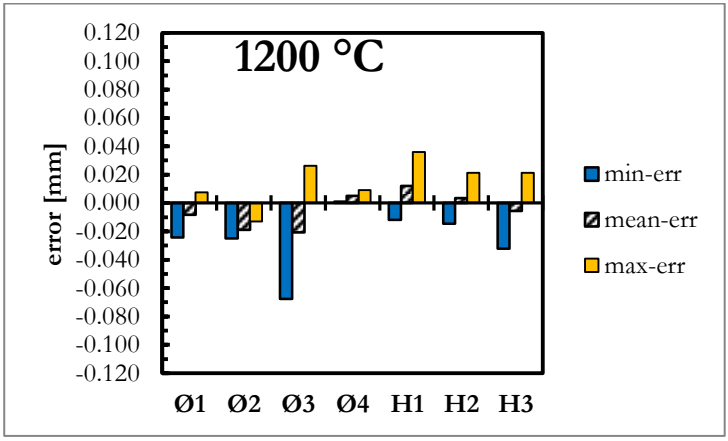

Fig. [5.21] Robustness test results, 1200 °C.

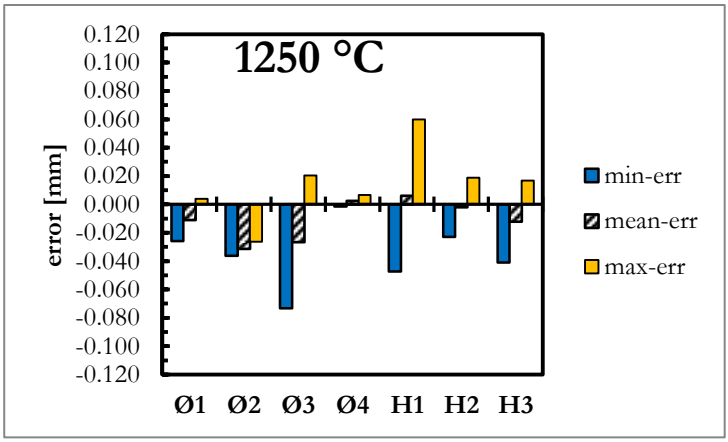

Fig. [5.22] Robustness test results, 1250 °C.

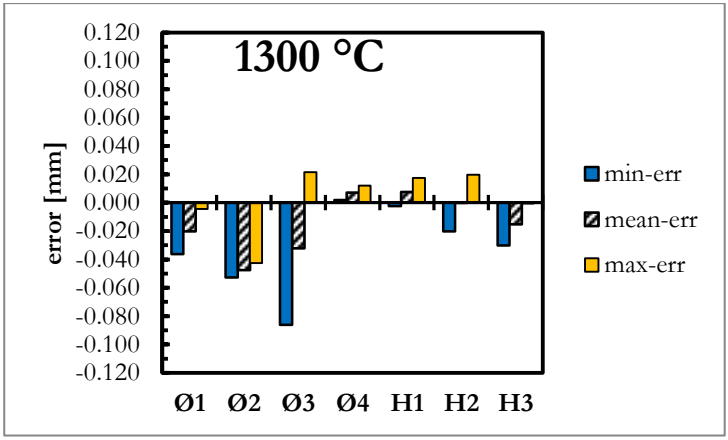

Fig. [5.23] Robustness test results, 1300 °C.

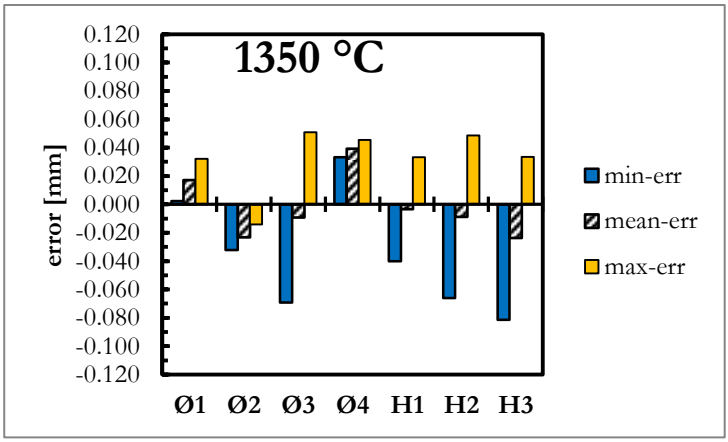

Fig. [5.24] Robustness test results, 1350 °C.

Considering the results reported from figure [5.20] to figure [5.24] the mean error seems to be similar to the one coming from the stability tests, while the minimum and the maximum errors are significantly higher. The robustness is the way the model is directly influenced by the process capability. In this test the role of the process capability has proven to be very important. When values with a high deviation from the mean are processed, then the precision of the model is heavily influenced.

5.3.4 Reliability.

The overall reliability of the model has been studied varying all the parameters. The test conditions are summarized in table [5.11].

	Test3: reliability
$[X]_g$	varying
$[X]_s$	varying
ε_i	varying

Tab. [5.11] Reliability test parameters.

At the end of the simulation the mean error has been computed as well as the maximum error and the minimum error. The results are summarized in figures from [5.25] to [5.29].

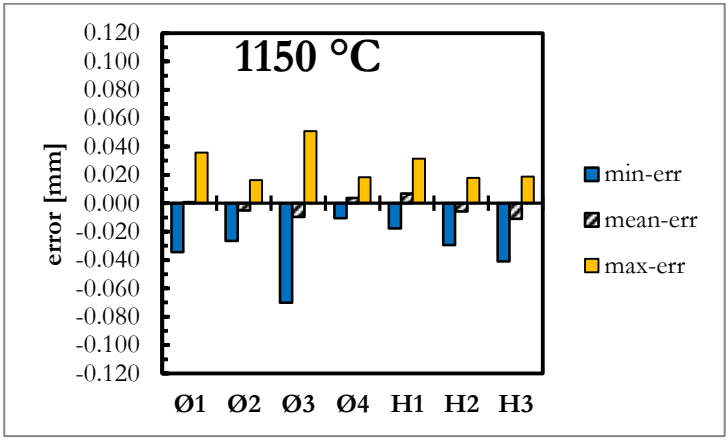

Fig. [5.25] Reliability test results, 1150 °C.

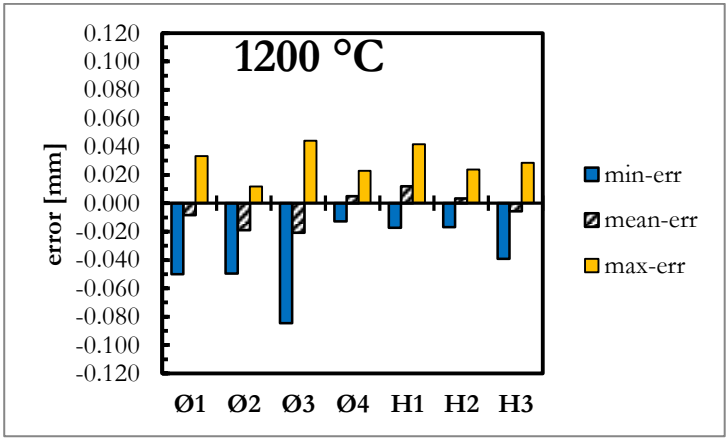

Fig. [5.26] Reliability test results, 1200 °C.

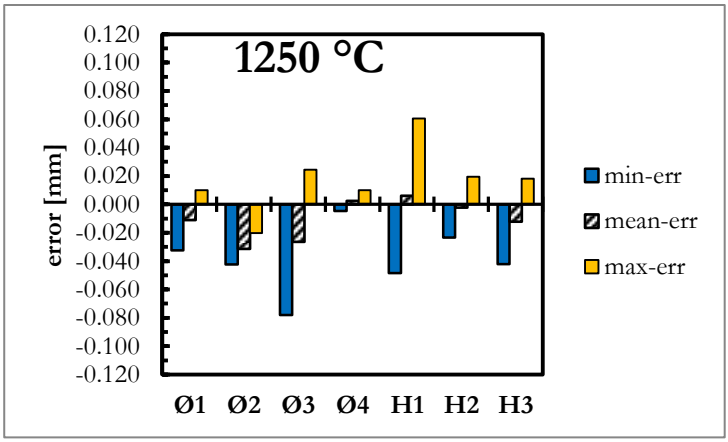

Fig. [5.27] Reliability test results, 1250 °C.

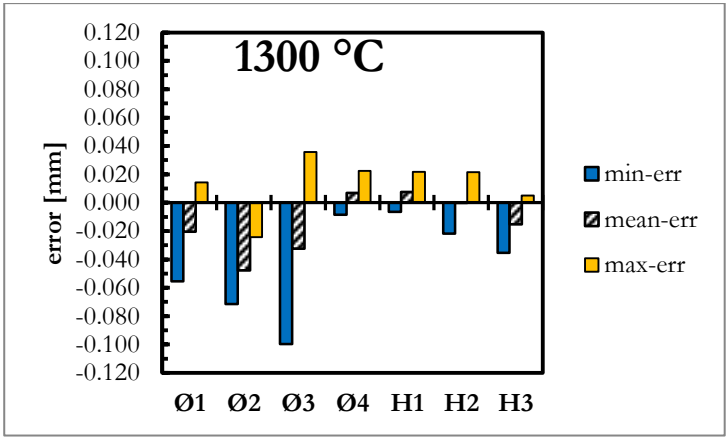

Fig. [5.28] Reliability test results, 1300 °C.

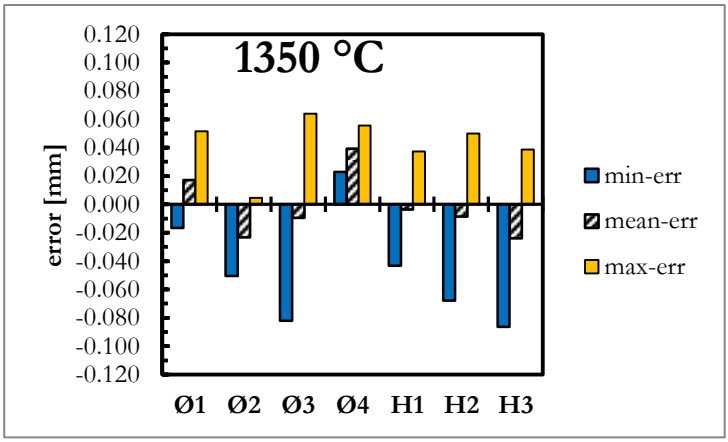

Fig. [5.29] Reliability test results, 1350 °C.

The reliability is the result of the combination of stability and robustness, therefore the precision of the prediction is lower than that of each single test, this leads to a wider distribution of the test outcome as it can be observed from figures [5.25] to [5.29]. The error distribution is represented in figures [5.30] to [5.34].

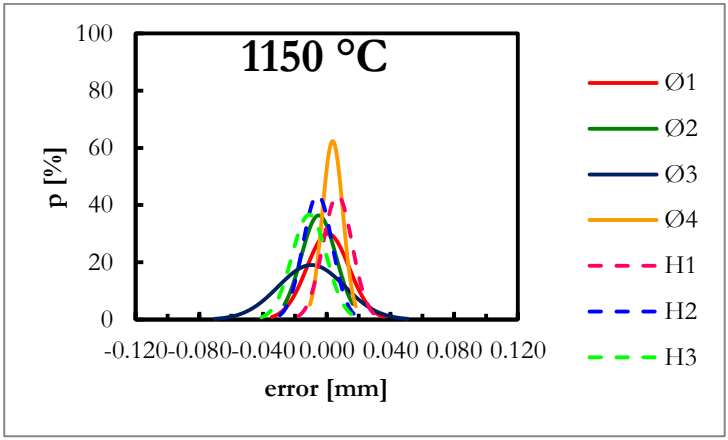

Fig. [5.30] Error dispersion test distribution, 1150 °C.

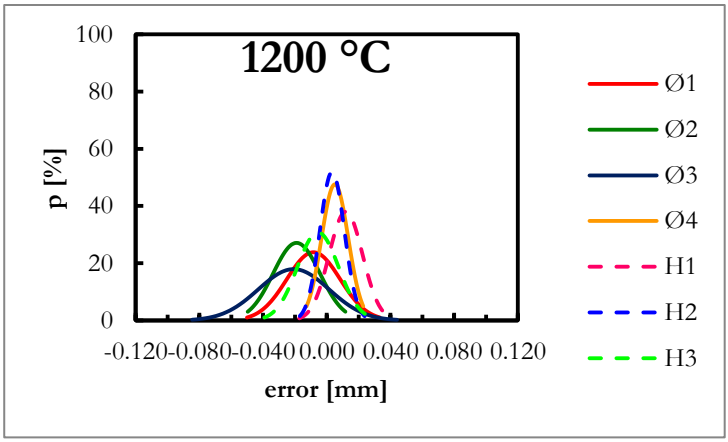

Fig. [5.31] Error dispersion test distribution, 1200 °C.

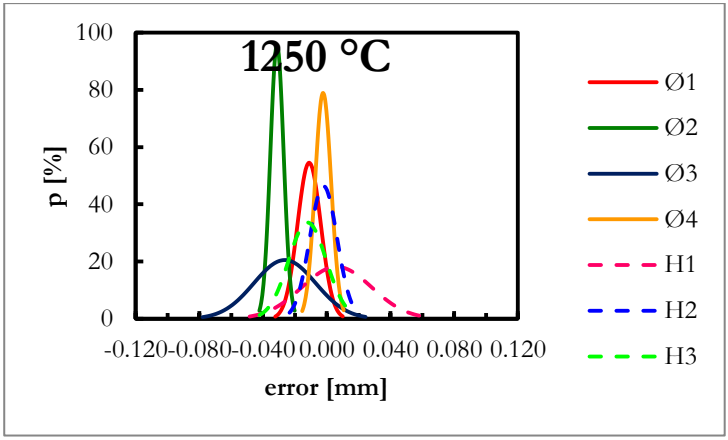

Fig. [5.32] Error dispersion test distribution, 1250 °C.

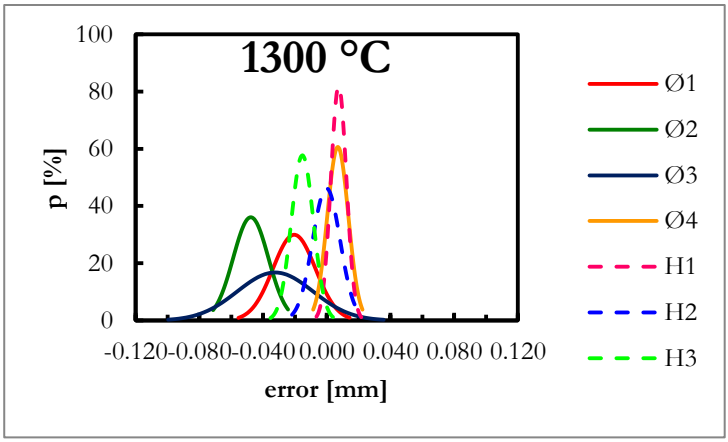

Fig. [5.33] Error dispersion test distribution, 1300 °C.

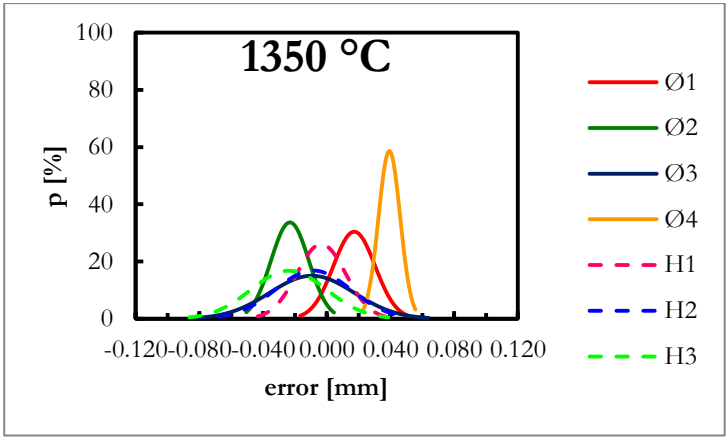

Fig. [5.34] Error dispersion test distribution, 1350 °C.

The error distribution represents the accuracy and the precision of the prediction procedure. The closer to the null value the distribution peak is, the higher is the accuracy, since the mean error is close to zero. The narrower the distribution is, the higher is the precision, since the density probability is closer to the mean value. Despite the accuracy being closer to the one coming from the validation test, the precision is highly influenced by the process capability. This means that the most efficient way to improve the behavior of the model is to reduce the scatter of the dimensions. The results also show that there is no clear evidence of an influence of the sintering temperature on the reliability of the model. This conclusion leads to two main

considerations. First, the model effectiveness is not affected by the magnitude of the dimensional variation, Second, and most important, the predictive model can be used to estimate the dimensional variation of the sintered parts on a wide range of process conditions with a good reliability, since the parameter depending on the process conditions is ε_i. Moreover the level of confidence related to the goodness of the estimation can be evaluated with an opportune consideration of the process capability, since it is the most influent parameter on the error distribution. By first approximation it is reasonable to assume that the error distribution of the predictive procedure can be considered the same as the process capability.

5.4 Conclusions

The model to predict the anisotropy of the dimensional variations has been developed in chapter four. This model, combined with the definition of the anisotropy parameter given in chapter three, has been implemented in a procedure, which can estimate the dimensional change on sintering of an axi-symmetric PM part, and in turn the final dimensions of the sintered part. This procedure is divided in three steps. In the first step the part is broken down to an n-level structure, which reminds of the powder columns during compaction. The second operation is the prediction of the dimensional variation for the n concentric rings that have been generated. Once all the dimensional variations are predicted in the last step the geometrical congruence has to be restored and the dimensions of the sintered part are provided.

The prediction of the dimensional variation for a given ring is possible by means of a model which can be described by a box model, where the inputs are the isotropic dimensional variation and the green dimensions, and the outputs are the sintered dimensions. This model has been validated on a mechanical component produced using Chromium steel powder. The results of the prediction have been satisfactory since the estimated error of prediction revealed to be lower than the tolerance level typical of the sintered components.

Being the design parameters affected by the variation due to the process capability, the model has been tested to evaluate its reliability. The reliability has been evaluated by a Monte Carlo method, where the design procedure has been perturbed by a noise simulating the process capability or the variation of ε_i, in other words the variability of the input parameters. The results have been collected and processed to obtain some error dispersion curves in order to evaluate the accuracy and the precision of the model. The error has been revealed to be influenced mostly by the process capability, rather than the parameter ε_i. This means that the model developed on the basis of the experimental correlation between ε_i and the anisotropy has a solid validity. Finally, no significant trend describing the influence of the sintering temperature has been highlighted.

5.5 References

1. H.E. Exner; G. Petzow, A critical evaluation of shrinkage equations, Proceedings of the fifth international conference on sintering and related phenomena, (1980), Material Science Research: 13, Plenum Press G. C. Kuczynsky Editor
2. Eugene A. Olevsky, Theory of sintering: from discrete to continuum, Materials Science and Engineering R23 (1998) pp 41- 100
3. Hunghai Su; D. Lynn Johnson - Master Sintering Curve: A Practical Approach to Sintering - Journal of the American ceramic society 79, 12 (1996) pp 3211 - 3217
4. Randall M. German, Sintering: From Empirical Observations to Scientific Principles (2014) 1st ed. Elsevier Butterworth-Heinemann
5. N. Corsentino; C. Menapace; I. Cristofolini; M. Pilla; M. Larsson; A. Molinari, The influence of the liquid phase on anisotropic dimensional change on sintering iron alloys, The International Journal of Powder Metallurgy 51, 2 (2015) pp 27 - 38
6. Cristofolini, I., Corsentino, N., Pilla, M., Molinari, A., Larsson, M., 2013, "Influence of the geometry on the anisotropic dimensional change of PM parts", proc. "Advances in Powder Metallurgy and Particulate Materials 2013", Chicago – IL, June 24-27, (2013), vol.11, pp. 49 - 61
7. Molinari, A., Emanuelli, L., Menapace, C., Cristofolini, I., Larsson, M., 2014, "Influence of Sintering Temperature on Shrinkage Anisotropy in Cr-Mo Low Alloy Steel Green Compacts", Advances in Powder Metallurgy and Particulate Materials 5 (2014) pp 99 - 107
8. A. Zavaliangos; J.M. Missiaen; D. Bouvard, Anisotropy in Shrinkage During Sintering, Science of Sintering 38, 1, (2006) pp 13 -26
9. A. Molinari; C. Menapace; E. Torresani; I. Cristofolini; M. Larsson, A study of sintering shrinkage kinetics of cold compacted ferrous green parts Metal Powder Industries Federation in ADVANCES IN POWDER METALLURGY AND PARTICULATE MATERIALS; 1; 05-25-05-32; Powder metallurgy & particulate materials (2013)
10. Robert L. Mott, P.E. Machine elements in mechanical design 5th edition (2013) PearsonChoiche
11. G.F. Bocchini, Influence of process parameters on precision of PM parts, Powder Metallurgy 28 (1985) pp 155 - 165
12. UNI EN 20286-1:1995, ISO 286/1
13. ASSINTER - Guida alla progettazione dei componenti sinterizzati - (technical gudelines from the Italian society of PM parts producers)
14. Sheldon M. Ross - Special Random Variables - Introduction to Probability and Statistics for Engineers and Scientists 3rd Edition (2004) Elsevrier
15. David G. Ullman - Product generation - the mechanical design process 4th Edition (2010) Mc Graw Hill Higher Education

Conclusions

The aim of this work is to provide a straight answer to the complex question regarding the prediction of the dimensional variations on sintering of PM parts, in particular to evaluate the influence of the part's geometry and the process parameters.

The method used to study this phenomenon has been principally experimental. The sampling analyzed has been designed from previous experimental studies. The experimental work has been carried out on disks and rings of different dimensions, designed to have a progressive height to thickness ratio. These samples comprehend a wide range of sizes typical of the press and sinter process. The material used for this explorative experimental campaign has been iron powder, being iron alloys the most used materials in PM press and sinter. All the samples have been measured with a Coordinate Measuring Machine. This method allowed to determine the dimensions of the specimen with high precision and accuracy, by scanning a high density of points on the sample's surfaces.

From an analytical point of view the definition of anisotropy has been formalized, being the several pre-existing definitions not satisfactory for the scope of this work. This step has been of fundamental importance not only for the analysis of the data but also for the development of a predicting procedure for the anisotropic dimensional variation of the sintered part. The analytical description of anisotropy has been derived from the definition of the dimensional variations and from two main assumptions:

- The volume of a part is always evaluable by the measured dimensions.
- The volume variation only depends on the densification despite the amount of anisotropy.

The first assumption implies that the geometrical characteristics of the parts are kept, without significant distortions. The second has been the basis to define the parameter called isotropic dimensional variation. Under these assumptions, the change in volume has been analytically defined by means of the isotropic dimensional change, and by means of the anisotropic dimensional changes. The relationship among these entities allowed defining an anisotropy parameter K, representing how far are the actual, anisotropic dimensional variations from the isotropic behavior.

The samples have been measured before and after the sintering process, three different temperatures under the same operative conditions were considered. The dimensional variations have been computed and analyzed. Three are the main results:

- On increasing the sintering temperature the dimensional variations increase as well.
- The dimensional variations are anisotropic at all three temperatures.

- There is a linear dependence between the variation of the internal diameter and the external diameter. This variation has been described with a linear equation, the coefficients of which depend on the height of the ring and on the internal to external diameter ratio.

The anisotropy coefficient has been computed for all the geometries and the sintering conditions. This parameter has been referred to as the isotropic dimensional variation and two important relations have been found:

- On increasing the isotropic dimensional variation the anisotropy parameter decreases with a non-linear monotonic relation. This implies that the higher the densification, the higher is the dimensional variation, the lower is the amount of anisotropy.
- With respect to the geometrical parameters, no monotonic trend could be highlighted for the sampling analyzed.

An inversely proportional model to fit the anisotropy coefficient value versus the isotropic dimensional variation has been proposed, the coefficient of this model has been found to be dependent on the diameters ratio, well fitted by a second order polynomial. This model based on experimental data is the basis for the prediction of the anisotropy of the dimensional variation.

The model separates the contribution of the process form the contribution of the geometry. The contribution of the geometry is expressed by the dimensions measured on the green sample. The contribution of the process parameters is given by the isotropic dimensional variation, which is related to the densification occurring during the sintering process, in turn affected by all the process parameters (powder, compaction and sintering).

The prediction of the dimensional variation has been possible thanks to a set of equations based on the anisotropy coefficient. This has been the starting point of a design procedure able to predict the sintered dimensions of an axi-symmetric PM part. This procedure has been developed on the basis that any PM component produced by rigid die compaction can be seen as composed by a series of concentric rings representing the powder columns during the compaction step. The main steps of this procedure are:

1. Part break-down to n concentric rings.
2. Prediction of the dimensional variation of each ring independently, using the model based on the anisotropic coefficient to account for the anisotropic dimensional variations.
3. Part build-up and restoring the geometrical congruence.
4. Estimation of the sintered part's dimensions from the known green part's dimensions.

This procedure has been validated on four structural chromium steel parts produced by press and sinter process. These parts have been measured before and after the sintering process at different temperatures. The dimensions of the sintered part have been estimated by applying the aforementioned procedure and then compared with the actual dimensions measured on the sintered parts. This analysis has provided the estimation error computed as the difference between the predicted value and the actual value. The error of estimation has been then used to compute the normalized ISO – IT tolerance class in order to evaluate the precision of the procedure. The results proved that this procedure predicts the sintered part's dimensions with a precision which is always higher than the precision of the process.

In the last part of this work a statistical simulation to evaluate the reliability of this procedure has been set up and performed. The procedure to predict the dimensional variations has been studied in terms of inputs and outputs. The inputs of this procedure are the dimensions of the green part and the densification parameter written as the isotropic dimensional variation. The output parameters are the predicted sintered part's dimensions and the estimation error. A Monte Carlo method has been used to simulate the variability of the inputs in order to simulate a perturbation of the value which is due to process capability. This noise signal has been iterated within the design procedure and the estimation error recorded. The reliability of this test has been divided into two contributions:

- Error on the densification parameter, which is a design parameter that has to be estimated. The precision of the outputs with respect to the variation of this parameter has been defined as stability, and it is related to the intrinsic precision of the model.
- Error on the dimensions, which is due to the physiologic variability of an industrial process (Robustness test, representing the precision of the outputs with respect to the variation of these parameters. This is related to the limit of application.

The results of these simulations revealed that the higher influence on the error distribution is due to the variation of the dimensional parameters, while the influence of the densification variability is negligible. This important result confirms that the design procedure is able to predict the dimensional variations accounting for the anisotropy within an error dispersion which depends basically on the process capability.

Future perspectives

From an experimental point of view the model presented in this work can be furtherly improved, in terms of both precision of estimation and correlation between the geometrical parameters, by the addition of some experimental points to the curve of the anisotropy coefficient versus the isotropic dimensional variation. An important step

may be the application of this approach also to non axi-symmetric shapes. Another investigation might involve a larger quantity of different materials to build the anisotropic coefficient's curves.

Form a theoretical side, the anisotropy of the dimensional variations could be interestingly related to the mechanisms involved during the compaction and the sintering processes, again considering the influence of the geometry of the part.

The prediction procedure has been evaluated only on the critical dimensions of the part (heights and diameters). An interesting development may be the implementation of this model in a software assisted simulation, which is able to handle and process the tri-dimensional geometrical complexity in order to evaluate the dimensional variations also on the details characterizing the mechanical component. This might enhance the precision of the die design and hopefully decrease the amount of secondary operations needed to achieve the required dimensional tolerances.

Appendix A.

Anisotropy design chart.

Using the set of equations [4.3, 4.4, 4.5, 4.6], a design chart has been built, figure [A.1a] and figure [a.1b]. This design chart can be used to estimate the dimensional variations accounting for their anisotropic behavior. In figure [A.1] is shown a scheme a design method using the anisotropy design chart.

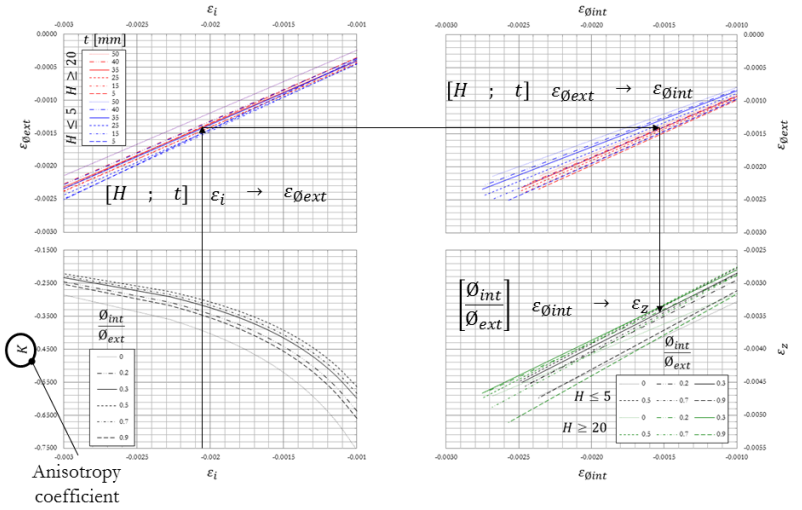

Fig. [A.1] Design method example for the anisotropy chart.

As depicted in figure [A.1] the anisotropy chart is made of four sub-charts each one representing one step of the design process for a ring-shaped part. The first step is left on top where the $\varepsilon_{\emptyset ext}$ yields from ε_i in function of the height and the wall thickness. In turn on the right top $\varepsilon_{\emptyset int}$ yields from $\varepsilon_{\emptyset ext}$ in function of the height and the wall thickness as well. Right on the bottom ε_z yields from $\varepsilon_{\emptyset int}$ in function of the diameter ratio. Left on the bottom a chart represents the anisotropy coefficient as a function of the isotropic dimensional variation.

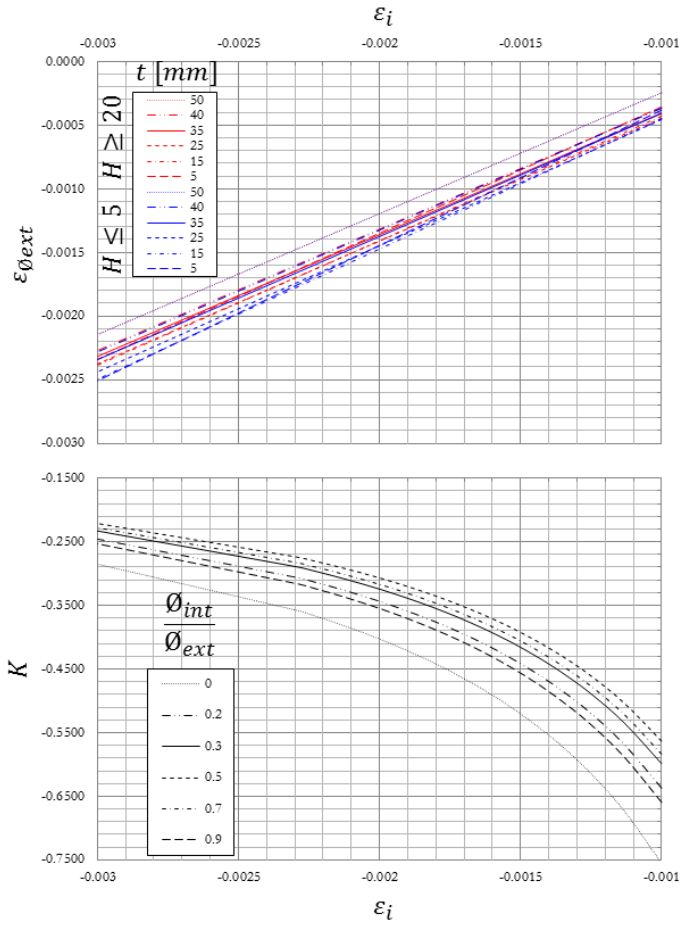

Fig. [A.2a] Anisotropy chart, (p 1/2) left.

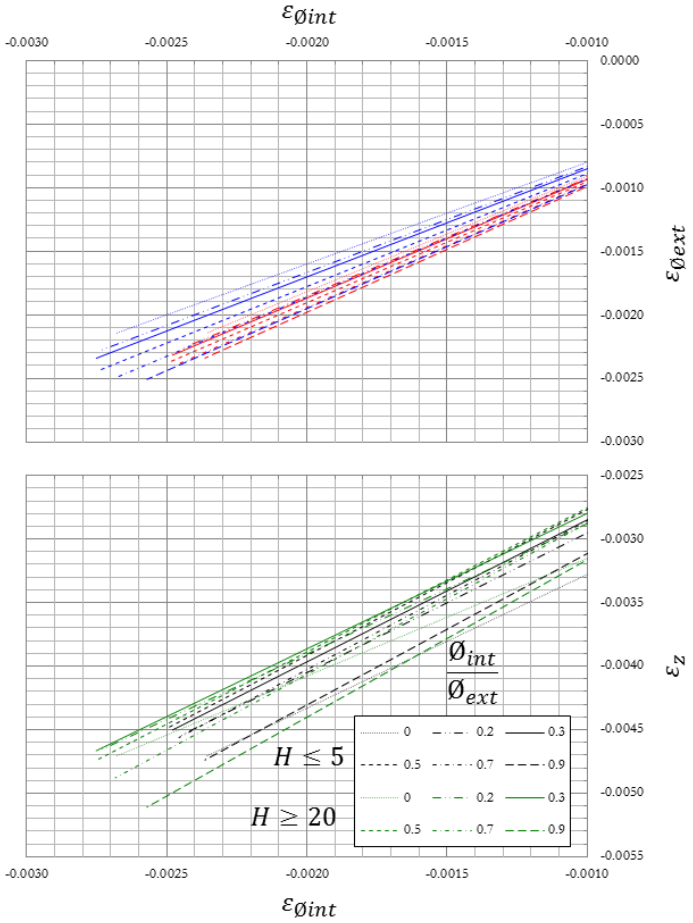

Fig. [A.2ab] Anisotropy chart, (p 2/2) right.

Appendix B.

Case of study: pulley.

Material: Fe-3%Cr-0.5%Mo-C.

B.1 Part and process description.

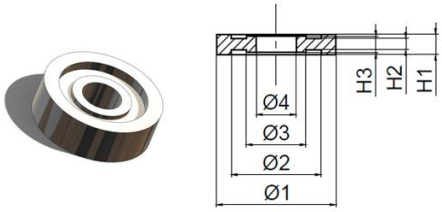

Fig. [B.1] Pulley, critical dimensions evaluated.

Label	Compaction speed [mm/s]	Green density [g/cm³]
665v05	5	6.65
665v20	20	6.65
68v05	5	6.8
68v20	20	6.8
68v50	50	6.8

Tab. [B.1a] Compaction conditions.

Sintering temperature [°C]	Heating rate [°C/min]	**Sintering** time [min]	Sintering atmosphere	Cooling rate [°C/min]
1250	5	30	Vacuum + N_2 backfill	5
1250	5	30	Vacuum + N_2 backfill	5
1250	5	30	Vacuum + N_2 backfill	5
1250	5	30	Vacuum + N_2 backfill	5
1250	5	30	Vacuum + N_2 backfill	5

Tab. [B.1b] Sintering conditions.

B.1.1 Part breakdown strategy

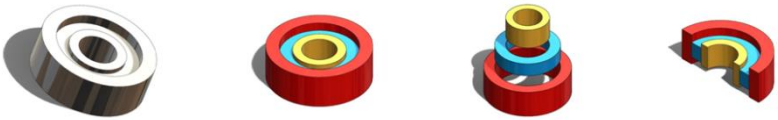

Fig. [B.2] Component break-down.

B.1.2 Actual dimensions, before and after sintering.

	∅1	∅2	∅3	∅4	H1	H2	H3
	60,133	45,053	30,026	19,983	20,010	10,092	15,987

Tab. [B.2a] Dimensions of the green samples.

	∅1	∅2	∅3	∅4	H1	H2	H3
665v05	-0,005	-0,005	-0,005	-0,005	-0,007	-0,007	-0,006
665v20	-0,005	-0,005	-0,005	-0,005	-0,007	-0,007	-0,006
68v05	-0,005	-0,005	-0,005	-0,005	-0,007	-0,006	-0,006
68v20	-0,005	-0,005	-0,005	-0,005	-0,007	-0,006	-0,006
68v50	-0,005	-0,005	-0,005	-0,005	-0,007	-0,007	-0,006

Tab. [B.2b] Dimensional variations in sintering.

	∅1	∅2	∅3	∅4	H1	H2	H3
665v05	59,841	44,839	29,896	19,885	19,857	9,959	15,834
665v20	59,836	44,836	29,893	19,886	19,826	9,954	15,784
68v05	59,874	44,860	29,910	19,893	19,903	10,062	15,945
68v20	59,870	44,855	29,906	19,893	19,885	10,075	15,912
68v50	59,870	44,856	29,907	19,894	19,864	10,057	15,875

Tab. [B.2c] Dimensions of the sintered samples.

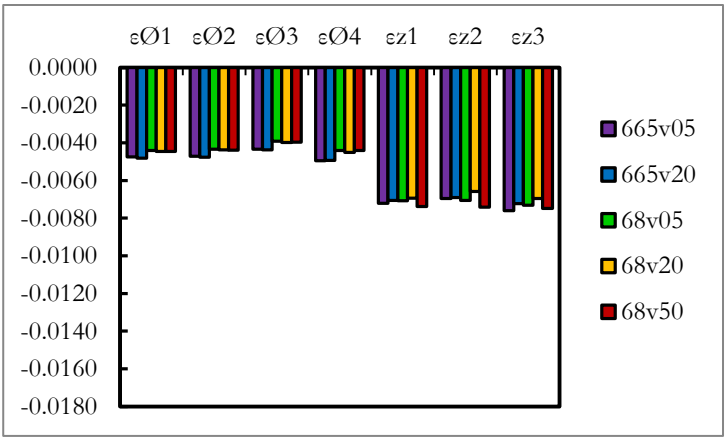

Fig. [B.3] Measured dimensional variations.

B.1.3 Design procedure. Estimation of the dimensional variation due to sintering.

	ε1	K	K	K
665v05	-0,006	-0,149	-0,145	-0,145
665v20	-0,006	-0,149	-0,145	-0,145
68v05	-0,005	-0,153	-0,150	-0,149
68v20	-0,005	-0,154	-0,150	-0,150
68v50	-0,005	-0,151	-0,147	-0,147

Tab. [B.3] Measured isotropic dimensional variations and computed anisotropy parameters.

	V2			V2			V3		
	εØext	εØint	εZ	εØext	εØint	εZ	εØext	εØint	εZ
665v05	-0,0050	-0,0053	-0,0072	-0,0049	-0,0052	-0,0067	-0,0048	-0,0050	-0,0065
665v20	-0,0050	-0,0053	-0,0072	-0,0049	-0,0052	-0,0068	-0,0048	-0,0050	-0,0065
68v05	-0,0048	-0,0050	-0,0069	-0,0047	-0,0049	-0,0065	-0,0046	-0,0048	-0,0062
68v20	-0,0047	-0,0050	-0,0069	-0,0046	-0,0049	-0,0064	-0,0045	-0,0047	-0,0062
68v50	-0,0049	-0,0052	-0,0071	-0,0048	-0,0051	-0,0066	-0,0047	-0,0049	-0,0064

Tab. [B.4] Predicted dimensional variations for each level.

	Ø1	Ø2	Ø3	Ø4	H1	H2	H3
665v05	59,841	44,839	29,896	19,885	19,857	9,959	15,834
665v20	59,836	44,836	29,893	19,886	19,826	9,954	15,784
68v05	59,874	44,860	29,910	19,893	19,903	10,062	15,945
68v20	59,870	44,855	29,906	19,893	19,885	10,075	15,912
68v50	59,870	44,856	29,907	19,894	19,864	10,057	15,875

Tab. [B.5a] Actual dimensions. Measured dimensions of the sintered parts.

	Ø1	Ø2	Ø3	Ø4	H1	H2	H3
665v05	59,824	44,818	29,875	19,883	19,858	9,962	15,852
665v20	59,823	44,816	29,874	19,884	19,824	9,955	15,796
68v05	59,851	44,833	29,884	19,886	19,907	10,068	15,962
68v20	59,854	44,833	29,884	19,888	19,887	10,076	15,924
68v50	59,841	44,824	29,878	19,883	19,870	10,065	15,892

Tab. [B.5a] Predicted dimensions. Computed dimensions of the sintered parts.

B.1.4 Error of estimation.

	Ø1	Ø2	Ø3	Ø4	H1	H2	H3
665v05	-0,017	-0,021	-0,020	-0,002	0,001	0,002	0,018
665v20	-0,013	-0,020	-0,019	-0,002	-0,003	0,002	0,012
68v05	-0,023	-0,027	-0,026	-0,008	0,003	0,006	0,017
68v20	-0,017	-0,023	-0,022	-0,005	0,002	0,001	0,012
68v50	-0,028	-0,032	-0,029	-0,011	0,006	0,008	0,018

Tab. [B.6] Errors of estimation.

	Ø1	*Ø2*	*Ø3*	*Ø4*	*H1*	*H2*	*H3*
665v05	6	7	7	3	3	3	7
665v20	5	6	7	3	3	3	6
68v05	6	7	7	5	3	5	7
68v20	6	7	7	4	3	3	6
68v50	7	7	8	6	5	6	7

Tab. [B.7] ISO-IT tolerances, values lower that 3 has been considered with the tolerance class IT 3.

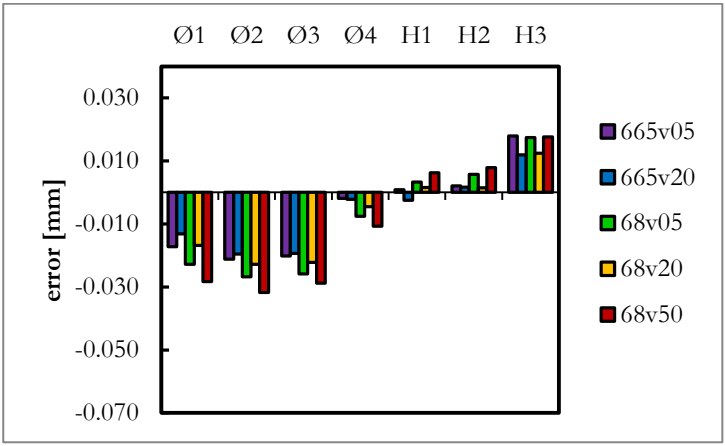

Fig [B.4] Difference between the actual value and the predicted one.

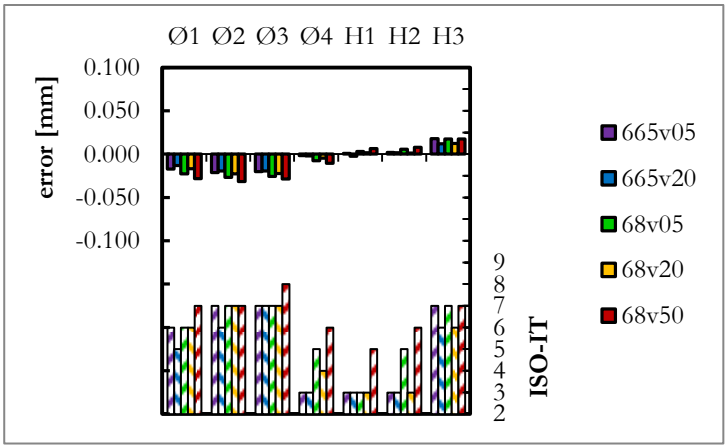

Fig. [B.5] Error and relative tolerance class.

B.2 Reliability

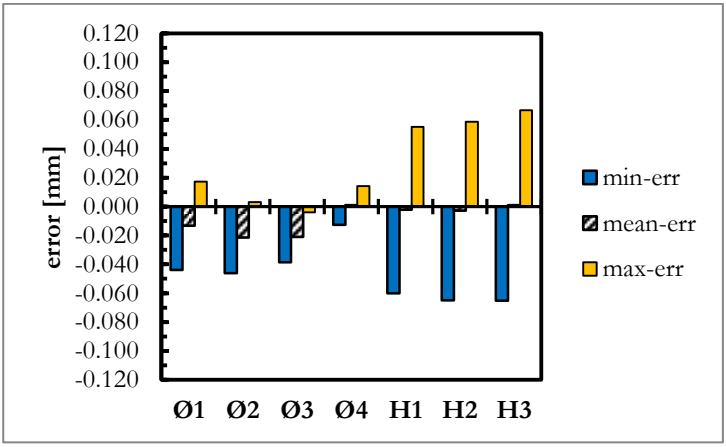

Fig. [B.6] Reliability test results,665v05.

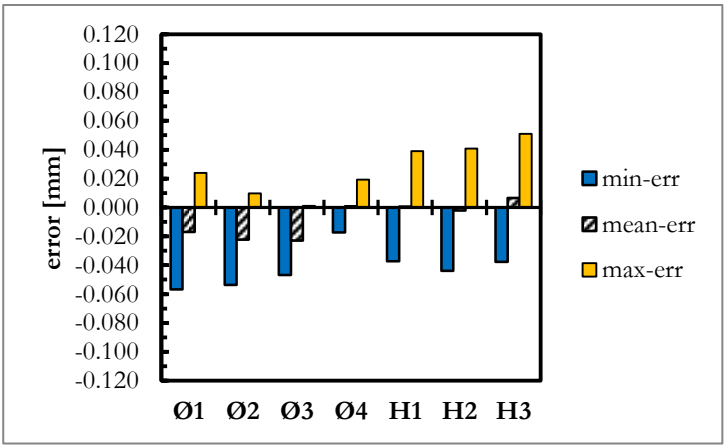

Fig. [B.7] Reliability test results,665v20.

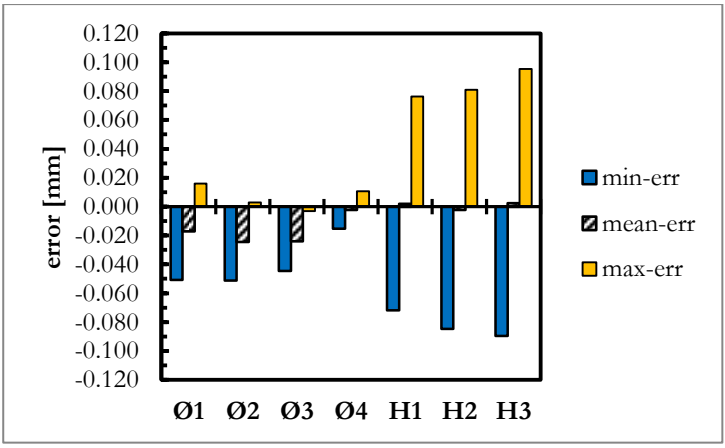

Fig. [B.8] Reliability test results,68v05.

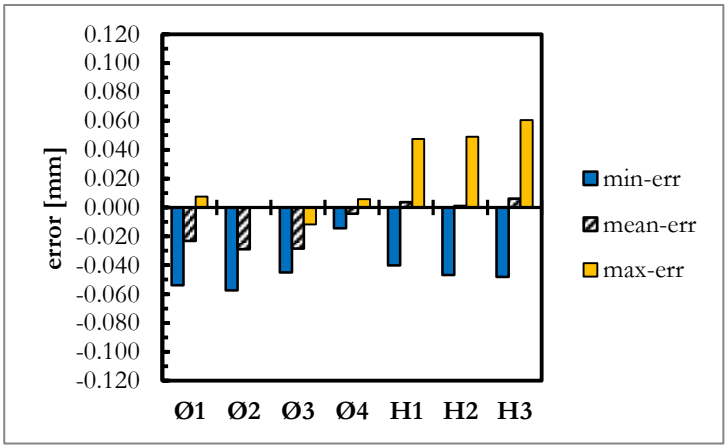

Fig. [B.9] Reliability test results,68v20.

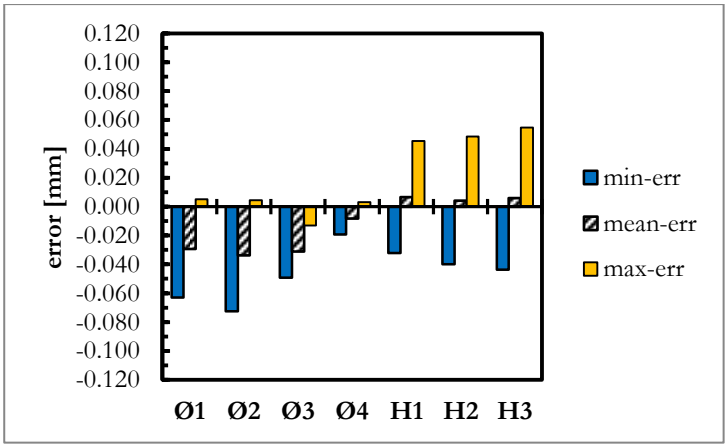

Fig. [B.10] Reliability test results,68v50.

Appendix C.

Case of study: flange.

Material: Fe-1.5%Cr-0.2%Mo-0.7%C.

C.1 Part and process description.

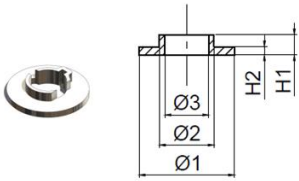

Fig. [C.1] Flange, critical dimensions evaluated.

Sintering temperature [°C]	Heating rate [°C/min]	**Sintering** time [min]	Sintering atmosphere	Cooling rate [°C/min]
1180	5	30	Vacuum + N_2 backfill	5
1360	5	30	Vacuum + N_2 backfill	5

tab. [C.1] (sintering conditions)

C.1.1 Part breakdown strategy

Fig. [C.2] Component break-down.

C.1.2 Actual dimensions, before and after sintering.

Ø1	Ø2	Ø3	H1	H2
48,210	27,633	22,251	4,056	10,310

Tab. [C.2a] Dimensions of the green samples.

	Ø1	Ø2	Ø3	H1	H2
1180°C	-0,004	-0,004	-0,004	-0,006	-0,006
1360°C	-0,011	-0,011	-0,011	-0,014	-0,014

Tab. [C.2b] Dimensional variations in sintering.

	Ø1	Ø2	Ø3	H1	H2
1180°C	48,078	27,550	22,181	4,018	10,254
1360°C	47,703	27,349	22,062	4,007	10,222

Tab. [C.2c] Dimensions of the sintered samples.

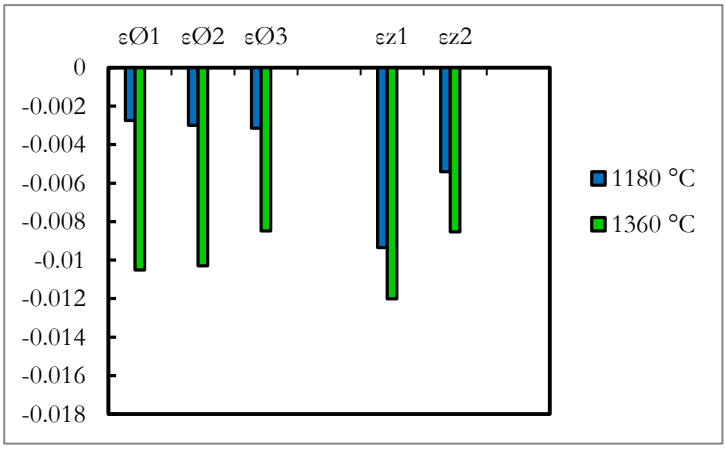

Fig. [C.3] Measured dimensional variations.

C.1.3 Design procedure. Estimation of the dimensional variation due to sintering.

	εi	K	K
1180°C	-0,004	-0,173	-0,185
1360°C	-0,012	-0,094	-0,099

Tab. [C.3] Measured isotropic dimensional variations and computed anisotropy parameters.

	V1			V2		
	εØext	εØint	εZ	εØext	εØint	εZ
1180°C	-0,0036	-0,0039	-0,0056	-0,0033	-0,0036	-0,0059
1360°C	-0,0110	-0,0119	-0,0138	-0,0103	-0,0111	-0,0144

Tab. [C.4] Predicted dimensional variations for each level.

	Ø1	Ø2	Ø3	H1	H2
1180°C	48,078	27,550	22,181	4,018	10,254
1360°C	47,703	27,349	22,062	4,007	10,222

Tab. [C.5a] Actual dimensions. Measured dimensions of the sintered parts.

	Ø1	Ø2	Ø3	H1	H2
1180°C	48,036	27,530	22,170	4,033	10,249
1360°C	47,680	27,317	22,003	4,000	10,161

Tab. [C.5a] Predicted dimensions. Computed dimensions of the sintered parts.

C.1.4 Error of estimation.

	Ø1	Ø2	Ø3	H1	H2
1180°C	-0,042	-0,021	-0,011	0,015	-0,005
1360°C	-0,023	-0,032	-0,059	-0,007	-0,061

Tab. [C.6] Errors of estimation.

	Ø1	Ø2	Ø3	H1	H2
1180°C	8	7	6	8	5
1360°C	7	8	9	6	10

Tab. [C.7] ISO-IT tolerances, values lower that 3 has been considered with the tolerance class IT 3.

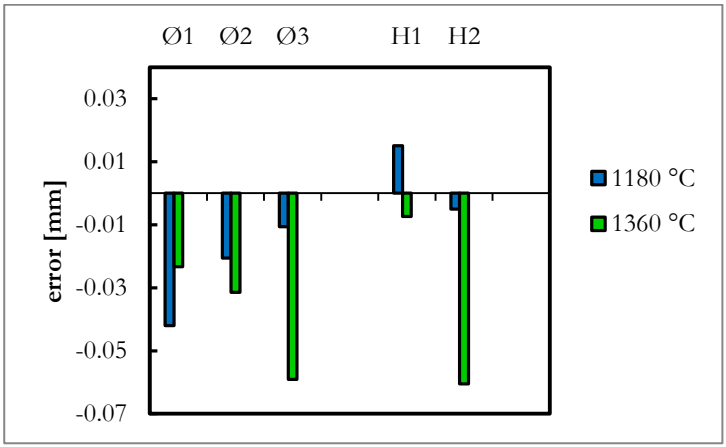

Fig [C.11] Difference between the actual value and the predicted one.

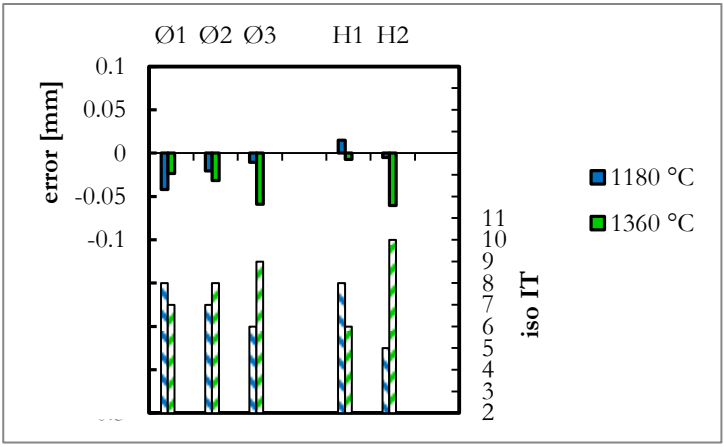

Fig. [C.12] Error and relative tolerance class.

C.2 Reliability.

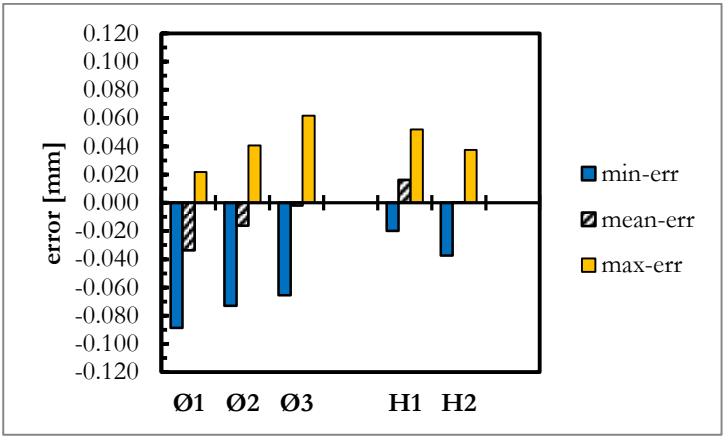

Fig. [C.13] Reliability test results,1180 °C.

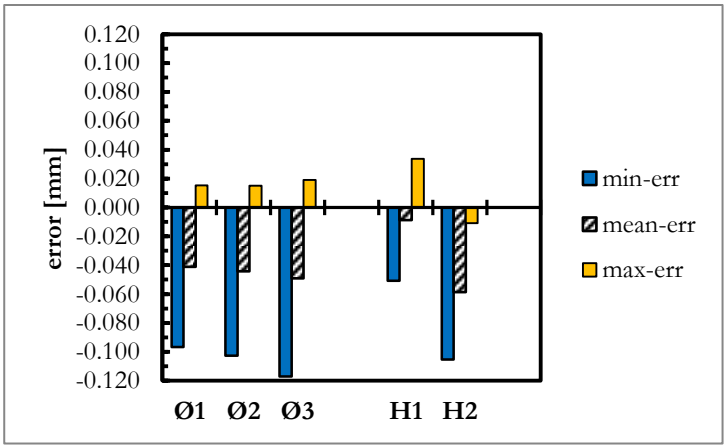

Fig. [C.14] Reliability test results,1360 °C.

Appendix D.

Case of study: braking device.

Material: 0.3%Cr 0.5%Mo.

D.1 Part and process description.

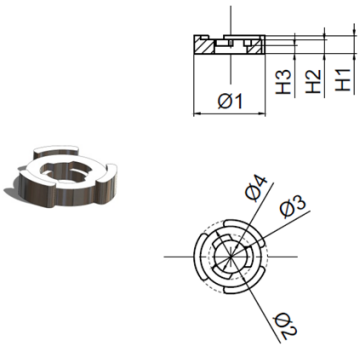

Fig. [D.1] Device, critical dimensions evaluated.

Sintering temperature [°C]	Heating rate [°C/min]	**Sintering** time [min]	Sintering atmosphere	Cooling rate [°C/min]
1150	5	30	Vacuum + N_2 backfill	5
1200	5	30	Vacuum + N_2 backfill	5
1250	5	30	Vacuum + N_2 backfill	5
1300	5	30	Vacuum + N_2 backfill	5
1350	5	30	Vacuum + N_2 backfill	5

Tab. [D.1b] (sintering conditions)

D.1.1 Part breakdown strategy

Fig. [D.2] Component break-down.

D.1.2 Actual dimensions, before and after sintering.

	Ø1	Ø2	Ø3	Ø4	H1	H2	H3
	37,186	30,579	22,541	16,573	9,088	7,050	3,937

Tab. [D.2a] Dimensions of the green samples.

	Ø1	Ø2	Ø3	Ø4	H1	H2	H3
1150°C	-0,002	-0,002	-0,002	-0,002	-0,004	-0,004	-0,004
1200°C	-0,003	-0,003	-0,003	-0,003	-0,006	-0,005	-0,005
1250°C	-0,005	-0,005	-0,005	-0,005	-0,008	-0,007	-0,007
1300°C	-0,006	-0,006	-0,006	-0,006	-0,009	-0,008	-0,008
1350°C	-0,009	-0,009	-0,009	-0,009	-0,013	-0,012	-0,012

Tab. [D.2b] Dimensional variations in sintering.

	Ø1	Ø2	Ø3	Ø4	H1	H2	H3
1150°C	37,135	30,533	22,509	16,546	9,058	7,011	3,919
1200°C	37,077	30,493	22,470	16,525	9,041	7,013	3,916
1250°C	37,022	30,451	22,445	16,496	9,024	7,019	3,917
1300°C	36,950	30,396	22,389	16,463	9,013	6,991	3,903
1350°C	36,861	30,329	22,351	16,418	8,970	6,970	3,880

Tab. [D.2c] Dimensions of the sintered samples.

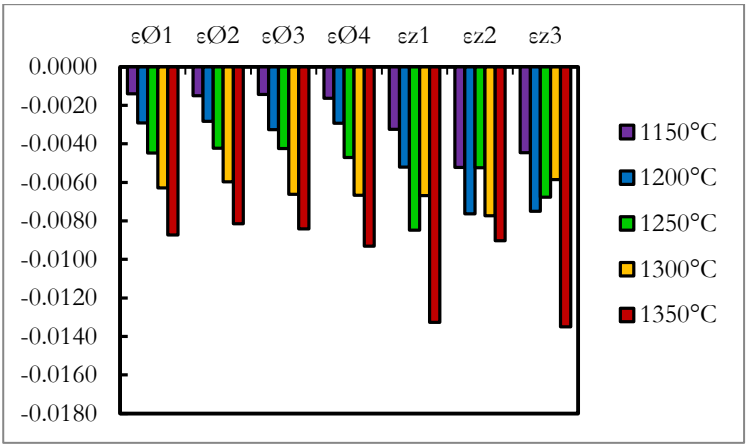

Fig. [D.3] Measured dimensional variations.

D.1.3 Design procedure. Estimation of the dimensional variation due to sintering.

	εi	K	K	K
1150°C	-0,002	-0,303	-0,290	-0,290
1200°C	-0,004	-0,192	-0,184	-0,184
1250°C	-0,005	-0,156	-0,151	-0,151
1300°C	-0,006	-0,138	-0,134	-0,134
1350°C	-0,010	-0,109	-0,105	-0,105

Tab. [D.3] Measured isotropic dimensional variations and computed anisotropy parameters.

	V1			V2			V3		
	εØext	εØint	εZ	εØext	εØint	εZ	εØext	εØint	εZ
1150°C	-0,0016	-0,0016	-0,0038	-0,0016	-0,0016	-0,0036	-0,0016	-0,0016	-0,0035
1200°C	-0,0032	-0,0033	-0,0059	-0,0033	-0,0034	-0,0055	-0,0033	-0,0033	-0,0055
1250°C	-0,0045	-0,0046	-0,0075	-0,0046	-0,0047	-0,0070	-0,0045	-0,0046	-0,0069
1300°C	-0,0055	-0,0057	-0,0088	-0,0057	-0,0058	-0,0082	-0,0056	-0,0057	-0,0081
1350°C	-0,0087	-0,0088	-0,0127	-0,0088	-0,0090	-0,0118	-0,0087	-0,0088	-0,0117

Tab. [D.4] Predicted dimensional variations for each level.

	Ø1	Ø2	Ø3	Ø4	H1	H2	H3
1150°C	37,135	30,533	22,509	16,546	9,058	7,011	3,919
1200°C	37,077	30,493	22,470	16,525	9,041	7,013	3,916
1250°C	37,022	30,451	22,445	16,496	9,024	7,019	3,917
1300°C	36,950	30,396	22,389	16,463	9,013	6,991	3,903
1350°C	36,861	30,329	22,351	16,418	8,970	6,970	3,880

Tab. [D.5a] Actual dimensions. Measured dimensions of the sintered parts.

	Ø1	Ø2	Ø3	Ø4	H1	H2	H3
1150°C	37,129	30,530	22,504	16,547	9,053	7,023	3,922
1200°C	37,065	30,478	22,468	16,518	9,034	7,028	3,924
1250°C	37,021	30,439	22,436	16,498	9,032	7,007	3,917
1300°C	36,978	30,405	22,410	16,479	8,994	6,988	3,894
1350°C	36,864	30,308	22,340	16,426	8,974	6,951	3,887

Tab. [D.5b] Predicted dimensions. Computed dimensions of the sintered parts.

D.1.4 Error of estimation.

	Ø1	Ø2	Ø3	Ø4	H1	H2	H3
1150°C	-0,006	-0,003	-0,004	0,000	-0,005	0,012	0,004
1200°C	-0,012	-0,015	-0,002	-0,007	-0,006	0,015	0,008
1250°C	-0,001	-0,011	-0,009	0,001	0,009	-0,012	-0,001
1300°C	0,028	0,010	0,020	0,016	-0,019	-0,003	-0,009
1350°C	0,003	-0,020	-0,011	0,008	0,005	-0,019	0,007

Tab. [D.6] Errors of estimation.

	Ø1	Ø2	Ø3	Ø4	H1	H2	H3
1150°C	4	3	4	3	5	7	5
1200°C	5	6	3	5	5	7	6
1250°C	3	5	5	3	6	7	3
1300°C	7	5	7	7	8	4	6
1350°C	3	7	6	5	5	8	6

Tab. [D.7] ISO-IT tolerances, values lower that 3 has been considered with the tolerance class IT 3.

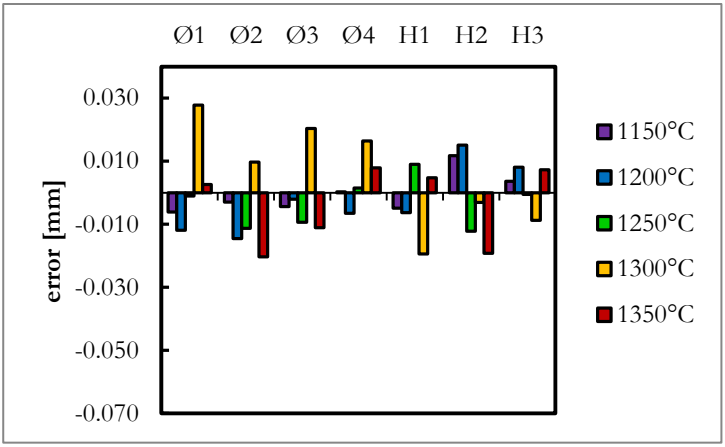

Fig [D.11] Difference between the actual value and the predicted one.

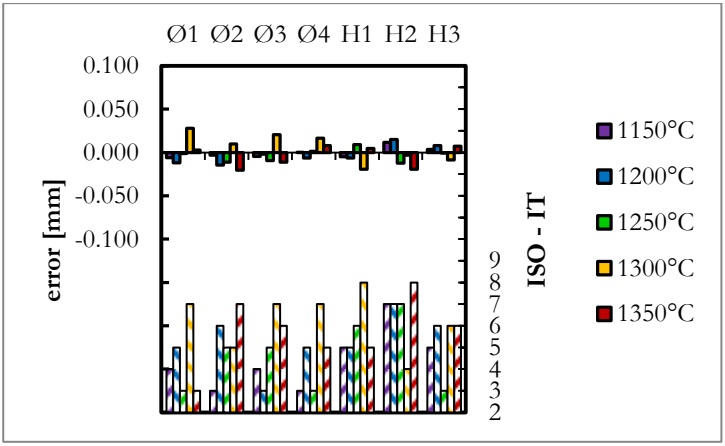

Fig. [D.12] Error and relative tolerance class.

D.2 Reliability.

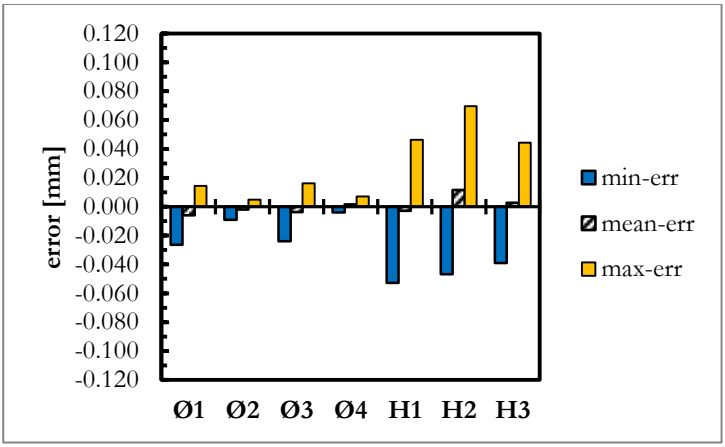

Fig. [D.13] Reliability test results, 1150 °C.

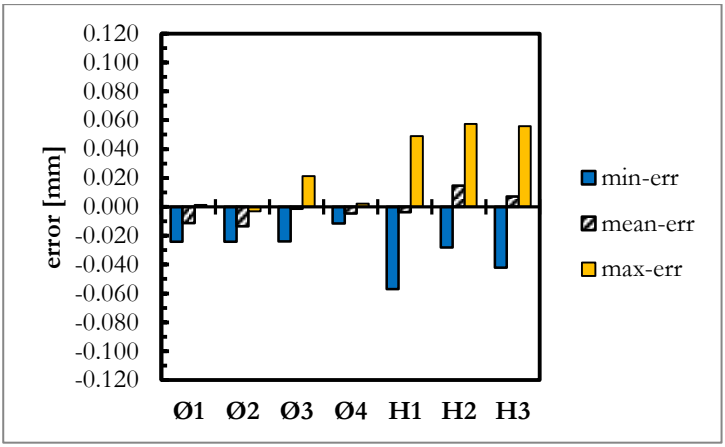

Fig. [D.14] Reliability test results, 1200 °C.

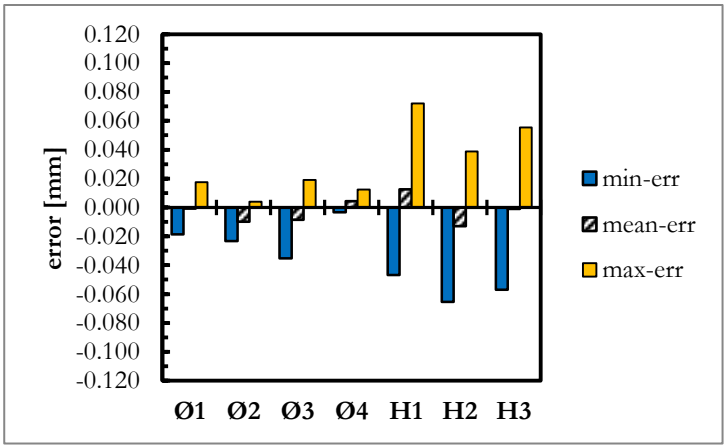

Fig. [D.15] Reliability test results, 1250 °C.

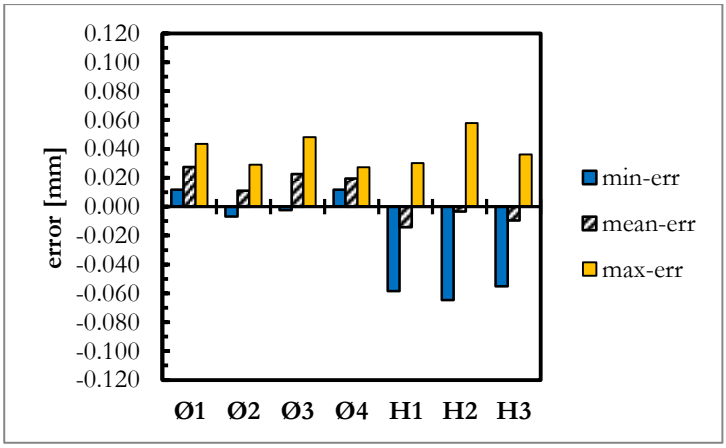

Fig. [D.16] Reliability test results,1300 °C.

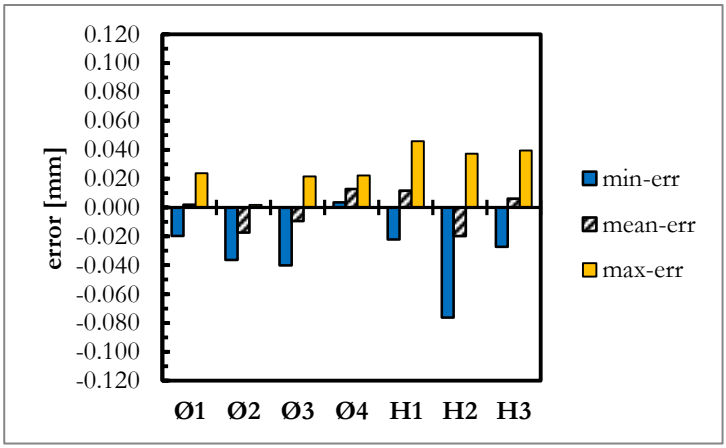

Fig. [D.17] Reliability test results,1350 °C.

List of publications

Papers on journal.

N. Corsentino, C. Menapace, I. Cristofolini, M. Larsson, A. Molinari, "The influence of the liquid phase on anisotropic dimensional change on sintering iron alloys", International Journal of Powder Metallurgy, 51/2, Spring 2015, pp. 27-38.

I. Cristofolini, N. Corsentino, A. Molinari, M. Larsson, "Study of the Influence of Material and Geometry on the Anisotropy of Dimensional Change on Sintering of Powder Metallurgy Parts " in International Journal of Precision Engineering and Manufacturing, v. 15, n. 9 (2014), pp. 1865-1873.

N. Corsentino, I. Cristofolini, M. Larsson, A. Molinari, "Modello analitico delle variazioni dimensionali in sinterizzazione di componenti in ferro", La Metallurgia Italiana n.10 2015, pp. 5-14.

Conference proceedings.

I. Cristofolini, N. Corsentino, M. Pilla, A. Molinari, M. Larsson, "Influence of the geometry on the anisotropic dimensional change of PM parts", Advances in Powder Metallurgy and Particulate Materials, 2013 vol. 2 n. 11 pp. 49-61.

I. Cristofolini, N. Corsentino, A. Molinari, M. Larsson, "A design procedure accounting the anisotropic dimensional change on sintering of ferrous PM parts", Advances in Powder Metallurgy and Particulate Materials, 2014 vol. 1 pp. 115-127.

I. Cristofolini, N. Corsentino, M. Larsson, A. Molinari, "Analytical model of the anisotropic dimensional change on sintering of ferrous parts", congress proceedings Sintering 2014, Dresden, August 24-28, 2014.

N.Corsentino, I.Cristofolini, S. Libardi, A. Molinari, "Effect of High Sintering Temperature on the Dimensional and Geometrical Precision of PM Cr-Mo Steel Parts", Euro PM2014 Proceedings, Salzburg, September 21-24, 2014.

N.Corsentino, I.Cristofolini, M.Larsson, A.Molinari, "Modello analitico delle variazioni dimensionali in sinterizzazione di componenti in ferro", atti di congresso 35° Convegno nazionale AIM, Roma, 5-7 Novembre, 2014.

N.Corsentino, I.Cristofolini, S. Libardi, A. Molinari, "Effect of High Sintering Temperature on the Dimensional and Geometrical Precision of PM Cr-Mo Steel Parts", Euro PM2015 Proceedings, Reims, October 04-07, 2015.

I. Cristofolini, N. Corsentino, A. Molinari, M. Larsson, "Influence of Geometry and Process Variables on the Anisotropy Parameter K ", Advances in Powder Metallurgy and Particulate Materials, 2015 vol. 1 pp. 31-40